## STIC-ILL

**From:** Davis, Minh-Tam
**Sent:** Wednesday, September 15, 2004 3:39 PM
**To:** STIC-ILL
**Subject:** Reprint request for 09/721864

NPL ___ Adonis
MIC ___ BioTech ✓ MAIN ___
NO ___ Vol NO ___ NOS ___
Ck Cite ___ Dupl Request ___
Call # RC 268.6 .C6
9/15 VD

1) 07821600 PMID: 3390350
Uptake of indium-111-labeled monoclonal antibody ZME-018 as a function of tumor size in a patient with melanoma.
Macey D J; Denardo S J; Denardo G L; Goodnight J K; Unger M W
Department of Radiology, University of California Davis Medical Center, Sacramento 95817.
American journal of physiologic imaging (UNITED STATES) 1988, 3 (1) p1-6, ISSN 0885-8276 Journal Code: 8610225

2) Rapid imaging of human melanoma xenografts using an scFv fragment of the human monoclonal antibody H11 labelled with 111In.
Reilly R M; Maiti P K; Kiarash R; Prashar A K; Fast D G; Entwistle J; Dan ; Narang S A; Foote S; Kaplan H A
Division of Nuclear Medicine, Toronto General Hospital, University Health Network, ON, Canada. raymond.reilly@utoronto.ca
Nuclear medicine communications (England) May 2001, 22 (5) p587-95, ISSN 0143-3636 Journal Code: 8201017

3) Treatment-related parameters predicting efficacy of Lym-1 radioimmunotherapy in patients with B-lymphocytic malignancies.
Lamborn K R; DeNardo G L; DeNardo S J; Goldstein D S; Shen S; Larkin E C; Kroger L A
Brain Tumor Research Center, Department of Neurological Surgery, University of California San Francisco Medical Center, San Francisco, California 94143, USA.
Clinical cancer research - an official journal of the American Association for Cancer Research (UNITED STATES) Aug 1997, 3 (8) p1253-60, ISSN 1078-0432 Journal Code: 9502500

4) 4368891 PMID: 10365793
Biodistribution of filamentous phage-Fab in nude mice.
Yip Y L; Hawkins N J; Smith G; Ward R L
School of Medicine (St. Vincent's Hospital), University of NSW, Sydney, Australia.
Journal of immunological methods (NETHERLANDS) May 27 1999, 225 (1-2) p171-8, ISSN 0022-1759 Journal Code: 1305440

5) Radiolabeling, biodistribution, and dosimetry of (123)I-mAb 14C5: a new mAb for radioimmunodetection of tumor growth and metastasis in vivo.
Lahorte Christophe M M; Bacher Klaus; Burvenich Ingrid; Coene Elisabeth D ; Cuvelier Claude; De Potter Christian; Thierens Hubert; Van de Wiele Christophe; Dierckx Rudi A; Slegers Guido
Department of Radiopharmacy, Faculty of Pharmaceutical Sciences, Gent University, Gent, Belgium. christophe.lahorte@ugent.be
Journal of nuclear medicine - official publication, Society of Nuclear Medicine (United States) Jun 2004, 45 (6) p1065-73, ISSN 0161-5505 Journal Code: 0217410

Thank you
MINH TAM DAVIS
ART UNIT 1642, ROOM 3A24, MB 3C18
272-0830

# Treatment-related Parameters Predicting Efficacy of Lym-1 Radioimmunotherapy in Patients with B-Lymphocytic Malignancies[1]

**Kathleen R. Lamborn, Gerald L. DeNardo,[2] Sally J. DeNardo, Desiree S. Goldstein, Sui Shen, Edward C. Larkin, and Linda A. Kroger**

Brain Tumor Research Center, Department of Neurological Surgery, University of California San Francisco Medical Center, San Francisco, California 94143 [K. R. L.], and Departments of Internal Medicine [G. L. D., S. J. D., D. S. G., S. S., L. A. K.] and Pathology [E. C. L.], University of California Davis Medical Center, Sacramento, California 95817

## ABSTRACT

**This study was designed to evaluate dosimetric, pharmacokinetic, and other treatment-related parameters as predictors of outcome in patients with advanced B-lymphocytic malignancies. Fifty-seven patients were treated with radiolabeled Lym-1 antibody in early phase trials between 1985 and 1994. Logistic regression and proportional hazards models were used to evaluate treatment parameters for their ability to predict outcome, taking into account patient risk group based on Karnofsky performance status and serum lactic dehydrogenase. The occurrence of a partial or complete response (31 of 57 patients) and development of human antimouse antibody (HAMA) predicted improved survival using a time-dependent proportional hazards model. The final multivariate model for survival with parameters significant at $P \leq 0.05$ included overall response and pretreatment risk group. Although some of the dosimetric and pharmacokinetic parameters were predictive in univariate analyses, only longer half-time of radionuclide in the blood showed any indication of improved prediction beyond that provided by the lactic dehydrogenase/Karnofsky performance status-based risk groups. Splenic volume, splenectomy, and malignant tissue Lym-1 reactivity were not contributory. In this patient group, the effect of radiolabeled Lym-1 treatment as indicated by measurable tumor response was associated with improved survival. Development of HAMA was also associated with improved survival, indicating that concern about HAMA should not preclude exploration of radioimmunotherapy. Although dosimetry has a role in determining safety based on dose to normal organs, when adjusted for baseline clinical features, dosimetric and pharmacokinetic parameters showed limited ability to improve outcome prediction.**

## INTRODUCTION

To effectively evaluate novel therapies such as RIT,[3] it is important to identify and to take into account patient characteristics that might influence outcome. The need to determine factors that predict therapeutic outcome in patients with non-Hodgkin's lymphoma has led to a number of studies (1–6), including the recent IPFP (7). In the IPFP, over 2000 patients treated with doxorubicin-based combination chemotherapy were evaluated to determine which pretreatment clinical features predicted for improved survival. Age, tumor stage, serum LDH, performance status, and number of extranodal disease sites were found to be significant in a multivariate stepwise analysis and were used to construct a model that predicted patients' relative risk of death.

Candidates for radioimmunotherapy represent a different patient group than those considered in the IPFP. The histological types of the RIT patients are less homogeneous, and extent of disease is heavily weighted toward Ann Arbor stages 3 and 4. Furthermore, RIT patients have been extensively treated with combination chemotherapy (8–10) and external beam radiotherapy. Additionally, RIT represents a different therapeutic modality than chemotherapy or standard radiotherapy, and it cannot be assumed that the same set of pretherapy parameters would be predictive of outcome.

For that reason, the predictive value of 21 pretherapy parameters were evaluated in patients with B-lymphocytic malignancies that were subsequently treated with $^{131}$I- or $^{67}$Cu-labeled Lym-1 antibody (11–16). It was found that these patients with advanced disease could effectively be categorized into low, medium, and high risk groups for early failure and death based on LDH (percentage above normal range) and performance status, two of the five parameters found to be of importance in the IPFP. As an indication of the population differences, it is of interest that the IPFP risk factor of stage (I and II *versus* III and IV) was not applicable to these patients because they all were stage III or IV.

The present report evaluates parameters specifically relevant to RIT, including HAMA, dosimetry, and pharmacokinet-

Received 12/2/96; revised 3/24/97; accepted 4/2/97.
The costs of publication of this article were defrayed in part by the payment of page charges. This article must therefore be hereby marked *advertisement* in accordance with 18 U.S.C. Section 1734 solely to indicate this fact.
[1] Supported by National Cancer Institute Grant PHS CA 47829 and Department of Energy Grant DE-FG03-84ER60233.
[2] To whom requests for reprints should be addressed, at the Molecular Cancer Institute, 1508 Alhambra Boulevard, Room 214, Sacramento, CA 95816. Fax: (916) 451-2857.

[3] The abbreviations used are: RIT, radioimmunotherapy; IPFP, International Non-Hodgkin's Lymphoma Prognostic Factors Project; LDH, lactic dehydrogenase; HAMA, human antimouse antibody; KPS, Karnofsky performance status; CR, complete remission; PR, partial response; TTP, time to disease progression.

ics. To reduce the possibility that these treatment-related parameters may serve as surrogates for overall patient status, general baseline risk factors were also included in the analyses. This type of analysis is critical to the evaluation of potential therapies, providing information relative to appropriate patient selection and radionuclide dosage planning.

## MATERIALS AND METHODS

**Patient Selection.** Fifty-seven heavily pretreated, adult patients with B-lymphocytic malignancies whose disease was progressing despite standard therapy were entered into clinical trials of Lym-1-based RIT between September 1985 and March 1994. Fifty-three patients received treatment with $^{131}$I-Lym-1 and 4 received treatment with $^{67}$Cu-Lym-1. The clinical trials were early phase studies (two were maximum tolerated dose trials). Patient doses were based on the assigned dose level at the time of patient enrollment. RIT doses were repeated at 2–6-week intervals. The median number of infusions was three (range, 1–16). Patients were evaluated immediately before and approximately 1, 4, 8, 12, 24, 36, and 48 weeks after radiolabeled antibody infusion and at 6-month intervals thereafter. Before treatment, all patients were advised of the investigational nature of the study and signed an informed consent for protocols that were approved by the University of California at Davis Human Subjects and Radiation Use Committees under an Investigational New Drug authorization from the United States Food and Drug Administration.

Fifty-two patients had non-Hodgkin's lymphoma (11, 32, and 9 classified as low, intermediate, and high grade, respectively, based on the Working Formulation) and 5 had chronic lymphocytic leukemia. There were 34 men and 23 women. Median age was 55 years (range, 30–74). Median KPS was 70 (range, 40–90). The median number of prior chemotherapy regimens was 4 (range, 1–13). All 57 patients had malignancies that showed evidence for Lym-1 reactivity as demonstrated by immunophenotypic studies.

**Patient Risk Groups for Early Failure and Death.** For the purpose of this study, patients were categorized into three risk groups based on their LDH and KPS values using information from the proportional hazards model for survival developed previously (11). In that model, the patient's LDH as a ratio of upper range of normal was categorized on a scale of 1–4 based on the following criteria: 1, <0.9; 2, 0.9–1.11; 3, 1.12–1.9; and 4, >1.9. From the model, the formula for risk assignment was 0.70 (LDH grade)–0.05 (KPS). Using this model, an increase in LDH grade by one level increased the logarithm of the hazard by 0.7. This increase roughly corresponded to a decrease in KPS of 10 units, which increased the log hazard by 0.5. The relationship between risk groups and histological grades was weak, and all histological grades were represented in each risk group.

**Quantitative HAMA.** Quantitative HAMA assays for reactivity against Lym-1 were performed by ELISA using serum from a patient with Lym-1 antiglobulin (HAMA) titer as the positive standard. In this study, HAMA titer was considered positive at 5.0 μg/ml (17). For protocol entry, prior immunotherapy was permitted, but a negative HAMA was required.

**Therapeutic Study Agents.** Lym-1 is an IgG2a mouse monoclonal antibody that is B lymphocyte specific and has avidity for a membrane-associated antigen found on most malignant B cells (18). $^{131}$I-labeled Lym-1 was prepared using chloramine-T at a mass ratio of about 1 μg of chloramine-T:10 μg of Lym-1 (19). $^{67}$Cu-labeled Lym-1 ($^{67}$Cu-2-iminothiolane-6-[p-(bromoacetamido)benzyl]-1,4,8,11-tetraazacyclotetradecane-*N,N′,N″,N‴*-tetraacetic acid-Lym-1) was prepared by the methods described previously (20). At least 90% of radioactivity was associated with Lym-1 by immunochemical characterization, and the pharmaceutical exhibited at least 65% immunoreactivity (19–21).

**Pharmacokinetics and Radiation Dosimetry.** Methods for collecting the pharmacokinetic data and calculating radiation absorbed dose have been described previously (22, 23). Briefly, planar images of conjugate views were acquired immediately, 2–6 h, and daily up to 10 days after administration of the radiopharmaceutical. The amount of activity in organs and tumors was determined using either geometric-mean or effective-point-source methods, depending on whether the source object could be identified on both or one conjugate view (22–25). Coincidence at high counting rates was corrected using a reference source (26). Blood samples were collected during imaging sessions, and the radioactivity in each sample was determined using a gamma well-counter.

Cumulated activity was determined by fitting pharmacokinetic data to a monoexponential function except for the blood, where a biexponential fit was used (22, 23, 27). Radiation dose was calculated based on Medical Internal Radiation Dose formalism (28, 29). A uniform distribution of radionuclide in the tissues was assumed, and Medical Internal Radiation Dose data for "standard man" was used for the organ S factors (30, 31) except for spleen, where actual volume was used. Spleen volume was determined using computed tomography images except for four patients, where single-photon emission computed tomography images were used (32) because computed tomography images of the spleen were not available. Patients that had a splenectomy were considered to have zero volume and zero cumulative activity for the purposes of analysis. For other spleen parameters, these patients were excluded from analysis.

Two patients in this study had an immunoadsorption procedure at 6 h after infusion of the $^{131}$I-Lym-1 dose to reduce the radiation dose to normal tissues (33). The cumulated activity was calculated for these patients by summing the activity over time that was separately determined before and after the immunoadsorption procedure.

Tumor radionuclide uptake measurements were made only for those tumors for which adequate dosimetry could be expected based on previous work using tumor phantoms (34). This included a criterion that the tumor be at least 2 cm in diameter. Eight patients had no tumors that met these criteria; 13 patients had only one tumor that met the criteria. To provide an overall picture of tumor dosimetry when multiple tumors were present, the tumors that had the least and greatest rads/mCi dose were selected for each patient from among those that could be quantitated. When only one tumor met the criteria, the dose to this tumor was included in analysis of lowest tumor dose and greatest tumor dose as predictors of outcome.

To assess radiation to the marrow, penetrating radiation from the body, nonpenetrating radiation from the blood (27, 35),

*Table 1* Dosimetric therapy-related parameters evaluated for predictive potential

| | Description |
|---|---|
| Tumor[a] | |
| Radiation dose (rads/mCi)<br>45; 3.8 (0.3–12.7)[b] | Dose to tumor from the first treatment per unit of injected mCi dose of radionuclide. Reflects tumor radiation dose independent of the injection dose or dosing schedule. |
| Radiation dose (rads)<br>45; 241 (16–1485) | Total radiation dose to tumor from the first treatment. |
| Blood | |
| Cumulative activity ($\mu$Cihr $\times$ $10^6$)<br>51; 0.41 (0.003–3.78) | Time-dependent integration of radionuclide level (equivalent to area under the curve for drug concentration). Directly linked to radiation dose by the physical constants for the specific radionuclide. |
| Bone marrow | |
| Nontargeted radiation dose (rads)<br>51; 22 (4–90) | Sum of the radiation doses contributed by penetrating radiation from the body and nonpenetrating radiation from the blood. |
| Targeted radiation dose (rads)<br>50; 16.6 (0.6–55.9) | Contribution from nonpenetrating radiation from radionuclide targeted to marrow elements. |
| Total radiation dose (rads)<br>50; 41 (7–126) | Sum of targeted and nontargeted radiation dose. |
| Spleen | |
| Radiation dose (rads/mCi)<br>37; 1.9 (0.3–8.2) | Dose to the spleen from the first treatment using the patient's tomographic splenic volume. |
| Cumulative activity as percentage of total body (%)<br>51; 3.38 (0–15.1) | Cumulative activity for the spleen divided by the total body cumulative activity. Calculated by time dependent integration of radionuclide level. Used as a measure of the spleen as a "sink" for the radiolabeled antibody. |

[a] Tumor with maximum radiation dose (rads/mCi).
[b] Number of patients; median (range).

and nonpenetrating radiation from targeting of the marrow (36) were considered.

**Outcome Assessment.** Complete staging by X-ray, physical exam, and computerized tomography was performed prior to RIT. Tumor sites were reevaluated during treatment and at 1–6-month intervals thereafter.

To qualify as a response, tumor regression must have persisted for at least 4 weeks. Responses were classified as: CR, the complete absence of demonstrable disease including negative bone marrow examination; PR, a decrease in the sum of the products of all tumor dimensions by at least 50%, or all tumor volumes by at least 70%; stable disease; and progression, an increase of at least 25% in the size of any lesion or the development of new lesions.

TTP was measured from the start of treatment. Survival time was measured from the start of treatment to death or the date of the last follow-up for surviving patients.

**RIT-specific Predictive Factors.** All dosimetric and pharmacokinetic parameters potentially related to treatment outcome were considered for analysis. In general, these parameters were selected based on their relevance to either antitumor activity or normal tissue toxicity. A list of these parameters together with definitions are provided in Table 1 (dosimetry) and Table 2 (pharmacokinetics).

**Statistical Methods.** Statistical analyses were done using SAS version 6.08 (37). Analysis of potential predictors of CR and CR + PR (overall response) was done using logistic regression. Analysis of TTP and survival was done using proportional hazards models (38). A multivariate analysis including the LDH/KPS-based risk group was done for all parameters significant at $P = 0.1$ in univariate analysis to evaluate the degree to which the new parameters would increase the ability to predict beyond prediction based on the general information known about the patient. All parameters that continued to be significant at $P = 0.1$ were considered for the final multivariate analysis with retention based on $P \leq 0.05$. Initial multivariate analyses included only those patients with values for all parameters under consideration, as required by the modeling method. The final model included all patients because all patients had the required information based on the final parameters selected.

Parameters that varied with time were included as time-dependent variables in the analysis of TTP and survival (38). For example, patients were not grouped as responders *versus* nonresponders with time to event calculated separately for the two groups, a method known to be biased (39). Instead, at each follow-up time, all patients without an event to that point were categorized as having had a response by that time or not, and this information was used in the calculation of a hazard ratio.

The usual proportional hazards model assumes a linear increase in the log hazard as a function of the predictor. However, when data include extreme values, the relationship can often be more accurately described assuming a linear relationship with a log transformation of the predictor values. For this reason, natural logarithms of the HAMA titers were used for the purpose of the time-dependent analysis of maximum HAMA. All patients were assigned a score of zero at baseline (based on the fact that all were considered HAMA negative at start of study). For patients that became HAMA positive, at each subsequent evaluation the log of the maximum HAMA titer to that point was used.

Analyses involving pharmacokinetics and dosimetry (administered radionuclide dose and radiation dose) included only those patients that received $^{131}$I-Lym-1 to prevent confounding due to differences in the radionuclide. The two patients that

*Table 2* Pharmacokinetic therapy-related parameters evaluated for predictive potential

| | Description |
|---|---|
| Tumor[a] | |
| Biologic clearance half-life (days)<br>43; 1.4 (0.5–7.2)[b] | Time required to clear one-half of the radionuclide from the tumor after correcting for radionuclide decay; determined by fitting the observed concentrations (%ID/g) for the tumor using a monoexponential function. |
| Peak concentration (%ID/g)<br>45; 0.03 (0.001–0.48) | Maximum measured concentration of radionuclide, usually observed at 6 or 24 h after infusion using quantitative radionuclide imaging. |
| Immediate concentration (%ID/g)<br>45; 0.13 (<0.001–0.54) | Measured concentration of radionuclide observed immediately after infusion using quantitative radionuclide imaging. |
| Extrapolated zero time concentration (%ID/g)<br>43; 0.02 (0.001–0.48) | Concentration of radionuclide calculated to be present at time zero by extrapolation of the monoexponential fit of subsequently observed concentrations. |
| Blood | |
| Alpha half-time (h)<br>50; 2.6 (0.1–13.1) | Initial rapid biological clearance half-time. Time required for one-half the initial rapid clearance corrected for radionuclide decay. Based on biexponential function adjusting for slow phase fit. |
| Beta half-time (h)<br>50; 29 (15–63) | Slow biological clearance half-time. Determined by fitting the later observed radionuclide levels to a monoexponential function. |
| VDss (liters)<br>50; 18 (5–80) | Volume of distribution of radionuclide after equilibration leads to steady state. Reflects the equilibrated space of the radiolabeled antibody. |
| Total body | |
| Total body clearance (h)<br>49; 29 (21–54) | Biological clearance half-time determined by fitting the observed percentage of injected dose over time to a monoexponential function. |
| Spleen | |
| Immediate uptake (%ID)<br>49; 4.4 (0–24.7) | Spleen uptake measured immediately after infusion using radionuclide imaging. |

[a] Tumor with maximum radiation dose (rads/mCi).
[b] Number of patients; median (range).

received immunoadsorption were also excluded for analyses involving clearances from tumor, total body and blood and extrapolated zero time tumor uptakes because values for these patients were modified by the immunoadsorption.

A number of supplementary analyses were done to confirm the results. These included a second multivariate analysis using the same parameters but including only patients in the two better risk groups, because it is possible that identifying a patient as high risk precludes further distinctions and, therefore, would invalidate the modeling assumptions. Analyses of parameters where it was felt chronic lymphocytic leukemia patients might be inherently different from lymphoma patients were repeated without this group. The analyses of HAMA and overall response as predictors of survival were repeated excluding the four patients receiving $^{67}$Cu-Lym-1 and the two who underwent an immunadsorption procedure. The risk groups used for this study were developed based on studying a relatively small number of patients, compared, for example, to the IPFP study, so that some risk factors might have been missed. Therefore, the two parameter analyses, including risk group and either HAMA or overall response as predictors of survival, were repeated using the IPFP risk groups. Because all of these supplementary analyses were consistent with the primary analysis, only the primary analysis is reported.

## RESULTS

Thirty-one patients achieved at least a PR, including 11 with CRs. Eighty-seven % of the responders had at least a partial response in less than 9 weeks from start of treatment, with a median of 4 weeks. At the time of this analysis, all patients had progressed. Four patients (all in the low risk group) remained alive at 6.3, 4.2, 3.5, and 2.1 years after initiation of treatment.

**Treatment-related Predictors.** The values for key treatment-related parameters are summarized in Tables 1–4. Table 5 lists characteristics found significant on a univariate basis for one or more of the outcome measures. The only pretherapy parameter found significant at $P = 0.1$ was larger initial dose (mCi), which was predictive for CR. Among parameters measured following the first treatment dose, longer $\alpha$ and $\beta$ half-times (h) for blood clearance predicted for CR and improved TTP. Increased cumulative activity in the blood ($\mu$Cihr), increased bone marrow nontargeted radiation dose (rads), increased peak concentration (%ID/g), and extrapolated zero time concentration (%ID/g) for the tumor receiving the maximum dose (rads/mCi) were also predictive for CR.

Among the time-dependent variables, CR and overall response (CR or PR) predicted for prolonged time to progression and survival. Nineteen of 57 patients developed positive serum HAMA levels, and higher HAMA score analyzed as a time-dependent variable predicted for improved survival. HAMA activity interrupted therapy in only seven patients (12%).

With a limited number of patients, it is possible that predictive parameters might not achieve statistical significance. For this reason, the distributions of key parameters not found significant in univariate analyses were reviewed for patients who had a CR and for patients who had any response. Complete response occurred in patients with a total radiation dose to a tumor site from the first treatment dose as low as 31 rads and with a spleen volume as large as 968 ml. The median spleen volume for all patients with responses was 251 ml. These numbers suggest that responses can occur in patients often considered unlikely to benefit from RIT and that although there may be an association between these parameters and outcome, it is limited in degree.

*Table 3* Pretherapy parameters evaluated for predictive potential

| | |
|---|---|
| Initial dose ($mCi/m^2$) 57; 36 (14–100)[a] | Radioactive dose planned per injection per meter squared of body surface area. |
| % Lym-1 reactivity (%) 49; 60 (10–97) | Percentage of malignant cells binding to Lym-1 based on immunophenotypic studies. |
| Spleen volume (ml) 47; 251 (0–2077) | Measured prior to therapy. |
| Splenectomy 8 | Splenectomy prior to therapy. |

[a] Number of patients; median (range).

All variables found significant at $P = 0.1$ in a univariate analysis were then tested in a two-parameter model that also included baseline risk category (graded 1, 2, or 3 for low, medium, or high risk). Parameters predicting improved CR rate with $P \leq 0.1$ in the two-parameter model were longer blood clearance $\alpha$ and $\beta$ half-times ($P = 0.08$ in each case). For TTP, longer blood clearance $\beta$ half-time met this criterion ($P = 0.06$). For survival, peak HAMA level and overall response evaluated as time-dependent variables remained predictive by this criterion ($P = 0.06$ and $P = 0.02$, respectively).

**Final Multivariate Models.** The final predictive models were defined to include variables significant at $P = 0.05$. With risk group in the model, none of the treatment-related parameters met this criterion for CR, overall response, or TTP. For survival prediction, the final model included risk category ($P < 0.001$) and overall response ($P = 0.02$). The hazard ratio for risk category was 3.5. This indicates that, based on the model, at any point in time the relative risk of death increased by 3.5-fold for each increase in risk category (*e.g.*, low to medium or medium to high). The hazard ratio for overall response was 0.4. This indicates that for each point in time, a patient with a response had a relative risk of death of 0.4 that of a patient alive at that point but without a response.

## DISCUSSION

Since the initial reports on the efficacy of radioimmunotherapy in B-cell malignancies (13, 14), a number of investigators have reported promising results from clinical trials using Lym-1 (12, 15, 16, 40, 41) and other radiolabeled antibodies (42–46), suggesting significant therapeutic potential for this novel therapy in patients with non-Hodgkin's lymphoma and chronic lymphocytic leukemia. To effectively evaluate new therapies such as RIT, it is useful to study treatment parameters unique to the nature of the therapy to determine their role in predicting outcome. Also, if preliminary results indicate that patients do respond, it is important to determine if that response influences survival.

In this heavily pretreated population, no spontaneous remissions were to be expected. Therefore, the presence of responses indicated therapeutic effect. This study analyzed CR and overall response as time-dependent variables to determine if they predicted improved TTP and survival from the time of occurrence. Overall response predicted improved TTP and survival with a high degree of significance ($P < 0.001$). Presence *versus* absence of a CR was also predictive. Because most of the CRs and many of the PRs occurred in the low risk group, it is not surprising that information on these outcomes did not substantially increase prediction for TTP when risk group was also included in the multivariate model. However, even after adjustment for risk group, overall response was predictive of improved survival.

On initial consideration, it might appear that the prediction of longer survival based on the presence of a response is self evident. However, there have been studies of other therapies that have demonstrated therapeutic effect in terms of response, but where response did not result in improved survival (39). Among other reasons, this can occur when the response is not durable or when patients die at a more rapid rate following failure than if they had received alternative treatment. Therefore, demonstration of a survival benefit following response, where the analysis is done in a way that avoids the bias of using responder/nonresponder as patient categories, and which does so after adjustment for patient baseline risk factors, indicates meaningful benefit from treatment.

Historically, the possibility of anaphylaxis and other immune reactions were of concern in RIT using murine antibodies. Studies to date have shown that these reactions are not a major problem (47). However, repeat dosing may be limited or dose effect reduced due to changes in biodistribution secondary to HAMA. In spite of this, there are reports of increased HAMA titer associated with improved outcome (48). In the study reported here, patients whose HAMA titers increased during and following treatment had improved survival with $P = 0.06$, even when adjusted for patient risk group. The fact that high peak HAMA titers predicted improved survival may represent the effect of a functioning immune system. It may also suggest generation of anti-idiotypic antibodies mimicking the tumor cell antigen and facilitating host recognition of tumor (49, 50). Whether or not high HAMA titers ultimately prove to be predictive, it is clear from this study and others that concern about HAMA should not *a priori* preclude use of RIT.

Because blood represents the input function of radiolabeled antibody to organs and tumor, parameters related to radionuclide kinetics in the blood were considered potentially predictive. Longer $\alpha$ and $\beta$ blood clearance half-times were found to be predictive of CR and TTP in the univariate analysis. Even with risk included in the model, the $\beta$ half-time was almost significant for TTP at $P = 0.06$. Prediction based on longer half-times is consistent with the concept that rapid clearance from the blood prevents sufficient radiolabeled antibody from reaching the tumors, and these parameters are analogous to parameters describing the area under the curve for a chemotherapeutic agent.

The lack of association between outcome and spleen parameters found in this study is of interest because of other reports indicating a relationship of spleen size to radionuclide biodistribution for patients receiving $^{131}I$ antibody therapy (45, 46). In those studies, patients received therapy only if they were considered likely to have a favorable biodistribution, with every assessable tumor predicted to receive a higher absorbed dose of radiation than key normal organs. Patients with enlarged spleens generally did not have favorable biodistribution based on tracer studies and were, therefore, not enrolled in the therapeutic portion of the trial. A larger spleen is associated with a greater number of normal and malignant B-lymphocytes that can take

*Table 4* Time-dependent parameters evaluated for predictive potential

| | Description |
|---|---|
| Peak HAMA (μg/ml)<br>19; 88 (7–1802)[a] | Defined for each time evaluated in a specific analysis as maximum HAMA score observed to that time for those who became HAMA positive (quantitative value exceeded 5 μg/ml). |
| Cumulative dose (mCi/m$^2$)<br>57; 131 (15–508) | For each time evaluated in an analysis, the sum of the radionuclide doses per meter squared received to that time. |
| CR<br>11; 9 (3–38)[b] | Denoted as positive for all times after a patient has achieved a CR. |
| Response<br>31; 4 (0.3–16)[b] | Denoted as positive for all times after a patient has achieved a response (partial or complete). |

[a] Number of patients; median (range) for maximum per patient.
[b] Number of patients; median (range) for time to event in weeks for those with event.

*Table 5* $P$ for treatment-related parameters significant in univariate analysis at $P = 0.1$ for one or more of the outcome measures.

| | CR | Response | TTP | Survival | Better outcome |
|---|---|---|---|---|---|
| Initial dose (mCi/m$^2$) | 0.03 | NS[a] | NS | NS | Higher dose |
| Peak concentration (%ID/g) for the high dose tumor | 0.09 | NS | NS | NS | Higher peak |
| Extrapolated zero time concentration (%ID/g) for the high dose tumor | 0.1 | NS | NS | NS | Higher concentration |
| Blood cumulative activity (μCihr) | 0.1 | NS | NS | NS | Higher cumulative activity |
| Alpha half-time (h) | 0.01 | NS | 0.02 | NS | Longer time |
| Beta half-time (h) | 0.06 | NS | 0.08 | NS | Longer time |
| Nontargeted marrow dose (rads) | 0.09 | NS | NS | NS | Higher dose |
| Peak HAMA (μg/ml) | NA | NA | NS | 0.02 | Higher HAMA |
| CR | NA | NA | 0.04 | 0.005 | CR |
| Response | NA | NA | <0.001 | <0.001 | Response |

[a] NS, not significant at $P = 0.1$; NA, not applicable (time-dependent variables were not considered as possible predictors for CR or Response).

up antibody, resulting in less antibody available for tumor binding outside the spleen. In our studies, patients with enlarged spleens were not excluded, and many patients had spleen volumes that deviated greatly from normal. Therefore, the data were useful for determining whether spleen size and/or dose to spleen were predictive of outcome from Lym-1 RIT. Analysis showed no relation between spleen parameters and outcome, even in univariate models. However, the antibodies studied target distinctly different antigens: CD20 and CD37 *versus* HLA-Dr (Lym-1)(18, 45). An enlarged spleen may present an overwhelming antigen sink for some antibodies, requiring adjustments such as pretherapy loading doses or splenectomy for successful therapy. This will need to be evaluated on an individual antibody basis.

Bone marrow dosimetric parameters were considered because of their potential for limiting RIT doses. The only parameter significant in univariate analysis was marrow radiation contributed by blood and body sources, which predicted higher likelihood of CR with higher dose (rads). This result may reflect the higher initial injected doses, which tended to be given to the patients without extensive marrow malignancy. However, none of the bone marrow variables proved predictive once patient risk group was taken into account.

Because radiotherapeutic response results from energy deposition in the tumor tissue, parameters relevant to radionuclide uptake, clearance, and radiation dose for tumor could be useful predictors. Past studies have shown that radiation dose to tumor can vary considerably and is not easily predicted from the amount of radioconjugated-antibody or radionuclide given (41). In a study reported by Kaminski *et al.* (44), pretreatment antibody loading dose was selected based on the ratio of radiation dose to tumor and total body observed in tracer studies. As noted above, Press *et al.* (45, 46) selected patients for RIT by requiring that tumor dose be greater than that to normal organs. For patients reported here, dose adjustments were not made based on tumor uptake, allowing evaluation of tumor dose as a predictor. In our analysis, some tumor dose-related parameters were predictive in univariate analyses (Table 5), but none improved predictive ability beyond information already provided by risk group category for any of the outcomes studied. The lack of outcome prediction based on tumor dose may have multiple causes. It is generally recognized that radiation dose is not homogeneously distributed throughout the tumor and differs from tumor to tumor. Additionally, radiation dosimetry for radionuclide treatment has not reached the level of accuracy of radiation dosimetry for external beam radiotherapy. Finally, tumor response and survival are the result of complex interactions of variables including the inherent biology and radiosensitivity (radiobiology) of the tumor and the clinical and immunological status of the patient.

In summary, our intent is to present a model for how to approach evaluating RIT therapies, rather than a model for RIT therapy. Even with the limitations presented by relatively small sample size and the many sources of variability, there was still

an indication of positive long-term outcomes based on response to therapy. This reinforces the belief that even heavily pretreated patients can derive clinical benefit from treatment with Lym-1 RIT. It also demonstrates that concern about HAMA need not *a priori* preclude consideration of such therapy. Review of the extensive information available to us concerning pharmacokinetics and dosimetry on these patients found them to be of limited predictive value once basic patient characteristics were considered. It will be important for others to complete similar reviews of their data. In the interim, although the use of radiation dosimetry to project safe dose levels based on potential organ toxicity may have a role in treatment planning, we should be cautious in using tumor dosimetry to determine patient eligibility or to select administered dose of radionuclide.

## ACKNOWLEDGMENTS

Work was done within the Department of Internal Medicine, University of California Davis Medical Center, Sacramento, CA. We acknowledge the assistance of Drs. Pavel L. Lomen and Robert T. O'Donnell in manuscript review and Edward Dolber-Smith in data assembly and manuscript preparation.

## REFERENCES

1. Bastion, Y., Berger, F., Byron, P., Felman, P., Ffrench, M., and Coiffer, B. Follicular lymphomas: assessment of prognostic factors in 127 patients followed for 10 years. Ann. Oncol., *2* (Suppl.): 123–129, 1991.

2. Coiffer, B., Gisselbrecht, C., Vose, J., Tilly, H., Herbrecht, R., Bosly, A., and Armitage, J. Prognostic factors in aggressive malignant lymphoma: description and validation of a prognostic index that could identify patients requiring a more intensive therapy. J. Clin. Oncol., *9:* 211–219, 1991.

3. Cowan, R., Jones, M., Harris, M., Steward, W., Radford, R., Wagstaff, J., Deakin, D., and Crowther, D. Prognostic factors in high and intermediate grade non-Hodgkin's lymphoma. Br. J. Cancer, *59:* 276–282, 1989.

4. Jagannath, S., Velasquez, W., Tucker, S., Fuller, L., McLaughlin, P., Manny, J., North, L., and Cabanillas, F. Tumor burden assessment and its implication for a prognostic model in advanced diffuse large-cell lymphoma. J. Clin. Oncol., *4:* 859–865, 1986.

5. Kaminski, M., Coleman, C., Colby, T., Cox, R., and Rosenberg, S. Factors predicting survival in adults with stage I and II large-cell lymphoma treated with primary radiation therapy. Ann. Intern. Med., *104:* 747–756, 1986.

6. Shipp, M., Harrington, D., Klatt, M., Jochelson, M., Pinkus, G., Marshall, J., Rosenthal, D., Skarin, A., and Canellos, G. Identification of major prognostic subgroups of patients with large-cell lymphoma treated with m-BACOD or M-BACOD. Ann. Intern. Med., *104:* 757–765, 1986.

7. Shipp, M., Harrington, D., Anderson, J., Armitage, J., Bonadonna, G., Brittinger, G., Cabanillas, F., Canellos, G., Coiffer, B., Connors, J., Cowan, D., Crowther, D., Dahlberg, S., Engelhard, M., Fisher, R., Gisselbrecht, C., Horning, S., Lepage, E., Lister, A., Meerwaldt, J., Montserrat, E., Nissen, N., Oken, M., Peterson, B., Tondini, C., Velasquez, W., and Yeap, B. A predictive model for aggressive NHL: the international non-Hodgkin's lymphoma prognostic factors project. N. Engl. J. Med., *329:* 987–994, 1993.

8. Fisher, R., Gaynor, E., Dahlberg, S., Oken, M., Grogan, T., Mize, E., Glick, J., Coltman, C., and Miller, T. Comparison of a standard regimen (CHOP) with three intensive chemotherapy regimens for advanced non-Hodgkin's lymphoma. N. Engl. J. Med., *328:* 1002–1006, 1993.

9. McMaster, M., Greer, J., Wolff, S., Johnson, D., Greco, F., Mize, E., Stein, R., Lousar, J., Flexner, J., and Hainsworth, J. Results of treatment with high intensity, brief duration chemotherapy in poor prognosis non-Hodgkin's lymphoma. Cancer (Phila.), *68:* 233–241, 1991.

10. Shipp, M., Yeap, B., Harrington, D., Klatt, M., Pinkus, G., Jochelson, M., Rosenthal, D., Skarin, A., and Canellos, G. The M-BACOD combination chemotherapy regimen in large-cell lymphoma: analysis of the completed trial and comparison with the M-BACOD regimen. J. Clin. Oncol., *8:* 84–93, 1990.

11. DeNardo, G., Lamborn, K., DeNardo, S., Goldstein, D., Dolber-Smith, E., Kroger, L., Larkin, E., and Shen, S. Prognostic factors for radioimmunotherapy in patients with B-lymphocytic malignancies. Cancer Res., *55* (Suppl.): 5893–5898, 1995.

12. DeNardo, G., and DeNardo, S. Treatment of B-lymphocytic malignancies with $^{131}$I-Lym-1 and $^{67}$Cu-2IT-BAT-Lym-1 and opportunities for improvement. *In:* D. Goldenberg (ed.), Cancer Therapy with Radiolabeled Antibodies, pp. 217–227. Boca Raton: CRC Press, Inc., 1995.

13. DeNardo, S., DeNardo, G., O'Grady, L., Macey, D., Mills, S., Epstein, A., Peng, J., and McGahan, J. Treatment of a patient with B-cell lymphoma by I-131 Lym-1 monoclonal antibodies. Int. J. Biol. Markers, *2:* 49–53, 1987.

14. DeNardo, S., DeNardo, G., O'Grady, L., Levy, N., Mills, S., Macey, D., McGahan, J., Miller, C., and Epstein, A. Pilot studies of radioimmunotherapy of B cell lymphoma and leukemia using I-131 Lym-1 monoclonal antibody. Antib. Immunoconjug. Radiopharm., *1:* 17–33, 1988.

15. DeNardo, G., Lewis, J., DeNardo, S., and O'Grady, L. Effect of Lym-1 radioimmunoconjugate on refractory chronic lymphocytic leukemia. Cancer (Phila.), *73:* 1425–1432, 1994.

16. Lewis, J., DeNardo, G., and DeNardo, S. Radioimmunotherapy of lymphoma: a UC Davis experience. Hybridoma, *14:* 115–120, 1995.

17. DeNardo, G., Mirick, G., Kroger, L., Lamborn, K., and DeNardo, S. HAMA response after a series of injections of Lym-1 monoclonal antibody in patients with B-lymphocytic malignancies. J. Nucl. Med., *36:* 215P, 1995.

18. Epstein, A., Marder, R., Winter, J., Stathopoulos, E., Chen, F., Parker, J., and Taylor, C. Two new monoclonal antibodies, Lym-1 and Lym-2, reactive with human-B-lymphocytes and derived tumors, with immunodiagnostic and immunotherapeutic potential. Cancer Res., *47:* 830–840, 1987.

19. DeNardo, S., Peng, J., DeNardo, G., Mills, S., and Epstein, A. Immunochemical aspects of monoclonal antibodies important for radiopharmaceutical development. Int. J. Radiat. Appl. Instrum. Part B, *13:* 303–310, 1986.

20. Kukis, D., DeNardo, G., DeNardo, S., Mirick, G., Miers, L., Greiner, D., and Meares, C. Effect of the extent of chelate substitution on the immunoreactivity and biodistribution of 2IT-BAT-Lym-1 immunoconjugates. Cancer Res., *55:* 878–884, 1995.

21. Kukis, D., Diril, H., Greiner, D., DeNardo, S., DeNardo, G., Salako, Q., and Meares, C. A comparative study of copper-67 radiolabeling and kinetic stabilities of antibody-macrocycle chelate conjugates. Cancer (Phila.), *73:* 779–786, 1994.

22. DeNardo, G., DeNardo, S., Macey, D., and Macey, D. Quantitative pharmacokinetics of radiolabeled monoclonal antibodies for imaging and therapy in patients. *In:* S. Srivastava (ed.), Radiolabeled Monoclonal Antibodies for Imaging and Therapy, pp. 293–310. New York: Plenum Publishing Corp., 1988.

23. Macey, D., DeNardo, G., and DeNardo, S. A treatment planning program for radioimmunotherapy. *In:* J. Vaeth (ed.), Frontiers of Radiation Therapy and Oncology, Vol. 24, pp. 123–131. Basel: S. Karger AG, 1990.

24. Eary, J., Appelbaum, F., Durack, L., and Brown, P. Preliminary validation of the opposing view method for quantitative gamma camera imaging. Med. Phys. (New York), *16:* 382–387, 1989.

25. Thomas, S., Maxon, H., and Kereiakes, J. *In vivo* quantitation of lesion radioactivity using external counting methods. Med. Phys. (New York), *3:* 253–255, 1976.

26. Sorenson, J. Deadtime characteristics of Anger cameras. J. Nucl. Med., *16:* 284–288, 1975.

27. DeNardo, G., Mahe, M., DeNardo, S., Macey, D., Mirick, G., Erwin, W., and Groch, M. Body and blood clearance and marrow radiation dose of $^{131}$I-Lym-1 in patients with B-cell malignancies. Nucl. Med. Commun., *14:* 587–595, 1993.

28. Loevinger, R., and Berman, M. A Revised Schema for Calculating the Absorbed Dose from Biologically Distributed Radionuclides. MIRD Pamphlet No. 1. New York: Society of Nuclear Medicine, 1976.

29. Shen, S., DeNardo, G., DeNardo, S., Salako, Q., Morris, G., Banks, D., Yuan, A., and DeNardo, D. Dosimetric evaluation of $^{64}$Cu-2IT-BAT-Lym-1 in $^{67}$Cu-2IT-BAT-Lym-1 for radioimmunotherapy. J. Nucl. Med., *37:* 146–150, 1996.

30. Snyder, W., Ford, M., Warner, G., and Watson, S. "S," Absorbed Dose Per Unit Cumulated Activity for Selected Radionuclides and organs. MIRD Pamphlet No. 11. New York: Society of Nuclear Medicine, 1975.

31. Weber, D., Eckerman, K., Dillman, L., and Ryman, J. MIRD: Radionuclide Data and Decay Schemes, pp. 72–75. New York: Society of Nuclear Medicine, 1989.

32. Pretoris, H., Aswegen, A., Lotter, M., Herbst, C., Nel, M., and Otto, A. Verification of a varying threshold edge detection SPECT technique for spleen volume: a comparison with computed tomography volumes. J. Nucl. Med., *34:* 963–967, 1993.

33. DeNardo, G., Maddock, S., Sgouros, G., Scheibe, P., and DeNardo, S. Immunoadsorption: an enhancement strategy for radioimmunotherapy. J. Nucl. Med., *34:* 1020–1027, 1993.

34. DeNardo, G., Shen, S., DeNardo, S., Liao, S., Yu, S., and Macey, D. Validation of nuclear quantitation of tumor size and I-131 amount in an Alderson phantom by planar imaging. J. Nucl. Med., *33:* 925, 1992.

35. Siegel, J., Wessels, B., Waston, E., Stabin, M., Vriesendorp, H., Bradley, E., Badger, C., Brill, A., Kwok, C., Stickney, D., Eckerman, K., Fisher, D., Buchsbaum, D., and Order, S. Bone marrow dosimetry and toxicity for radioimmunotherapy. Antib. Immunoconjug. Radiopharm., *3:* 213–233, 1990.

36. Macey, D., DeNardo, S., DeNardo, G., DeNardo, D., and Shen, S. Estimation of radiation absorbed doses to the red marrow in radioimmunotherapy. Clin. J. Nucl. Med., *20:* 117–125, 1995.

37. SAS/STAT Users Guide. Version 6.08. Cary, NC: SAS Institute Inc., 1994.

38. Buyse, M., Staquet, M., and Sylvester, R. (eds.). Cancer Clinical Trials: Methods and Practice. New York: Oxford University Press, 423–452, 1984.

39. Anderson, J. Analysis of survival by tumor response. J. Clin. Oncol., *1:* 710–719, 1983.

40. Kuzel, T., Rosen, S., Zimmer, A., Silverstein, E., Spies, S., Saletan, S., Norvitch, M., Birkhofer, M., Shochat, D., LoBuglio, A., Meredith, R., Khazaeli, M., Polansky, A., Hu, E., Chen, D., Lee, K., and Watkins, K. A Phase I escalating-dose safety, dosimetry and efficacy study of radiolabeled monoclonal antibody Lym-1. Cancer Biother., *8:* 3–16, 1993.

41. Meredith, R., Khazaeli, M., Plott, G., Wheeler, R., Russel, C., Shochat, D., Norvitch, M., Saletan, S., and LoBuglio, A. Comparison of diagnostic and therapeutic doses of $^{131}$I-Lym-1 in patients with non-Hodgkin's lymphoma. Antib. Immunoconjug. Radiopharm., *6:* 1–11, 1993.

42. Czuczman, M., Straus, D., Divgi, C., Graham, M., Garin-Chesa, P., Finn, R., Myers, J., Old, L., Larson, S., and Scheinberg, D. Phase I dose-escalation trial of iodine 131-labeled monoclonal antibody OKB7 in patients with non-Hodgkin's lymphoma. J. Clin. Oncol., *11:* 2021–2029, 1993.

43. Goldenberg, D. Targeting, dosimetry, and radioimmunotherapy of B-cell lymphomas with iodine-131 labeled LL2 monoclonal antibody. J. Clin. Oncol., *11:* 548–564, 1991.

44. Kaminski, M., Zasadny, K., Francis, I., Milik, A., Ross, C., Moon, S., Crawford, S., Burgess, J., Petry, N., Butchko, G., Glenn, S., and Wahl, R. Radioimmunotherapy of B-cell lymphoma with [$^{131}$I] anti-B1 (anti-CD20) antibody. N. Engl. J. Med., *329:* 459–465, 1993.

45. Press, O. Radiolabeled-antibody therapy of B-cell lymphoma with autologous bone marrow support. N. Engl. J. Med., *329:* 1219–1224, 1993.

46. Press, O., Eary, J., Appelbaum, F., Martin, P., Nelp, W., Glenn, S., Fisher, D., Porter, B., Matthews, D., Gooley, T., and Bernstein, I. D. Phase II trial of $^{131}$I-B1 (anti-CD20) antibody therapy with autologous stem cell transplantation for relapsed B cell lymphomas. Lancet, *346:* 336–340, 1995.

47. Khazaeli, M., Conroy, R., and Lo Buglio, A. Human immune response to monoclonal antibodies. J. Immunol., *15:* 42–52, 1994.

48. Baum, R., Nieson, A., Hertel, A., Nancy, A., Hess, H., Donnerstag, B., Sykes, T., Sykes, C., Suresh, M., Noujaim, A., and Hör, G. Activating anti-idiotypic human anti-mouse antibodies for immunotherapy of ovarian carcinoma. Cancer (Phila.), *73:* 1121–1125, 1994.

49. Herlyn, D., Ross, A., and Koprowski, H. Anti-idiotype antibodies bear the internal image of a human tumor antigen. Science (Washington DC), *232:* 100–102, 1986.

50. Herlyn, D., Zaloudik, J., Somasundaram, R., Jacob, L., Benden, A., and Mastangelo, M. Anti-idiotype vaccine in colorectal cancer patients. Hybridoma, *12:* 515–520, 1993.

STIC-ILL 5/1225 #2510

**From:** Davis, Minh-Tam
**Sent:** Wednesday, September 15, 2004 3:39 PM
**To:** STIC-ILL
**Subject:** Reprint request for 09/721864

NPL ___ Adonis X
MIC ___ BioTech ___ MAIN ___
NO ___ Vol NO ___ NOS ___
Ck Cite ___ Dupl Request ___
Call # 9/15 VD

1) 07821600 PMID: 3390350
Uptake of indium-111-labeled monoclonal antibody ZME-018 as a function of tumor size in a patient with melanoma.
Macey D J; Denardo S J; Denardo G L; Goodnight J K; Unger M W
Department of Radiology, University of California Davis Medical Center, Sacramento 95817.
American journal of physiologic imaging (UNITED STATES) 1988, 3 (1) p1-6, ISSN 0885-8276 Journal Code: 8610225

2) Rapid imaging of human melanoma xenografts using an scFv fragment of the human monoclonal antibody H11 labelled with 111In.
Reilly R M; Maiti P K; Kiarash R; Prashar A K; Fast D G; Entwistle J; Dan ; Narang S A; Foote S; Kaplan H A
Division of Nuclear Medicine, Toronto General Hospital, University Health Network, ON, Canada. raymond.reilly@utoronto.ca
Nuclear medicine communications (England) May 2001, 22 (5) p587-95, ISSN 0143-3636 Journal Code: 8201017

3) Treatment-related parameters predicting efficacy of Lym-1 radioimmunotherapy in patients with B-lymphocytic malignancies.
Lamborn K R; DeNardo G L; DeNardo S J; Goldstein D S; Shen S; Larkin E C; Kroger L A
Brain Tumor Research Center, Department of Neurological Surgery, University of California San Francisco Medical Center, San Francisco, California 94143, USA.
Clinical cancer research - an official journal of the American Association for Cancer Research (UNITED STATES) Aug 1997, 3 (8) p1253-60, ISSN 1078-0432 Journal Code: 9502500

4) 4368891 PMID: 10365793
Biodistribution of filamentous phage-Fab in nude mice.
Yip Y L; Hawkins N J; Smith G; Ward R L
School of Medicine (St. Vincent's Hospital), University of NSW, Sydney, Australia.
Journal of immunological methods (NETHERLANDS) May 27 1999, 225 (1-2) p171-8, ISSN 0022-1759 Journal Code: 1305440

5) Radiolabeling, biodistribution, and dosimetry of (123)I-mAb 14C5: a new mAb for radioimmunodetection of tumor growth and metastasis in vivo.
Lahorte Christophe M M; Bacher Klaus; Burvenich Ingrid; Coene Elisabeth D ; Cuvelier Claude; De Potter Christian; Thierens Hubert; Van de Wiele Christophe; Dierckx Rudi A; Slegers Guido
Department of Radiopharmacy, Faculty of Pharmaceutical Sciences, Gent University, Gent, Belgium. christophe.lahorte@ugent.be
Journal of nuclear medicine - official publication, Society of Nuclear Medicine (United States) Jun 2004, 45 (6) p1065-73, ISSN 0161-5505 Journal Code: 0217410

Thank you
MINH TAM DAVIS
ART UNIT 1642, ROOM 3A24, MB 3C18
272-0830

| | |
|---|---|
| Article title | Rapid imaging of human melanoma xenografts using an scFv fragment of the human monoclonal antibody H11 labelled with ^1^1^1In |
| Article identifier | 014336360100089X |
| Authors | Reilly_R_M Maiti_P_K Kiarash_R Prashar_A_K Fast_D_G Entwistle_J Dan_M_D Narang_S_A Foote_S Kaplan_H_A |
| Journal title | Nuclear Medicine Communications |
| ISSN | 0143-3636 |
| Publisher | Lippincott Williams and Wilkins |
| Year of publication | 2001 |
| Volume | 22 |
| Issue | 5 |
| Supplement | 0 |
| Page range | 587-595 |
| Number of pages | 9 |
| User name | Adonis |
| Cost centre | |
| PCC | $25.00 |
| Date and time | Thursday, September 16, 2004 9:21:32 PM |

18069302
*Nuclear Medicine Communications*, 2001, **22**, 587–595

**Nuclear Medicine** *Communications*

# Rapid imaging of human melanoma xenografts using an scFv fragment of the human monoclonal antibody H11 labelled with $^{111}$In

R.M. REILLY,[1,4,*] P.K. MAITI,[2] R. KIARASH,[1] A.K. PRASHAR,[2] D.G. FAST,[2] J. ENTWISTLE,[2] M.D. DAN,[2] S.A. NARANG,[3] S. FOOTE[3] and H.A. KAPLAN[2]

[1]*Division of Nuclear Medicine, Toronto General Hospital, University Health Network, Toronto, Canada;* [2]*Viventia Biotech Inc., Winnipeg, Canada;* [3]*Institute for Biological Sciences, National Research Council of Canada, Ottawa, Canada; and* [4]*Departments of Pharmaceutical Sciences and Medical Imaging, University of Toronto, Toronto, Canada*

Received 13 October 2000, in revised form 10 November 2000 and accepted 15 November 2000

## Summary

H11 is a human IgM monoclonal antibody which recognizes a novel tumour-associated antigen expressed on melanoma, glioma, breast cancer, colon cancer, prostate cancer, lung cancer and B-cell lymphoma. In this study, a recombinant single-chain Fv (scFv) fragment of H11 labelled with $^{111}$In was investigated for tumour imaging in athymic mice implanted subcutaneously with A-375 human melanoma xenografts. H11 scFv was derivatized with diethylenetriaminepentaacetic acid (DTPA) for labelling with $^{111}$In. The immunoreactivity of DTPA-H11 scFv against A-375 cells *in vitro* ranged from 23% to 36%. $^{111}$In-DTPA-H11 scFv was rapidly eliminated from the blood and most normal tissues (except the kidneys) reaching maximum tumour/blood ratios of 12:1 at 48 h post-injection. Tumours were imaged as early as 40 min after injection. The kidneys accumulated the highest concentration of radioactivity (up to 185% injected dose/g). Tumour uptake was 1–3% injected dose/g. The whole-body radiation absorbed dose predicted for administration of 185 MBq of $^{111}$In-DTPA-H11 scFv to humans was 37 mSv. The radiation absorbed dose estimates for the kidneys, spleen and intestines were 405 mSv, 698 mSv and 412 mSv, respectively. The results of this preclinical study and a concurrent phase I trial suggest a promising role for H11 scFv for tumour imaging. (© 2001 Lippincott Williams & Wilkins)

**Keywords:** scFv, imaging, indium-111, monoclonal antibody, melanoma.

## Introduction

Radiolabelled monoclonal antibodies (mAbs) directed against tumour-associated antigens are promising radiopharmaceuticals for diagnostic imaging of human malignancies. Despite some limitations [1], the results of clinical trials of these agents over the past 10–15 years have been encouraging, particularly for imaging breast [2–4], colorectal [5–8], and ovarian cancers [9]. Recently, several mAb-based radiopharmaceuticals have been approved by regulatory authorities and introduced into clinical practice (e.g. Oncoscint® and Prostascint®, Cytogen Inc., and CEA-Scan®, Immunomedics Inc.). Intact mAbs generated by conventional murine hybridoma technology are not ideal for tumour imaging in humans [1]. First, intact forms of the mAbs are eliminated very slowly from the blood resulting in relatively low tumour/blood (T/B) ratios, particularly at early time points, which in most cases necessitates delayed imaging studies from several days up to 1 week post-injection. Second, intact mAbs exhibit poor diffusion across the vascular endothelium into the extravascular space and incomplete penetration into tumour nodules. Third, intact mAbs accumulate non-specifically in normal tissues, such as the liver and spleen, due to interaction

*Address all correspondence to Dr Raymond M. Reilly, Division of Nuclear Medicine, Toronto General Hospital, University Health Network, 585 University Avenue, Toronto, ON, Canada M5G 2C4.
e-mail: raymond.reilly@utoronto.ca

of the Fc-domain with Fc receptors in these tissues. Fourth, murine forms of the intact mAbs are immunogenic in humans and elicit an immune response (human anti-mouse antibody, HAMA) which severely restricts the ability to perform repeated imaging studies.

One strategy to overcome the limitations of intact murine mAbs for tumour imaging is to utilize fully human mAb fragments (e.g. scFv or Fab). The heavy and light chain variable regions can be isolated from the genomic DNA of a human–human hybridoma [10] or from a phage display library of human immunoglobulins [11]. The isolated $V_H$ and $V_L$ sequences can be fused to a DNA sequence encoding a flexible polypeptide linker and inserted into an appropriate expression vector for production of the human protein in bacteria or eukaryotic cells. H11® is a fully human IgM mAb produced by a human–human hybridoma which recognizes a novel tumour-associated antigen expressed on the cell surface of a large number of human cancers, including melanoma, glioma, breast cancer, colon cancer, prostate cancer, lung cancer and B-cell lymphoma [12]. H11 scFv is a recombinant scFv fragment produced in *Escherichia coli* by an expression vector encoding the $V_H$ and $V_L$ sequences of the antibody linked by a flexible polypeptide sequence (P.K. Maiti *et al.* manuscript in preparation). Our objectives in this study were to evaluate H11 scFv labelled with $^{111}$In for imaging human melanoma xenografts in athymic mice and also to predict the corresponding radiation absorbed doses in humans.

## Methods

### *Establishment of melanoma xenografts*

A-375 human melanoma cells were obtained from the American Type Culture Collection (Rockville, MD) and were cultured in DMEM supplemented with 10% fetal calf serum (Sigma, St. Louis, MO). Single cells were recovered by trypsinization with 0.25% trypsin/EDTA (Sigma) and resuspended in sterile 150 mM sodium chloride. Approximately $3–5 \times 10^6$ cells were injected subcutaneously in the hind leg of 4–6 week old female Swiss athymic (*nu/nu*) mice (Charles River Laboratories, Boston, MA). The melanoma xenografts were allowed to grow to a size of 0.3–0.6 cm in diameter for the imaging and biodistribution studies.

### *H11 scFv*

H11 (Viventia Biotech Inc.) is a fully human monoclonal antibody (mAb H11) that recognizes a tumour-associated antigen widely expressed on different types of tumours [12]. H11 scFv is a recombinant antibody fragment retaining the same specificity as the parent molecule consisting of the $V_H$ and $V_L$ sequences of H11 fused through a flexible peptide linker [$(GGGGS)_3$]. H11 scFv was expressed in *E. coli* and purified by metal affinity chromatography and was supplied by Viventia Biotech Inc. as a 7.2 mg·ml$^{-1}$ solution in phosphate buffered saline pH 7.4.

### *Derivatization of H11 scFv with DTPA and radiolabelling with $^{111}$In*

H11 scFv was derivatized with the bicyclic anhydride of diethylenetriaminepentaacetic acid (DTPA bicyclic anhydride, Sigma Chemical Co., St. Louis, MO) for radiolabelling with $^{111}$In as previously described [13]. Briefly, H11 scFv was buffer-exchanged into trace metal-free 50 mM sodium bicarbonate buffer pH 7.5 in 150 mM sodium chloride using Centricon-30 (Amicon, Beverley, MA) ultrafiltration devices. A 5-fold molar excess of DTPA bicyclic anhydride was then dispensed as a 1 mg·ml$^{-1}$ suspension in chloroform (ACS grade, Fisher Scientific Inc.) into a glass Reacti-Vial® (Pierce Chemical Co., Rockford, IL) and the chloroform was evaporated under a gentle stream of nitrogen. H11 scFv (10 mg·ml$^{-1}$ in 50 mM sodium bicarbonate buffer pH 7.5, in 150 mM sodium chloride) was added and the reaction mixture incubated for 30 min at room temperature. The conjugation efficiency (molecules DTPA/molecule scFv) was determined by trace radiolabelling of an aliquot of the reaction mixture (5 μl, 50 μg) with $^{111}$In-acetate (0.9–1.85 MBq, 25–50 μCi) and separating radiolabelled scFv from free radiolabelled DTPA by silica gel instant thin layer chromatography (ITLC-SG) developed in 100 mM sodium citrate buffer, pH 5.0. The substitution level (molecules DTPA/molecule scFv) was calculated by multiplying the conjugation efficiency by the molar ratio (DTPA bicyclic anhydride:scFv) used in the reaction (5:1). DTPA-derivatized H11 scFv was purified from excess DTPA on a Sephadex G-25 mini-column and reconcentrated to 2–5 mg·ml$^{-1}$ on a Centricon-30 device. A control, irrelevant scFv directed against blood group A (AC1001 scFv) [14] was derivatized with DTPA identically to H11 scFv.

DTPA-derivatized H11 scFv was radiolabelled with $^{111}$In to a specifc activity of approximately 1.85–3.7 MBq·μg$^{-1}$ (50–100 μCi·μg$^{-1}$) by incubation with $^{111}$In acetate for 30 min at room temperature. $^{111}$In acetate was prepared by mixing equal volumes of $^{111}$In chloride (>3700 MBq·ml$^{-1}$, MDS-Nordion, Kanata, ON) and trace metal-free 1 M sodium acetate buffer, pH 6.0. Radiolabelled H11 scFv was purified from excess $^{111}$In on a Sephadex G-25 mini-column eluted with 150 mM sodium chloride. The radiochemical purity of $^{111}$In-DTPA-H11

scFv was determined by instant thin layer chromatography (ITLC-SG) in 100 mM sodium citrate pH 5.0.

*Immunoreactivity testing*

The immunoreactivity of DTPA-derivatized H11 scFv was compared with non-derivatized H11 scFv by flow cytometry or fixed-cell ELISA using A-375 human melanoma cells as previously described [12]. Flow cytometry was conducted by incubating H11 scFv with A-375 cells for 2 h at 37°C. Binding of H11 scFv was determined by subsequent incubation of the cells with a rabbit polyclonal anti-H11 scFv secondary antibody followed by a fluorescein-conjugated anti-rabbit IgG tertiary antibody. The mean fluorescence of the cells relative to that obtained by incubation with an irrelevant control scFv (AC1001 scFv) was measured for DTPA-derivatized H11 scFv and compared with non-derivatized H11 scFv.

The fixed-cell ELISA was conducted by suspending A-375 cells in Hank's balanced salt solution containing 0.5% formalin and plating approximately $10^4$ cells onto 96-well microtitre plates (50 $\mu$l/well). The plates were centrifuged at 1500 rpm for 10 min, the supernatant was removed and the plates were air dried at 37°C overnight. The plates were then incubated with blocking buffer (phosphate buffered saline containing 1% bovine serum albumin and 0.5% Tween 20), washed, and incubated with 2.5 $\mu g \cdot ml^{-1}$ of DTPA-H11 scFv, non-derivatized H11 scFv or control AC1001 scFv. The plates were washed again and incubated with a rabbit polyclonal anti-H11 scFv secondary antibody followed by an anti-rabbit IgG-horseradish peroxidase tertiary antibody. The complex was detected by adding TMB substrate (Kirkegaard Perry Laboratories, Gaithersburg, MD) and measuring the absorbance at 450 nm in a plate reader.

*Animal imaging and biodistribution studies*

Swiss athymic (*nu/nu*) mice bearing subcutaneous (s.c.) A-375 melanoma xenografts were injected intravenously in the tail vein with 1.85–3.7 MBq (50–100 $\mu$Ci, 0.5–1 $\mu$g) of $^{111}$In-DTPA-H11 scFv. At selected times up to 72 h post-injection, groups of three to seven mice were killed by cervical dislocation and the tumour and samples of normal tissues removed to measure levels of radioactivity. Additional groups of four to five mice were injected with $^{111}$In-DTPA-AC1001 control, scFv or with $^{125}$I-human serum albumin, a blood perfusion marker. $^{125}$I-human serum albumin was purchased from Drax-Image Inc. (Dorval, PQ). Tissue samples were weighed and counted along with a standard of the injectate in a gamma counter (Packard Auto Gamma 5650, Packard Instruments, Downer's Grove, IL) using a window of 150–270 keV for $^{111}$In. The tumour and normal tissue uptake of $^{111}$In-DTPA-H11 scFv was expressed as per cent injected dose per gram of tissue (% i.d./g) and as tumour/normal tissue (T/NT) ratios. Dynamic posterior whole-body images were obtained in some mice on a Siemens ZLC-3700 gamma camera (Siemens, Knoxville, TN) fitted with a medium energy pinhole collimator and interfaced to a General Electric Star 4000i computer (General Electric, Milwaukee, WI). Images were acquired at 10 min intervals for up to 2 h post-injection of $^{111}$In-DTPA-H11 scFv using a 20% window centred over the 172 and 247 keV photopeaks of $^{111}$In. Animal studies were conducted under an approved Animal Care Protocol (# 97-007) at Toronto General Hospital and following the Canadian Council on Animal Care (CCAC) guidelines.

*Radiation dosimetry calculations*

Radiation absorbed dose estimates for administration of $^{111}$In-DTPA-H11 scFv to humans were calculated based on the biodistribution of the radiolabelled antibody in mice. The organ uptake (% i.d./g) in mice at selected times post-injection was multiplied by the organ weights (g) to obtain the total percentage of the injected dose in the organs (% i.d.). For the purposes of radiation absorbed dose calculations, an injected dose of 1 Bq and an organ biodistribution (% i.d.) in humans identical to that in mice was assumed. The area under the radioactivity versus time curve for each organ (Bq·h) in mice was determined using the trapezoidal rule [15] and the mean residence time for each organ ($\tau$) was then calculated by dividing the area under the curve (kBq·h) by the injected dose (kBq). The radiation absorbed dose estimates ($\bar{D}$) in humans were calculated using the MIRDOSE computer program [16] as $\bar{D} = \tau S$, where $S$ is the mean absorbed radiation dose to a target organ per unit cumulated radioactivity in the source organ.

*Statistical analysis*

Statistical comparisons were made using Student's $t$-test ($P < 0.05$). Tumour and normal tissue uptake and tumour/normal tissue ratios were expressed as mean $\pm$ standard error of the mean.

## Results

*Radiolabelling of H11 scFv with $^{111}$In*

Reaction of H11 scFv with a 5-fold molar excess of the bicyclic anhydride of DTPA resulted in substitution of $1.5 \pm 0.4$ molecules of DTPA/molecule H11 scFv ($n = 8$). The immunoreactivity of DTPA-H11 scFv relative to non-derivatized H11 scFv was $23 \pm 16$% by flow cytometry

and 36±18% by fixed-cell ELISA. The radiolabelling efficiency of H11 scFv with $^{111}$In ranged from 70% to 95% but after purification, the final radiochemical purity was >95% as determined by ITLC-SG in 100 mM sodium citrate pH 5.0.

*Biodistribution and tumour imaging studies with $^{111}$In-DTPA-H11 scFv*

The tumour and normal tissue uptake of $^{111}$In-DTPA-H11 scFv and tumour/normal tissue (T/NT) ratios at selected times post-injection are shown in Fig. 1. The level of radioactivity of $^{111}$In-DTPA-H11 scFv in the blood decreased rapidly from 4.4±0.9% i.d./g at 3 h post-injection to 0.14±0.01% i.d./g at 72 h. The concentration of $^{111}$In-DTPA-AC1001 scFv (irrelevant control scFv) in the blood at 72 h post-injection was 0.19±0.01% i.d./g. Tumour uptake of $^{111}$In-DTPA-H11 scFv increased from 1.1±0.3% i.d./g at 3 h to 2.7±0.6% i.d./g at 48 h, then decreased to 1.2±0.2% i.d./g at 72 h. The tumour/blood (T/B) ratio (Fig. 2) increased from 0.3±0.1 at 3 h, to 2.9±0.9 at 24 h, reached a maximum of 12.0±3.4 at 48 h post-injection, then decreased to 8.8±1.4 at 72 h post-injection. The tumour uptake of In-DTPA-AC1001 at 72 h post-injection was 1.2±0.3% i.d./g and was not significantly different from that of $^{111}$In-DTPA-H11 scFv. The T/B ratio for $^{111}$In-DTPA-AC1001 scFv (6.2±1.4) was also not significantly different ($P$=0.24) to that for $^{111}$In-DTPA-H11 scFv (8.8±1.4) at 72 h post-injection. The T/B ratio for $^{125}$I-human serum albumin (a tumour perfusion marker) at 48 h post-injection (1.1±0.6) was significantly lower ($P$=0.04) to that for $^{111}$In-DTPA-H11 (12.0±3.4). There was a suggestion of a lower absolute tumour uptake for $^{125}$I-human serum albumin (0.9±0.5% i.d./g) compared to $^{111}$In-DTPA-H11 scFv (2.7±0.6% i.d./g) at 48 h post-injection, but the difference did not reach statistical significance ($P$=0.08).

Among normal tissues, the kidneys accumulated the highest concentration of $^{111}$In radioactivity (up to 185% i.d./g at 16 h), but renal radioactivity decreased more than 6-fold to 30–35% i.d./g at 48–72 h post-injection (Fig. 1). The concentration of radioactivity in the liver and spleen was relatively low, reaching maximum values of 4.5±0.8% i.d./g and 3.4±0.4% i.d./g, respectively, at 16 h post-injection. Tumour/normal tissue (T/NT) ratios at 48 h post-injection exceeded 2:1 for blood, heart, lungs, stomach and intestines, were approximately 1.5:1 for the liver and spleen, but were much less than 1:1 for the kidneys (due to high renal uptake of radioactivity) (Fig. 2). A dynamic imaging study (Fig. 3) in athymic mice with subcutaneous A-375 melanoma xenografts clearly demonstrated tumour uptake of radioactivity as early as 40 min post-injection of $^{111}$In-DTPA-H11 scFv. Tumours were also visualized at 24 h post-injection (not shown). The kidneys were the predominant normal tissue visualized on the images. Lower amounts of radioactivity were observed in the heart (blood pool), liver and bladder (due to urinary excretion).

*Radiation absorbed dose calculations*

Radiation absorbed dose estimates predicted for the administration of $^{111}$In-DTPA-H11 scFv to humans are shown in Table 1. The highest radiation absorbed doses

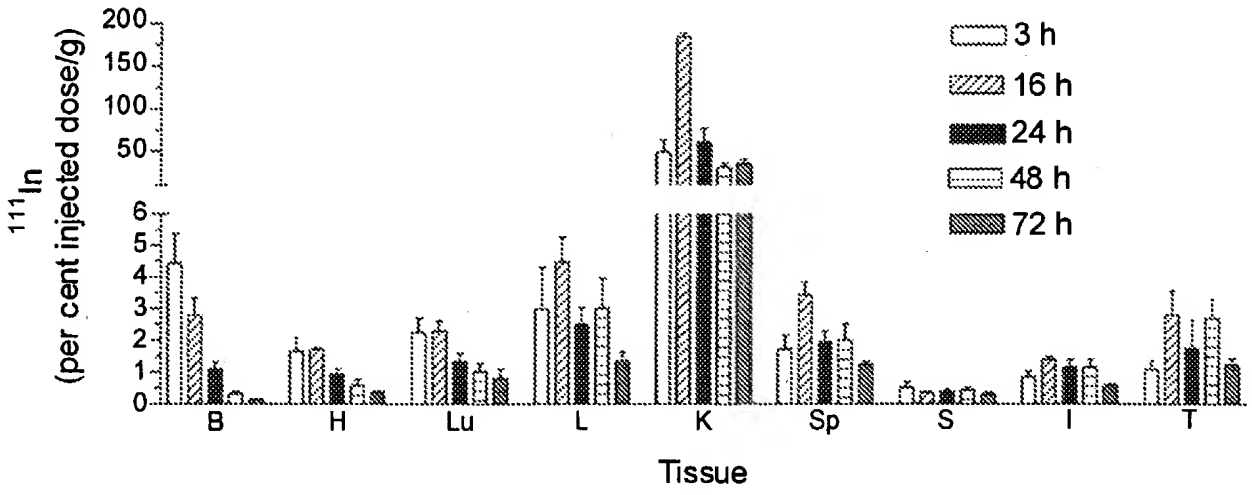


Fig. 1. Tumour and normal tissue localization (per cent injected dose/g) of $^{111}$In-DTPA-H11 scFv at selected times post-injection in athymic mice bearing subcutaneous A-375 human melanoma xenografts. Tissues shown are blood (B), heart (H), lungs (Lu), liver (L), kidneys (K), spleen (Sp), stomach (S), intestines (I) and tumour (T).

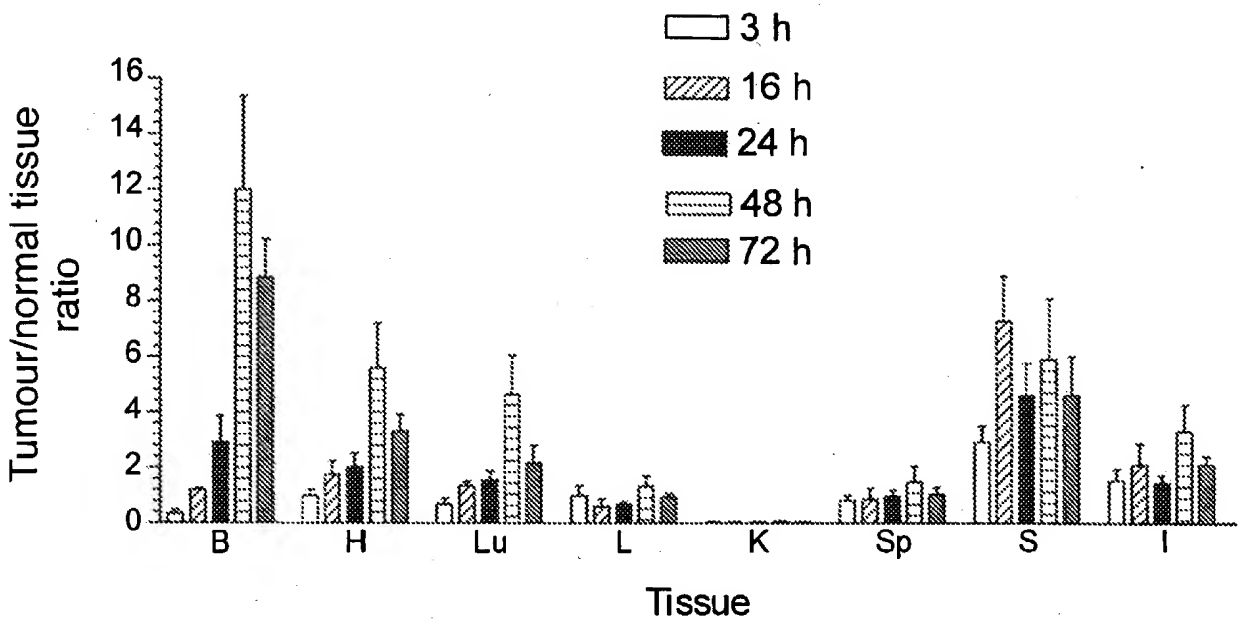


**Fig. 2.** Tumour/normal tissue ratios for $^{111}$In-DTPA-H11 scFv at selected times post-injection in athymic mice bearing subcutaneous A-375 human melanoma xenografts. Tissues shown are blood (B), heart (H), lungs (Lu), liver (L), kidneys (K), spleen (Sp), stomach (S) and intestines (I).

would be received by the kidneys, spleen and intestines. Assuming an injected dose of 185 MBq of $^{111}$In-DTPA-H11 scFv in humans, the radiation absorbed dose to the whole body would be approximately 37 mSv. The radiation absorbed dose to the kidneys, spleen and intestines from $^{111}$In-DTPA-H11 scFv would be 405 mSv, 698 mSv and 412 mSv, respectively.

## Discussion

MAb fragments (e.g. Fab' and scFv) are advantageous for tumour imaging because they are rapidly eliminated from the blood and normal tissues, exhibit low non-specific uptake by the liver, penetrate deeply into tumour nodules and have low immunogenicity in humans [1]. In this study, the tumour-imaging properties and radiation dosimetry of a recombinant scFv fragment H11 labelled with $^{111}$In were evaluated in athymic mice implanted with A-375 human melanoma xenografts. H11 recognizes a novel tumour-associated antigen that is expressed on the cell surface of several human cancers including melanoma, glioma, breast cancer, colon cancer, prostate cancer, lung cancer and B-cell lymphoma [12]. $^{111}$In-H11 scFv exhibited rapid tumour uptake and was quickly eliminated from the blood and most normal tissues (except the kidneys) allowing successful tumour imaging as early as 40 min after injection.

Flow cytometry and fixed-cell ELISA testing of H11 scFv following derivatization with DTPA demonstrated decreased immunoreactivity of the antibody *in vitro* (immunoreactivity of 23–36% relative to unconjugated H11 scFv). Decreased immunoreactivity of mAbs resulting from derivatization with the bicyclic anhydride of DTPA is well recognized [13, 17]. This can be particularly problematic for antibody fragments such as Fab and scFv, since DTPA groups may be inadvertently introduced near complementarity determining regions (CDRs). One possible means of addressing this issue may be to engineer a radiometal binding site directly into the scFv protein. For example, Pietersz *et al.* [18] incorporated the gene for metallothionein into an expression vector for an anti-CEA scFv to produce a recombinant scFv which contained an internal radiometal binding site for direct labelling with $^{99}$Tc$^{m}$.

The similar levels of tumour accumulation observed for H11 scFv and the AC1001 non-specific control scFv could be due to the low immunoreactivity of H11 scFv following derivatization with DTPA, but may also be due to other factors. Tumour uptake of radiolabelled antibodies is controlled by the rate of diffusion of the antibodies across the tumour vascular endothelium, their rate of elimination from the blood, extent of sequestration by normal tissues, and specific binding to tumour-associated antigens on cancer cells [1]. The relative contribution of each of these processes to tumour

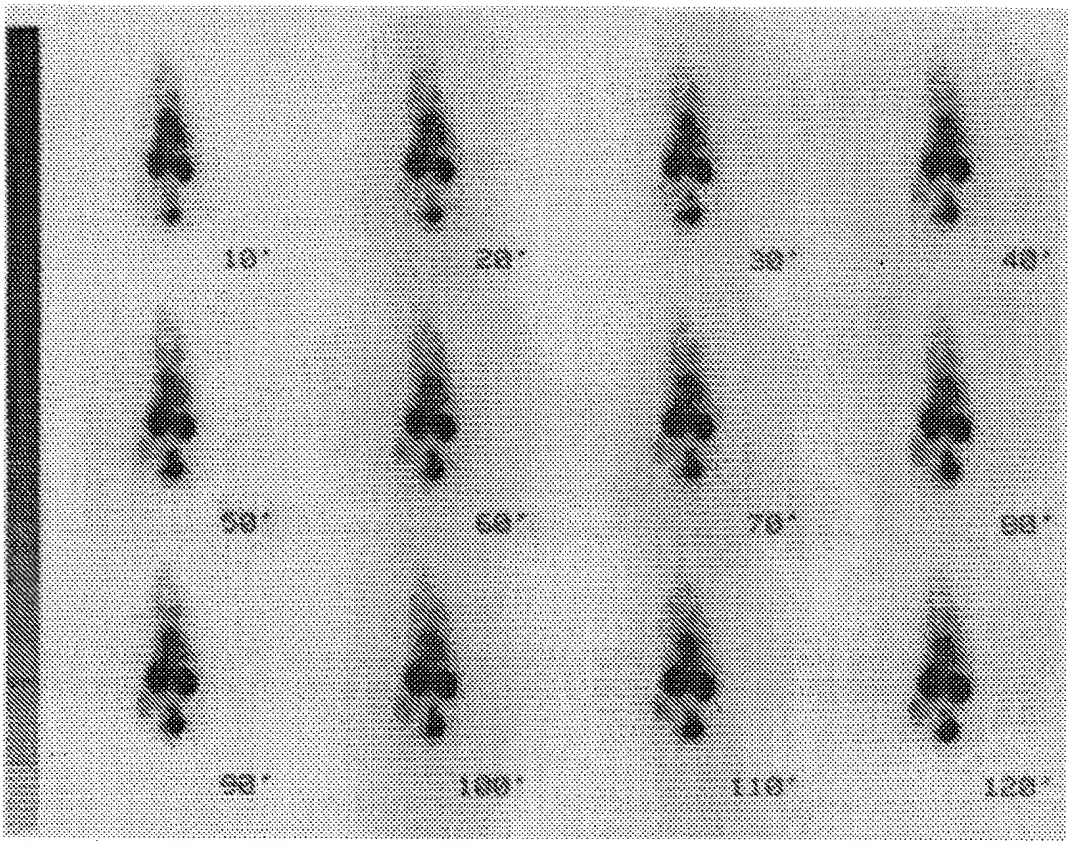

Fig. 3. Dynamic posterior whole-body images at 10 min intervals in an athymic mouse with a subcutaneous A-375 melanoma xenograft on the left hind leg administered $^{111}$In-DTPA-H11 scFv. The tumour was clearly visualized as early as 40 min after injection. Normal tissues also visualized on the images include the heart, liver, kidneys and urinary bladder.

**Table 1.** Radiation absorbed dose estimates* in humans from administration of $^{111}$In-DTPA-H11 scFv

| *Organ* | *Radiation absorbed dose† ($mSv \cdot Bq \times 10^{-7}$)* |
|---|---|
| Heart | 15.76 |
| Lungs | 6.32 |
| Liver | 6.27 |
| Kidneys | 21.92 |
| Spleen | 37.73 |
| Stomach | 14.57 |
| Intestine | 22.30 |
| Whole body | 2.00 |

*Radiation absorbed doses estimates in humans were based on the biodistribution of radiolabelled H11 scFv in athymic mice implanted with subcutaneous A375 melanoma xenografts. †Calculated using the MIRDose computer program.

localization is not known. Antigen-binding is recognized to be relatively weak for scFvs compared to intact mAbs due to their lower affinity and avidity (due to monovalency for antigen binding). Adams *et al.* [19] recently showed a direct relationship between the tumour uptake of $^{125}$I-labelled scFvs directed against the HER2/neu growth factor receptor in mice implanted with SK-OV-3 ovarian cancer xenografts and *in vitro* binding affinity. The tumour uptake ranged from as low as 0.2% i.d./g for C6G98A scFv ($K_d = 3.2 \times 10^{-7}$ M), to 0.8% i.d./g for C6.5 scFv ($K_d = 1.6 \times 10^{-8}$ M), to as high as 1.4% i.d./g for C6ML3-9 scFv ($K_d = 1 \times 10^{-9}$ M). Similar to our results, the tumour uptake of C6G98A scFv (which exhibited the lowest antigen binding affinity) was not significantly different from that of an irrelevant anti-digoxin control scFv (0.18% i.d./g), despite demonstration of specific antigen binding *in vitro*. T/B ratios at 24 h post-injection were slightly higher for C6G98 scFv (3.5:1) than for the irrelevant scFv (2.6:1).

The affinity of H11 scFv for its antigen may affect tumour localization but factors such as the diffusion rate into the tumour, elimination rate from the blood and

uptake by normal tissues may also play a prominent role. Nevertheless, the observation that the T/B ratios increased over time (Fig. 2) and the demonstration of specific binding to A-375 melanoma cells *in vitro* (by flow cytometry and fixed cell ELISA) suggest that antigen binding to tumour cells occurs *in vivo*. The tumour uptake of H11 scFv does not appear to be due to increased tumour blood flow, since the T/B ratio for $^{111}$In-DTPA-H11 scFv at 48 h post-injection (12:1) was significantly higher than that for $^{125}$I-human serum albumin (approximately 1:1), a marker of tumour blood perfusion. Nevertheless, improvements in the specific tumour uptake of H11 scFv could possibly be achieved by modifications to the radiolabelling method as previously discussed or by increasing its avidity through cross-linking of scFv molecules through one of the constant domains of human IgG (e.g. $C_H3$, 'minibody') [20] or through utilization of a dimeric form of the antibody fragment [21]. For example, Hu *et al.* [20] showed that the tumour uptake of T84.66 anti-CEA scFv minibody was increased at least 7-fold compared to monomeric scFv in athymic mice with LS174T human colon cancer xenografts. Pavlinkova *et al.* [21] recently observed that the tumour uptake of dimeric CC49 scFv directed against the TAG-72 antigen was improved more than 3-fold in mice with LS174T tumours compared to an earlier study [22] using monomeric CC49 scFv.

The radiation absorbed dose estimates for administration of 185 MBq (5 mCi) of $^{111}$In-DTPA-H11 scFv to humans suggest that the whole-body dose (Table 1) would be approximately 37 mSv ($2 \times 10^{-7}$ mSv·Bq$^{-1}$). The whole-body radiation absorbed dose is just slightly higher than that associated with common nuclear medicine procedures such as tumour imaging with $^{111}$In-satumomab pentetide (Oncoscint®, $1.5 \times 10^{-7}$ mSv·Bq$^{-1}$) [23] or $^{111}$In-pentetreotide (Octreoscan®, $1.2 \times 10^{-7}$ mSv·Bq$^{-1}$) [24]. The radiation absorbed dose to the kidneys predicted for administration of $^{111}$In-DTPA-H11 scFv to humans ($2.2 \times 10^{-6}$ mSv·Bq$^{-1}$) is higher than that for $^{111}$In-pentetreotide or $^{111}$In-satumomab pentetide ($0.5 \times 10^{-6}$ mSv·Bq$^{-1}$) [23, 24]. Preliminary results recently reported from a phase I clinical trial of $^{111}$In-DTPA-H11 scFv for imaging non-Hodgkin's lymphoma estimated the whole-body radiation dose in humans as $5 \times 10^{-7}$ mSv·Bq$^{-1}$, and the radiation absorbed dose to the kidneys as $9 \times 10^{-6}$ mSv·Bq$^{-1}$ [25].

The kidneys accumulated the highest amounts of $^{111}$In-DTPA-H11 scFv. High renal uptake of radioactivity has been previously reported for scFv fragments, [26, 27] particularly when conjugated to radiometals [28]. Kidney uptake is hypothesized to be due to filtration of the protein, followed by non-specific charge interactions with renal tubular cells [29]. Positively charged residues on the antibody (e.g. lysine amino acids) are thought to interact with the negatively charged cell membrane of renal tubular cells. At physiological pH, the ε-amino group on lysine residues would be protonated, which may promote charge interactions with renal tubular cells. Renal uptake could potentially be reduced through pre-treatment with lysine solutions to competitively inhibit the interaction of the lysine residues on the scFv with renal tubular cells [26, 29]. Preliminary studies in animals (unpublished results) suggest that the renal uptake of $^{111}$In-DTPA-H11 scFv can be reduced approximately 3- to 4-fold using this strategy. Another approach to reduce renal uptake may be to delete non-essential lysine residues by site-directed mutagenesis [30].

The liver uptake for H11 scFv was relatively low (3–5% i.d./g, Fig. 1) likely due to the absence of the Fc domain, which is thought to mediate liver uptake of antibodies through binding to Fc receptors on hepatocytes. The low liver uptake could be an advantage for the application of H11 scFv for imaging liver metastases, currently a difficult problem for intact radiolabelled anti-tumour mAbs [1]. Assuming an administered dose of 185 MBq (5 mCi) of $^{111}$In-DTPA-H11 scFv and a tumour accumulation in humans of 0.01% i.d./g [1], approximately 18.5 kBq (0.5 μCi) of radioactivity would be delivered to a 1 g tumour. We previously demonstrated in a phantom study [31] that a minimum tumour uptake of 11.1 kBq (0.3 μCi) of $^{111}$In is required for tumour detection under ideal circumstances. Therefore, we anticipate that the minimum size of tumour detectable in humans using $^{111}$In-DTPA-H11 scFv will be 0.5 g (approximately 1 cm in diameter). Our phantom study also demonstrated that a minimum T/NT ratio of 2:1 is required for tumour detection. Based on the results of this preclinical study of $^{111}$In-DTPA-H11 scFv, we anticipate that the minimum T/NT ratio in humans would be exceeded for most tissues except the kidneys ($<<$1:1) and possibly the liver and spleen (1.5:1).

The clinical utility of H11 scFv for tumour imaging was recently demonstrated in a pilot phase I trial in five patients with non-Hodgkin's lymphoma in which $^{111}$In-DTPA-H11 scFv successfully imaged known tumour sites in 4/5 cases [25]. H11 scFv conjugated to the fluorochrome Cy5 has also recently been successfully tested for immunofluoresence imaging of A-375 melanoma xenografts hosted in athymic mice [32]. Using a $^{123}$I-labelled MFE-23 anti-CEA scFv, Begent *et al.* [33] demonstrated successful tumour imaging in 10 patients with CEA-producing tumours. The results of our preclinical testing and the early phase I clinical results with H11 scFv, as well as those reported by Begent *et al.* [33] for $^{123}$I-MFE-23 scFv, suggest a promising role for anti-tumour scFvs in cancer imaging in the future.

## Conclusions

A recombinant scFv fragment of the fully human multi-carcinomic mAb H11 radiolabelled with $^{111}$In localized rapidly in subcutaneous A-375 melanoma xenografts in athymic mice and was eliminated quickly from the blood and most normal tissues (except the kidneys), allowing successful tumour imaging as early as 40 min after injection. The radiation absorbed doses predicted for radiolabelled H11 scFv in humans were similar to those for common nuclear medicine procedures. The results of the currently described preclinical study, and preliminary results from a concurrent pilot phase I trial in patients with non-Hodgkin's lymphoma suggest that H11 scFv is a promising tumour imaging agent in humans, although modifications to increase its avidity and affinity and improvements in the radiolabelling method could enhance the specificity of tumour targeting.

## Acknowledgements

The authors would like to acknowledge the expert technical assistance with the animal imaging studies provided by Wendy Denovan and Gina Capone-Civichino in the Division of Nuclear Medicine at Toronto General Hospital, University Health Network. This study was financially supported by a grant from Viventia Biotech Inc. and by a grant from the National Research Council of Canada, Industrial Research Assistance Program.

## References

1. Reilly RM, Sandhu J, Alvarez-Diez T, *et al.* Problems of delivery of monoclonal antibodies: Pharmaceutical and pharmacokinetic solutions. *Clin Pharmacokinet* 1995; **28:** 126–142.
2. Goldenberg DM, Nabi HA. Breast cancer imaging with radiolabeled antibodies. *Semin Nucl Med* 1999; **24:** 41–48.
3. Dessureault S, Koven I, Reilly RM, *et al.* Pre-operative assessment of axillary lymph node status in patients with breast adenocarcinoma using intravenous $^{99m}$technetium mAb-170H.82 (Tru-Scint AD$^{TM}$). *Breast Cancer Res and Treatment* 1997; **45:** 29–37.
4. Breitz H, Tyler A, Bjorn MJ, Lesley T, Weiden PL. Clinical experience with Tc-99m nofetumomab merpentan (Verluma) radioimmunoscintigraphy. *Clin Nucl Med* 1997; **22:** 615–620.
5. Abdel-Nabi HH, Doerr RJ. Multicenter clinical trials of monoclonal antibody B72.3-GYK- DTPA-$^{111}$In ($^{111}$In-CYT-103, Oncoscint CR103) in patients with colorectal carcinoma. In: Maguire RT, Van Nostrand D, eds. Diagnosis of colorectal and ovarian carcinoma. Application of immunoscintigraphic technology. New York: Dekker, 1992: 73–88.
6. Muxi A, Sola M, Bassa P, *et al* Radioimmunoscintigraphy of colorectal carcinoma with a $^{99}$Tc$^{m}$-labelled anti-CEA monoclonal antibody (BW431/26). *Nucl Med Commun* 1992; **13:** 261–270.
7. Gallinger S, Reilly RM, Kirsh J, *et al.* Comparative dual label study of first and second generation antitumor-associated glycoprotein-72 monoclonal antibodies in colorectal cancer patients. *Cancer Res* 1993; **53:** 271–278.
8. Smith AJ, Reilly RM, Kirsh JC, *et al.* Tumor imaging and pharmacokinetics of $^{99m}$Tc labelled monoclonal antibody 170H.82 in patients with colorectal cancer. *Antibody Immunocon Radiopharm* 1995; **8:** 203–214.
9. Gallup DG. Multicenter clinical trial of $^{111}$In-CYT-103 in patients with ovarian cancer. In: Maguire RT, Van Nostrand D, eds. Diagnosis of colorectal and ovarian carcinoma: Application of immunoscintigraphic technology. New York: Dekker, 1992.
10. Shirahata S, Katakura Y, Teruya K. Cell hybridization, hybridomas and human hybridomas. *Methods Cell Biol* 1998; **57:** 111–145.
11. Verhaar MJ, Chester KA, Keep P, *et al.* A single chain Fv derived from a filamentous phage library has distinct tumour targeting advantages over one derived from hybridoma. *Int J Cancer* 1995; **61:** 497–501.
12. Maiti PK, Dan MD, Prashar A, *et al.* Development and characterization of pancarcinoma specific human monoclonal antibody H11 (H11). *Biotech Internat* 1997; **1:** 85–93.
13. Reilly RM, Marks A, Law J, Lee NS, Houle S. *In-vitro* stability of EDTA and DTPA immunoconjugates of monoclonal antibody 2G3 labelled with In-111. *Appl Radiat Isot* 1992; (in press).
14. Patenaude SI, MacKenzie CR, Bilous D. Production, crystallization and diffraction to atomic resolution of an antibody Fv specific for the blood-group A oligosaccharide antigen. *Acta Crystallographica* 1998; **D54:** 1456–1459.
15. Gibaldi M, Perrier D, eds. Pharmacokinetics. 2nd edn. Appendix D. Estimation of areas. New York: Dekker, 1982: 445–449.
16. Watson E, Stabin M, Bolch W. MIRDOSE Ver. 3.0 (computer program). Oak Ridge, TN: Oak Ridge Associated Universities, 1994.
17. Paik CH, Ebbert MA, Murphy PR, *et al.* Factors influencing DTPA conjugation with antibodies by clyclic DTPA anhydride. *J Nucl Med* 1983; **24:** 1158–1163.
18. Pietersz GA, Patrick MR, Chester KA. Preclinical characterization and *in vivo* imaging studies of an engineered recombinant technetium-99m-labeled metallothionein-containing anti-carcinoembryonic antigen single-chain antibody. *J Nucl Med* 1998; **39:** 47–56.
19. Adams GP, Schier R, Marshall K, *et al.* Increased affinity leads to improved selective tumour delivery of single-chain Fv antibodies. *Cancer Res* 1998; **58:** 485–490.
20. Hu S, Shively L, Raubitschek A, *et al.* Minibody: A novel engineered anti-carcinoembryonic antigen antibody fragment (single-chain Fv-$C_H$3) which exhibits rapid high-level targeting of xenografts. *Cancer Res* 1996; **56:** 3055–3061.

21. Pavlinkova G, Booth BJM, Batra SK, Colcher D. Radioimmunotherapy of human colon cancer xenografts using a dimeric single-chain Fv antibody construct. *Clin Cancer Res* 1999; **5**: 2613–2619.
22. Milenic DE, Yokota T, Filpula DR, *et al.* Construction, binding properties, metabolism, and tumor targeting of a single-chain Fv derived from the pancarcinoma monoclonal antibody CC49. *Cancer Res* 1991; **51**: 6363–6371.
23. OncoScint® CR/OV Kit (satumomab pendetide) for the preparation of indium In 111 satumomab pendetide. Princeton, NJ: Cytogen, 1996.
24. Octreoscan Kit for the preparation of indium-111 pentetreotide. St Louis, MO: Mallinckrodt Medical Inc., 1995.
25. Percheson PB, Connors JM, Dan MD, *et al.* A phase I clinical study of $^{111}$indium-labeled H11 scFv, a recombinant human monoclonal antibody fragment, in patients with non-Hodgkin's lymphoma. *Clin Cancer Res* 1999; **5**: 3749s.–
26. Kobayashi H, Yoo, TM, Kim IS, *et al.* L-lysine effectively blocks renal uptake of $^{125}$I- or $^{99m}$Tc-labeled anti-Tac disulfide-stabilized Fv fragment. *Cancer Res* 1996; **56**: 3788–3795.
27. Webber KO, Kreitman RJ, Pastan I. Rapid and specific uptake of anti-Tac disulfide-stabilized Fv by interleukin-2 receptor-bearing tumors. *Cancer Res* 1995; **55**: 318–323.
28. Schott ME, Milenic DE, Yokota T, *et al.* Differential metabolic patterns of iodinated versus radiometal chelated anticarcinoma single-chain Fv molecules. *Cancer Res* 1992; **52**: 6413–6417.
29. Behr TM, Goldenberg DM, Becker W. Reducing the renal uptake of radiolabeled antibody fragments and peptides for diagnosis and therapy: present status, future prospects and limitations. *Eur J Nucl Med* 1998; **25**: 201–212.
30. Colcher D, Pavlinkova, G, Beresford G, Booth BJ, Choudhury A, Batra SK. Pharmacokinetics and biodistribution of genetically-engineered antibodies. *Q J Nucl Med* 1998; **42**: 225–241.
31. Reilly RM, Gariépy J. Factors influencing the sensitivity of tumor imaging with a receptor-binding radiopharmaceutical. *J Nucl Med* 1998; **39**: 1036–1043.
32. Ramjiawan B, Maiti P, Aftanas A, *et al.* Non-invasive localization of tumors by immunofluorescence imaging using a single chain Fv fragment of a human monoclonal antibody with broad cancer specificity. *Cancer* 2000; **89**: 1134–1144.
33. Begent RH, Verhaar MJ, Chester KA. Clinical evidence of efficient tumor targeting based on single-chain Fv antibody selected from a combinatorial library. *Nature Medicine* 1996; **2**: 979–984.

STIC-ILL

**From:** Davis, Minh-Tam
**Sent:** Wednesday, September 15, 2004 3:39 PM
**To:** STIC-ILL
**Subject:** Reprint request for 09/721864



1) 07821600 PMID: 3390350
Uptake of indium-111-labeled monoclonal antibody ZME-018 as a function of tumor size in a patient with melanoma.
Macey D J; Denardo S J; Denardo G L; Goodnight J K; Unger M W
Department of Radiology, University of California Davis Medical Center, Sacramento 95817.
American journal of physiologic imaging (UNITED STATES) 1988, 3 (1) p1-6, ISSN 0885-8276 Journal Code: 8610225

2) Rapid imaging of human melanoma xenografts using an scFv fragment of the human monoclonal antibody H11 labelled with 111In.
Reilly R M; Maiti P K; Kiarash R; Prashar A K; Fast D G; Entwistle J; Dan ; Narang S A; Foote S; Kaplan H A
Division of Nuclear Medicine, Toronto General Hospital, University Health Network, ON, Canada. raymond.reilly@utoronto.ca
Nuclear medicine communications (England) May 2001, 22 (5) p587-95, ISSN 0143-3636 Journal Code: 8201017

3) Treatment-related parameters predicting efficacy of Lym-1 radioimmunotherapy in patients with B-lymphocytic malignancies.
Lamborn K R; DeNardo G L; DeNardo S J; Goldstein D S; Shen S; Larkin E C; Kroger L A
Brain Tumor Research Center, Department of Neurological Surgery, University of California San Francisco Medical Center, San Francisco, California 94143, USA.
Clinical cancer research - an official journal of the American Association for Cancer Research (UNITED STATES) Aug 1997, 3 (8) p1253-60, ISSN 1078-0432 Journal Code: 9502500

4) 4368891 PMID: 10365793
Biodistribution of filamentous phage-Fab in nude mice.
Yip Y L; Hawkins N J; Smith G; Ward R L
School of Medicine (St. Vincent's Hospital), University of NSW, Sydney, Australia.
Journal of immunological methods (NETHERLANDS) May 27 1999, 225 (1-2) p171-8, ISSN 0022-1759 Journal Code: 1305440

5) Radiolabeling, biodistribution, and dosimetry of (123)I-mAb 14C5: a new mAb for radioimmunodetection of tumor growth and metastasis in vivo.
Lahorte Christophe M M; Bacher Klaus; Burvenich Ingrid; Coene Elisabeth D ; Cuvelier Claude; De Potter Christian; Thierens Hubert; Van de Wiele Christophe; Dierckx Rudi A; Slegers Guido
Department of Radiopharmacy, Faculty of Pharmaceutical Sciences, Gent University, Gent, Belgium. christophe.lahorte@ugent.be
Journal of nuclear medicine - official publication, Society of Nuclear Medicine (United States) Jun 2004, 45 (6) p1065-73, ISSN 0161-5505 Journal Code: 0217410

Thank you
MINH TAM DAVIS
ART UNIT 1642, ROOM 3A24, MB 3C18
272-0830

# Radiolabeling, Biodistribution, and Dosimetry of $^{123}$I-mAb 14C5: A New mAb for Radioimmunodetection of Tumor Growth and Metastasis In Vivo

Christophe M.M. Lahorte, MSc[1]; Klaus Bacher, MSc[2]; Ingrid Burvenich, MSc[1]; Elisabeth D. Coene, PhD[3]; Claude Cuvelier, MD, PhD[3]; Christian De Potter, MD, PhD[1]; Hubert Thierens, PhD[2]; Christophe Van de Wiele, MD, PhD[4]; Rudi A. Dierckx, MD, PhD[4]; and Guido Slegers, PhD[1]

*[1]Department of Radiopharmacy, Faculty of Pharmaceutical Sciences, Gent University, Gent, Belgium; [2]Department of Medical Physics and Radiation Protection, Gent University, Gent, Belgium; [3]Department of Pathology, N. Goormaghtigh Institute, Gent University, Gent, Belgium; and [4]Department of Nuclear Medicine, Gent University Hospital, Gent, Belgium.*

This study reports on the in vitro evaluation, biodistribution, and dosimetry of $^{123}$I-labeled monoclonal antibody (mAb) 14C5, a new antibody-based agent proposed for radioimmunodetection of tumor growth and metastasis in vivo. **Methods:** $^{123}$I-mAb 14C5 was prepared by direct iodination and tested for stability in vitro. Binding assays were performed on human SK-BR-3 and HeLa carcinoma cells to investigate the antigen expression, antibody affinity, and kinetics of tracer binding. For the biodistribution and dosimetry study, 3- to 4-wk-old NMRI mice were injected intravenously with $^{123}$I-mAb 14C5 (148.0 ± 7.4 kBq per mouse) and killed at preset time intervals. Organs, blood, urine, and feces were counted for radioactivity uptake, and the data were expressed as the percentage injected dose per gram tissue (%ID/g tissue) or %ID. The MIRDOSE3.0 program was applied to extrapolate the estimated absorbed radiation doses for various organs to the human reference adult. **Results:** $^{123}$I-mAb 14C5 was obtained in radiochemical yields of 85.0% ± 2.5% and radiochemical purities were >97%. The iodinated antibody demonstrated good in vitro stability with 93.6% ± 0.1% of $^{123}$I-mAb 14C5 remaining intact at 24 h after radiolabeling. $^{123}$I-mAb 14C5 bound to SK-BR-3 cells (dissociation constant [$K_d$] ≈ 0.85 ± 0.17 nmol/L) and HeLa cells ($K_d$ ≈ 1.71 ± 0.17 nmol/L) with nanomolar affinity and high specificity, whereas both cell types exhibited a high CA14C5 antigen expression (maximum number of binding sites [$B_{max}$] = 40.6 ± 5.2 and 57.1 ± 9.6 pmol/L, respectively). In mice, $^{123}$I-mAb 14C5 accumulated primarily in lungs (20.4 %ID/g), liver (15.1 %ID/g), and kidneys (11.1 %ID/g) within 5 min after injection. A delayed uptake was observed in stomach (12.8 %ID/g) and urinary bladder (8.7 %ID/g) at 3 and 6 h, respectively, after injection. Radioactivity clearance was predominantly urinary, with 44.9 + 4.5 %ID excreted during the initial 48 h after administration (cumulative amount). The highest absorbed radiation doses determined for the human reference adult were received by the urinary bladder wall (0.1200–0.1210 mGy/MBq), liver (0.0137–0.0274 mGy/MBq), uterus (0.0196–0.0207 mGy/MBq), and lower large intestine wall (0.0139–0.0258 mGy/MBq). The average effective dose resulting from a single $^{123}$I-mAb 14C5 injection was estimated to be 0.017–0.022 mSv/MBq. **Conclusion:** $^{123}$I-mAb 14C5 shows good in vitro biologic activity and favorable biodistribution properties for imaging carcinomas of different origin and provides an acceptable radiation dose to the patient.

**Key Words:** monoclonal antibody 14C5; cell substrate adhesion; metastasis; extracellular matrix; radioimmunodetection

**J Nucl Med 2004; 45:1065–1073**

The extracellular matrix (ECM) consists of a complex network of macromolecules, such as collagens, glycoproteins, and proteoglycans, which surrounds the connective tissue cells and is mainly being secreted by fibroblasts or other members of the fibroblast family, such as chondroblasts and osteoblasts (*1,2*). Apart from intercellular adhesion (i.e., cell-to-cell adhesion), the organization of cells within connective tissue is based on adhesion of these cells to ECM components (i.e., cell substrate adhesion) (*3*). Subsequently, cell substrate adhesion molecules are considered as essential regulators of cell migration, differentiation, and tissue integrity. They play a role in inflammation, but they also participate in the process of invasion and metastasis of malignant cells in the host tissue (*4–6*). In fact, cell substrate adhesion is a prerequisite for tumor invasion in normal mesenchymal tissue. Invasive tumor cells adhere to the ECM components, such as type IV collagen, laminin, and chondroitin and heparan sulfate proteoglycans, and are guided by them during their permeation through the basal lamina and underlying interstitial stroma of the connective tissue (*7,8*). Several ECM adhesion molecules and their protein receptors have been studied extensively for their

Received Sep. 8, 2003; revision accepted Jan. 15, 2004.
For correspondence contact: Christophe M.M. Lahorte, MSc, Department of Radiopharmacy, Faculty of Pharmaceutical Sciences, Gent University, Harelbekestraat 72, B-9000 Gent, Belgium.
E-mail: christophe.lahorte@ugent.be

involvement in tumor invasion and metastasis, including the integrins, lectins, selectins, and cadherins (*9–12*).

In search of new antibody therapeutics for inhibition of metastatic breast cancer, De Potter et al. (*13,14*) developed several mouse monoclonal antibodies (mAbs) against epitopes on the extracellular membrane of SK-BR-3 human breast cancer cells. One of these mAbs is the IgG1 mAb 14C5, which recognizes an extracellular plasma membrane antigen expressed on SK-BR-3 and MCF-7 human breast cancer cells (*13,14*). The antibody is capable of reversibly inhibiting the adhesion of SK-BR-3 cells on both culture-treated plastic and on pronectin-, fibronectin-, osteopontin-, and vibronectin-precoated culture plates. Furthermore, mAb 14C5 has been shown to prevent invasion and, subsequently, metastasis of SK-BR-3 and MCF-7 cells on host tissue in vitro (*13*). In addition, Giffels et al. (*15*) and Wagner et al. (*16*) demonstrated that mAb 14C5 and its antiidiotypic counterpart (mAb ACA 14C5) significantly inhibit tumor growth in a dose-dependent way in Sprague–Dawley rats bearing HH-16 clone 1/2 adenocarcinomas or fibrosarcomas overexpressing the CA14C5 antigen.

Immunohistochemical evaluation of human benign and malignant neoplastic tissues demonstrated that the 90-kDa CA14C5 antigen is highly expressed in most of the invasive ductal breast carcinomas but also on the cell membrane of several other epithelial malignant tumors, such as spinocellular carcinomas of the head and neck region, lung, skin, and oral mucosa. Adenocarcinomas of the stomach, colon, ovaries, and thyroid gland as well as squamous cell carcinomas also stained strongly positive (*14,17*). An even more pronounced antigen expression was found between and on the cell membrane of fibroblasts surrounding the tumor cells, especially at the invasive front of the tumor even in biopsy specimens in which tumor cells were negative. In general, the antigen was strongly expressed on the cell membrane of both poorly differentiated, highly invasive ductal carcinomas and in situ ductal carcinomas. In contrast, normal multilayered epithelial, muscle, and connective tissues as well as healthy breast tissue stained completely negative (*14*). High antigen expression has also been reported for granulation tissue, suggesting the involvement of CA14C5 in tissue repair and wound healing.

All of these findings suggest that the cancer-associated antigen CA14C5 plays a role in both the construction and the destruction of the connective tissue architecture and ECM and may, in fact, represent a cell substrate adhesion molecule, possibly related to the integrin family (*13*). However, the exact nature of the antigen has not yet been defined. This antigen may serve as a new effective target not only for passive and active cytotoxic immunotherapy but also for radioimmunodetection (RID) and radioimmunotherapy (RIT) of some carcinomas.

This study is focused on the $^{123}$I-labeled mAb 14C5 ($^{123}$I-mAb 14C5) that was recently developed by our group and on the evaluation of its in vitro binding properties to SK-BR-3 and HeLa tumor cells, expressing the CA14C5 antigen (*18*). Since mAb 14C5 is able to prevent cell substrate adhesion and tumor invasion by binding to its antigen, $^{123}$I-mAb 14C5 holds promise as a new marker for RID of tumor growth and metastasis by means of SPECT. Because information on the biologic behavior and radiation burden is mandatory for any new radiopharmaceutical before human application, the aim of this feasibility study was to investigate the biodistribution and dosimetry of $^{123}$I-mAb 14C5 in mice to establish absorbed radiation dose estimates for the human reference adult by means of the MIRDOSE3.0 program.

## MATERIALS AND METHODS

### Radiolabeling of $^{123}$I-mAb 14C5

The generation and purification of the mouse mAb 14C5 were described previously by De Potter et al. (*13*). Bovine serum albumin (BSA) and other reagents were purchased from Sigma-Aldrich unless stated otherwise. Radiolabeling of the mAb was performed using to the IODO-BEADS method (Pierce Biochemical Co.), as described earlier with minor modifications (*19*). Briefly, before use, IODO-BEADS were washed in 1 mL of 0.01 mol/L potassium phosphate buffer (pH 7.4) and allowed to dry on absorbent paper. Ten micrograms mAb 14C5 in phosphate-buffered saline (PBS) (43.2 mmol/L $K_2HPO_4$, 9.5 mmol/L $NaH_2PO_4 \cdot H_2O$, and 123.2 mmol/L NaCl, pH 7.4) were added to the reaction vial, buffered with 100 μL 0.1 mol/L potassium phosphate (pH 6.5) and placed in a lead-shielded container. $^{123}$I (5.55–222 MBq) in 0.05 mol/L NaOH (Tyco Healthcare) was transferred to the reaction vial and 2 IODO-BEADS were added to the reaction mixture. Radiolabeling was then allowed to proceed for 30 min at room temperature. The iodination of the antibody was terminated by removing the reaction mixture from the vial. IODO-BEADS were washed twice with 500 μL 0.1 mol/L potassium phosphate (pH 6.5) and the wash solutions were added to the reaction mixture. Afterward, $^{123}$I-mAb 14C5 was purified by size-exclusion chromatography on a PD10 (G25) Sephadex column (Amersham Pharmacia Biotech) using PBS (pH 7.4), supplemented with 0.25% BSA as eluent. Finally, the chemical and radiochemical purity of the eluted radioligand was determined by high-performance liquid chromatography (HPLC) on a Bio-Silect SEC 250-5 (7.8 × 300 mm) column (Bio-Rad Laboratories) using 0.01 mol/L potassium phosphate (pH 7.4) as the eluent at a flow rate of 0.8 mL/min.

### In Vitro Stability of $^{123}$I-mAb 14C5

$^{123}$I-mAb 14C5 was prepared and purified as described, starting with 200 MBq $^{123}$I. The radiolabeled antibody was stored at room temperature and aliquots were reinjected on the HPLC column at preset time points (0.5, 1, 3, 6, 21, and 32 h) up to 48 h after radiolabeling. The chemical and radiochemical purity of the injected samples was obtained under HPLC conditions identical to those described for the quality control of the radioligand immediately after purification. All tested time points were investigated in triplicate.

### In Vitro Binding of $^{123}$I-mAb 14C5 to Carcinoma Cells

*Cell Cultures.* The following ATCC cell lines were used: SK-BR-3 (breast adenocarcinoma), T47D (breast carcinoma), 791T (skeletal osteosarcoma), HeLa (cervix spinocellular carcinoma), and CoLo-16 (skin spinocellular carcinoma) cells. T47D, 791T, and CoLo-16 cells were cultured in RPMI 1640 medium contain-

ing *N*-(2-hydroxyethyl)piperazine-*N'*-(2-ethanesulfonic acid) (HEPES) and L-glutamine supplemented with 10% fetal calf serum (FCS). SK-BR-3 cells were grown in Eagle's minimal essential medium (EMEM) supplemented with 10% FCS, 60 IU/mL penicillin, 60 IU/mL streptomycin, and 2 mmol/L L-glutamine. Similarly, the culture medium for maintaining HeLa cells consisted of Dulbecco's minimal essential medium (DMEM) supplemented with 10% FCS, 65 IU/mL penicillin, 65 IU/mL streptomycin, and 2 mmol/L L-glutamine. The cell culture media RPMI 1640, EMEM, and DMEM were purchased from Bio-Whittaker, whereas all other cell culture reagents were obtained from Invitrogen.

*$^{123}$I-mAb 14C5 Immunoreactivity to Carcinoma Cells.* $^{123}$I-mAb 14C5 was initially screened for its binding capacity to SK-BR-3, T47D, 791T, and HeLa carcinoma cells (CA14C5 positive) as well as CoLo-16 cells (CA14C5 negative). Confluent SK-BR-3, T47D, 791T, HeLa, and CoLo-16 cells were washed twice with freshly prepared culture medium and mechanically detached from their culture plates (Nunc). After resuspending and homogenizing in cell culture medium, all cell suspensions were examined microscopically for cell viability, using 20% trypan blue dye (Invitrogen), and for morphology to confirm the absence of multicellular aggregates. Aliquots containing $1.4 \times 10^6$ cells in culture medium were then incubated in quadruplicate with $0.45 \pm 0.03$ nmol/L $^{123}$I-mAb 14C5 (150.0 ± 9.0 kBq) for 2 h at 37°C in an atmosphere of 5% $CO_2$ in air with gentle shaking of the incubation tubes. Afterward, all samples were centrifuged for 8 min at 400*g* at room temperature. The supernatant ($SN_1$) was withdrawn and the cell pellets washed with PBS (pH 7.4) and centrifuged again at 400*g* for 8 min. The supernatant ($SN_2$) was again removed and the cell pellet was resuspended with PBS (pH 7.4). Both supernatants and the pellet originating from each sample were counted for radioactivity on a NaI γ-counter (Canberra Packard) to determine the percentage of cell-bound $^{123}$I-mAb 14C5. Control samples without carcinoma cells were used to assess nonspecific radioligand binding to the incubation tubes. Specific $^{123}$I-mAb 14C5 binding to cells was calculated using Equation 1 to calculate the percentage of specific $^{123}$I-mAb 14C5 binding:

$$\% \text{ specific bound} = \left(\frac{\text{cpm (Pellet)}_{(\text{unknown})}}{\text{cpm (Total)}_{(\text{unknown})}} - \frac{\text{cpm (Pellet)}_{(\text{control})}}{\text{cpm (Total)}_{(\text{control})}}\right) \times 100, \quad \text{Eq. 1}$$

with cpm (Total) = cpm (Pellet + $SN_1$ + $SN_2$).

*Analysis of Saturation $^{123}$I-mAb 14C5 Binding.* Immediately after harvesting, aliquots—each containing either $1.4 \times 10^6$ SK-BR-3, HeLa, or CoLo-16 cells (as negative control)—were incubated for 1 h with increasing concentrations of $^{123}$I-mAb 14C5, ranging from 4.5 ± 0.4 pmol/L to 4.5 ± 0.3 nmol/L final concentration (49.0 ± 4.0 kBq to 49.4 ± 3.9 MBq). Incubation of the samples was performed under conditions identical to those described earlier. Each $^{123}$I-mAb 14C5 concentration was investigated in quadruplicate. Analysis of saturation binding was performed according to the method of Bylund and Yamamura et al. (*20*). $^{123}$I-mAb 14C5 binding to each cell line was expressed as specific binding versus radioligand concentration. The corresponding values of the dissociation constant ($K_d$) and the maximum number of binding sites ($B_{max}$) were generated by curve fitting of the saturation plots applying the GraphPad Prism 3.0 program and were expressed in nmol/L and pmol/L, respectively. The fitted curves, obtained by nonlinear regression analysis, were assumed to follow a 1-site fit unless the statistical analyses within the program indicated that the data gave a significantly better fit using a 2-site model. Additionally, the radioligand binding data (i.e., expressed as bound/free vs. free radioligand concentration) were also expressed as typical Scatchard plots.

*Kinetics of $^{123}$I-mAb 14C5 In Vitro Binding.* To determine the kinetics of radioligand binding to SK-BR-3, HeLa, and CoLo-16 carcinoma cells, binding of $^{123}$I-mAb 14C5 over time was studied using a constant radioligand concentration derived from the linear range of the Scatchard plots. SK-BR-3, HeLa, and CoLo-16 cells were harvested from confluent cultures and prepared as described. Samples containing $1.4 \times 10^6$ cells in cell culture medium were incubated with 0.45 ± 0.06 nmol/L of $^{123}$I-mAb 14C5 (4.8 ± 0.6 MBq) from 5 min to 3 h, at 37°C in an atmosphere of 5% $CO_2$ in air. Supernatants and cell pellets were processed as described and counted for activity on a NaI γ-counter. Each incubation time interval was investigated in quadruplicate. In addition, the binding experiment was repeated in a similar way for control samples containing no cells to determine nonspecific radioligand binding to the incubation tubes. The results were expressed as the percentage of cell-bound radioligand versus incubation time according to Equation 1.

### Biodistribution Studies in Mice

All animal experiments were approved by the local ethics committee of the Gent University, Faculty of Medicine (ethics protocol: Project ECP 00/17) in compliance with the principles of laboratory animal care. For the biodistribution study, 3- to 4-wk-old female NMRI mice ($n = 3$ per time point) (Iffa-Credo) were injected in the lateral tail vein with 148.0 ± 7.4 kBq of research-grade $^{123}$I-mAb 14C5 (0.10 ± 0.005 μg mAb 14C5) and killed at preset time points up to 48 h after tracer injection. Selected organs and tissues, blood, as well as urine and feces were collected and tissues were washed with saline. All samples were then counted for radioactivity on a NaI γ-counter (Canberra Packard). The uptake was expressed as the percentage of the injected dose per gram tissue (%ID/g tissue) or as %ID (in particular, for blood and urinary excretion).

### Dosimetric Calculations

Mean time–activity curves were generated for the organs of interest. Source organ residence times were determined from integration of the biexponential fit to the experimental biodistribution data. Extrapolation of the animal biodistribution to the human reference adult was performed by assuming that either the %ID/g tissue or the %ID in mice and humans was equal. Absorbed radiation dose estimates were then calculated for the target organs applying the MIRD methodology (*21*) for healthy adults using the MIRDOSE3.0 software package (*22,23*).

## RESULTS

### Radiolabeling and In Vitro Stability of $^{123}$I-mAb 14C5

Applying the IODO-BEADS method, $^{123}$I-mAb 14C5 could be obtained in radiochemical yields of 85.0% ± 2.5% when using starting activities up to 200–222 MBq/10 μg mAb 14C5. Purification of the radioligand on a PD10 (G25) Sephadex column, resulted in a chemical and radiochemical purity of >97% as shown by HPLC analysis. On average, specific activity was in the range of 17.0 ± 1.5 MBq/μg protein. HPLC radiochromatography of the radiolabeled antibody over time demonstrated that 93.6% ± 0.1% of

$^{123}$I-mAb 14C5 was found intact at 24 h after radiolabeling and slowly decreased to 89.7% ± 0.7% at 48 h.

### $^{123}$I-mAb 14C5 Immunoreactivity to Carcinoma Cells

As shown in Table 1, $^{123}$I-mAb 14C5 exhibited the highest immunoreactivity toward SK-BR-3 cells and HeLa cells with 3.91% ± 0.08% and 2.26% ± 0.24% of $^{123}$I-mAb 14C5 bound to the cells (i.e., total bound minus nonspecifically bound). In contrast, the T47D breast cancer cells (0.100% ± 0.023%) and 791T osteosarcoma cells (0.150% ± 0.009%) showed a significantly lower cell-associated radioactivity. These data were only slightly higher than those observed for the negative control CoLo-16 cells (0.070% ± 0.021%). Nevertheless, cell binding to both T47D and 791T cells was statistically different from that of CoLo-16 cells using a Student *t* test with $P = 0.01$ ($n = 6$). Binding data are presented as a fraction of the specifically bound $^{123}$I-mAb 14C5. The CA14C5 expression of all investigated cells and the biologic effect of mAb 14C5 binding on these cells (i.e., cell substrate adhesion inhibition) are given in Table 1.

### Analysis of Saturation $^{123}$I-mAb 14C5 Binding

Since $^{123}$I-mAb 14C5 displayed strongest immunoreactivity to SK-BR-3 and HeLa carcinoma cells, a second set of binding assays was performed, using increasing tracer concentrations, to study the affinity of $^{123}$I-mAb 14C5 binding as well as the degree of CA14C5 antigen expression on SK-BR-3 and HeLa cells in detail. CoLo-16 cells were used as negative controls to assess nonspecific cell binding. Analysis of the tracer binding data was based on the method of Bylund and Yamamura et al. (*20*). Saturation of $^{123}$I-mAb 14C5 binding to SK-BR-3 and HeLa cells is plotted as specific tracer binding versus tracer concentration in typical saturation plots (Figs. 1A and 1B). Curve fitting of the binding data was performed using nonlinear regression analysis to generate $K_d$ and $B_{max}$ values for each cell type ($r^2 > 0.95$). The corresponding Scatchard plots, shown as insets in Figures 1A and 1B, were derived from the binding data by applying linear regression analysis according to the method of least squares. $^{123}$I-mAb 14C5 specifically binds with nanomolar affinity to SK-BR-3 cells ($K_d \approx 0.85 \pm 0.17$ nmol/L) and HeLa cells ($K_d \approx 1.71 \pm 0.17$ nmol/L) and appears to recognize a single binding site. Both carcinoma cell types also exhibited a high CA14C5 antigen expression as reflected by the corresponding $B_{max}$ values derived from the Scatchard plots: $B_{max} = 40.61 \pm 5.19$ pmol/L for SK-BR-3 cells and $B_{max} = 57.08 \pm 9.57$ pmol/L for HeLa cells. Nonspecific binding, as determined by $^{123}$I-mAb 14C5 binding to CoLo-16 cells, was low and was comparable to nonpecific radioligand binding to the incubation tubes that did not contain any cells.

### Kinetics of $^{123}$I-mAb 14C5 In Vitro Binding

The kinetics of $^{123}$I-mAb 14C5 binding to SK-BR-3 and HeLa cells was evaluated using a time-dependent binding assay. As shown in the saturation curves (Figs. 2A and 2B), tracer binding to the cells lines proceeds rapidly. The incubation time needed to reach full saturation of the available CA14C5 antigen sites at 37°C was about 2–2.5 h for SK-BR-3 cells and 3 h for HeLa cells, resulting in 3.95% ± 0.23% and 2.36% ± 0.16% specific binding (total bound minus nonspecifically bound), respectively. On the contrary, a very low binding to CA14C5-negative CoLo-16 cells over time was observed.

### Biodistribution and Dosimetry in Mice

As shown in Figure 3, $^{123}$I-mAb 14C5 was slowly cleared from the blood (9.7 ± 1.4 %ID remaining at 48 h after injection) following a biexponential pharmacokinetic behavior. Fitting of the blood clearance curve was performed with the SPSS 10.0 software package, using the method of least squares, to calculate the biologic half-life ($t_{1/2}$) of the tracer ($r^2 > 0.95$). The biexponential blood clearance of $^{123}$I-mAb 14C5 was characterized by a fast phase ($t_{1/2,\alpha} = 1.43 \pm 0.42$ h, 62.8% of total circulating radioactivity in the

**TABLE 1**

In Vitro Binding of $^{123}$I-mAb 14C5 to Carcinoma Cells Compared with CA14C5 Expression and Biologic Activity (Cell Substrate Adhesion Inhibition) of Nonradiolabeled mAb 14C5

| Cell line | Origin | CA14C5 expression* | Cell substrate adhesion inhibition† | $^{123}$I-mAb 14C5 binding‡ (%) | |
|---|---|---|---|---|---|
| | | | | Average | SD |
| SK-BR-3 | Breast adenocarcinoma | +++ | +++ | 3.91 | 0.08 |
| T47D | Breast carcinoma | + | + | 0.10 | 0.02 |
| 791T | Skeletal osteosarcoma | + | – | 0.15 | 0.01 |
| HeLa | Cervical spinocellular carcinoma | +++ | + | 2.26 | 0.24 |
| CoLo-16 | Skin spinocellular carcinoma | – | – | 0.07 | 0.02 |

*CA14C5 expression based on previously performed immunohistochemical and fluorescent staining experiments (*25,26*).

†Inhibitory effect of nonradiolabeled mAb 14C5 on cell substrate adhesion as demonstrated by earlier reported adhesion inhibition experiments on artificial substrates in vitro (*13,14,25*).

‡Values represent percentage of specific $^{123}$I-mAb 14C5 binding to each carcinoma cell type (total bound minus nonspecifically bound) as determined by Equation 1 ($n = 6$).

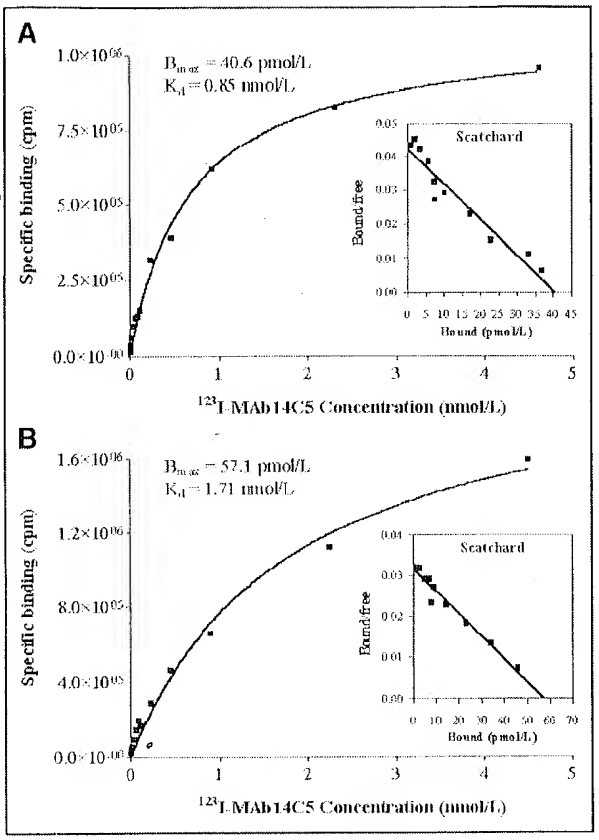


**FIGURE 1.** Saturation plots for $^{123}$I-mAb 14C5 binding to SK-BR-3 cells (A) and HeLa cells (B). Each point represents mean ± SD of 4 measurements. Corresponding curve fittings, as determined by GraphPad Prism 3.0 program, are indicated by solid lines. Insets show respective Scatchard plots derived from linear regression analysis of binding data.

blood) and a slow phase ($t_{1/2,\beta}$ = 130.4 ± 100.0 h, 37.2%). The remaining radioactivity (68 %ID) was rapidly distributed into the extravascular compartments in the initial phase of the tracer biodistribution. Kinetic parameters for blood clearance are presented in Table 2. Blood-pool activity was at any time substantially higher than tracer uptake in any of the other investigated organs. $^{123}$I-mAb 14C5 did not cross the blood–brain barrier as indicated by the low brain uptake (<1.0 %ID/g on average). The biodistribution data are presented in Table 3. The highest accumulation of radioactivity occurred in lungs (20.4 ± 3.7 %ID/g), liver (15.1 ± 1.4 %ID/g), and kidneys (11.1 ± 1.1 %ID/g) within 5 min after injection and to a lesser extent in the spleen (9.2 ± 2.4 %ID/g) at 20 min after injection. A delayed uptake was observed in stomach (12.8% ± 2.4 %ID/g) and urinary bladder (8.7 ± 5.2 %ID/g) at 3 and 6 h after injection, respectively (Table 3). $^{123}$I-mAb 14C5 was mainly cleared by kidneys, with 40.7 ± 2.9 %ID being excreted in urine at 48 h after injection, representing 90.8% of the total excreted radioactivity. Fecal excretion 48 h after tracer injection (4.1 ± 1.0 %ID) contributed only 9.2% to the total excreted activity as depicted in Figure 3.

Based on the biodistribution data given earlier, time–activity curves were generated for the whole body and several organs of interest, and data were expressed as %ID/g tissue and as %ID. Both types of time–activity curves were fitted using the SPSS 10.0 program to determine mean residence times. The residence times calculated from the biexponential fits for the source organs was highest for the remainder of the body in both dosimetric approaches, followed by the urinary bladder content, liver, and lungs (data not shown).

Mean radiation dose estimates were calculated for the human reference adult using time–activity curves and organ

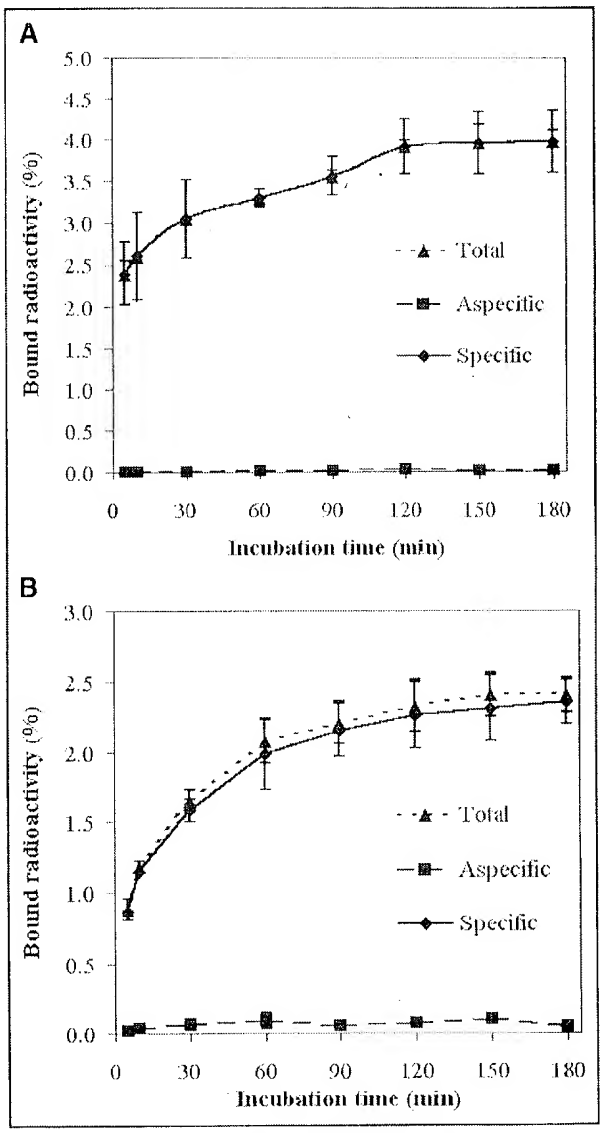


**FIGURE 2.** In vitro binding of $^{123}$I-mAb 14C5 over time to SK-BR-3 cells (A) and HeLa cells (B). Each time point represents mean ± SD of 4 measurements.

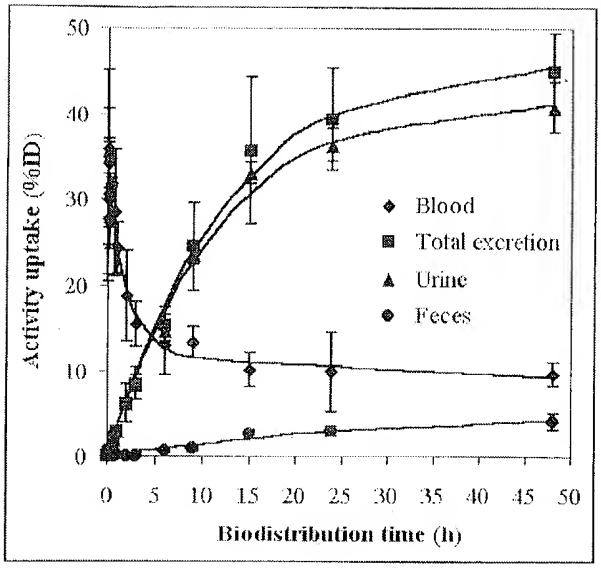


**FIGURE 3.** Blood clearance (◆) and urinary (▲) and fecal (●) excretion of $^{123}$I-mAb 14C5 (%ID) in mice after intravenous injection. Each time point represents mean ± SD of 3 animals. Corresponding curve fittings, as determined by SPSS 10.0 program, are indicated by solid lines.

residence times derived from mice biodistribution data. The MIRDOSE3.0 program was applied assuming that either the %ID/g tissue values or the %ID values for $^{123}$I-mAb 14C5 in mice are equal to those in humans. Dosimetry results according to both estimates are given in Table 4. In addition, the absorbed-dose estimate for the urine bladder wall was determined according to the dynamic bladder model as described by Cloutier et al. (*24*). In the applied bladder model, a biologic $t_{1/2}$ of 7.92 h was used with a bladder voiding interval of 4.8 h. The highest absorbed radiation dose was received by the urine bladder wall (0.1200–0.1210 mGy/MBq), liver (0.0137–0.0274 mGy/MBq), and uterus (0.0196–0.0207 mGy/MBq), followed by the lower large intestine wall (0.0139–0.0258 mGy/MBq) and stomach (0.0090–0.0292 mGy/MBq), as determined by the dosimetry estimations used. The predicted radiation dose for the thyroid was in the range of 0.0070–0.0084 mGy/MBq. The effective dose for the human reference adult was estimated to be approximately 0.0172–0.0223 mSv/MBq. When selecting the highest absorbed radiation dose for each organ out of both dosimetry estimations, this worst-case scenario would result in an effective dose of 0.0231 mSv/MBq, which is slightly higher compared with the upper limit value of the estimated effective dose for humans.

## DISCUSSION

The immunoreactivity of $^{123}$I-mAb 14C5 correlates well with the CA14C5 expression status of the investigated cells. This is in agreement with the previously reported immunohistochemistry data (Table 1) (*25,26*). SK-BR-3 and HeLa cells, strongly positive for the CA14C5 antigen, exhibited the highest tracer binding. T47D and 791T cells, characterized by a moderate-to-weak CA14C5 staining, showed low $^{123}$I-mAb 14C5 binding, almost at the same level of tracer binding to CA14C5-negative CoLo-16 cells. Visual assessment of the antigen expression by means of immunohistochemical staining is difficult to correlate accurately with quantitative methods, such as tracer binding assays. No true correlation was found between $^{123}$I-mAb 14C5 binding to T47D, 791T, and HeLa cells and the known biologic effect (cell substrate adhesion inhibition) that nonradiolabeled mAb 14C5 exerts on these cell lines (Table 1). Only for SK-BR-3 cells was a positive correlation found between both parameters.

The in vitro affinities of $^{123}$I-mAb 14C5 are in the range of affinities observed for radiolabeled antibodies or somewhat better by a factor of 2.9–5.9 than the nanomolar affinity, $K_d$ = 5 nmol/L, of trastuzumab (Herceptin; Genentech, Inc.) for breast cancer cells expressing the HER-2/neu receptor as reported by Coussens et al. (*27*) and Press et al. (*28*). Since binding affinities of better than $10^{-8}$ mol/L and receptor densities of 50,000–100,000 binding sites per tumor cell are considered as one of the requirements for efficient in vivo detection of solid tumors, RID of CA14C5-positive human carcinomas with $^{123}$I-mAb 14C5 seems achievable (*29*). However, it should be noted that the stroma surrounding the tumor cells often expresses higher levels of the CA14C5 antigen than that of the tumor cells. Previous immunohistochemical evaluation of tumor biopsy specimens clearly demonstrated that the strong signal of the connective tissue can be attributed to pronounced antigen expression in extracellular spaces and on the cell membrane of fibroblasts surrounding tumor cells, especially at the invasive front of the tumor (*13,14*). In some biopsy specimens, strong positive staining of the stroma was not accompanied by any staining of the tumor cells. In general, poorly differentiated, highly invasive ductal carcinomas showed the strongest staining (the stroma and both the tumor cell membranes and their cytoplasmic membrane extensions)

**TABLE 2**
Kinetic Parameters for Blood Clearance of $^{123}$I-mAb 14C5 in Mice

| Parameter | Average | SD |
|---|---|---|
| $A_\alpha$ | 20.29 | 2.45 |
| $t_{1/2,\alpha}$ (h) | 1.43 | 0.42 |
| $A_\beta$ | 12.03 | 2.41 |
| $t_{1/2,\beta}$ (h) | 130.42 | 100.00 |
| $r^2$ | 0.95 | |

$A_\alpha$ and $A_\beta$ represent activity fractions (%ID) in blood at any time (T) after tracer injection, corresponding to biologic half-lives $t_{1/2,\alpha}$ and $t_{1/2,\beta}$, respectively.

Clearance data were fit to the following equation using method of least squares: Activity = $A_\alpha \cdot e^{-(0.6931/t_{1/2,\alpha})\cdot T} + A_\beta \cdot e^{-(0.6931/t_{1/2,\beta})\cdot T}$.

compared with in situ ductal carcinomas, in which the antigen was only expressed on the cell membrane of the tumor cells (*13,14*). These histologic findings imply that the $^{123}$I-mAb 14C5 uptake in tumors could be considerably higher than that predicted from the $B_{max}$ values. Furthermore, it can expected that the extent of tracer uptake by tumors in vivo might correlate with the degree of differentiation and the invasive character of the investigated tumor.

Immunohistochemical evaluation of human benign and malignant neoplastic tissues has previously shown that the CA14C5 antigen is highly expressed in most of the invasive ductal breast carcinomas but also on the cell membrane of several other epithelial malignant tumors, such as spinocellular carcinomas of the head and neck region, lung, skin, and oral mucosa. Adenocarcinomas of the stomach, colon, ovaries, and thyroid gland as well as squamous cell carcinomas also stained strongly positive (*14,17*). Therefore, mAb 14C5 and radioimmunoconjugates thereof could offer much broader perspectives in (radio)immunotherapy and in vivo detection of cancer in addition to metastatic breast cancer therapy. CA14C5-negative tumors also might benefit from the treatment with unlabeled or radiolabeled mAb 14C5, since the connective tissue surrounding the tumor cells has also been shown to express the CA14C5 antigen.

When compared with $^{18}$F-FDG PET, in vivo imaging of CA14C5 tumor antigen expression could provide in vivo histopathologic information for diagnostic purposes, for targeted radionuclide therapy, and for therapy follow-up. With regard to therapy follow-up, in vivo imaging of changes over time in CA14C5 tumor expression, after instigation of specific "cytostatic" treatments targeting the underlying molecular abnormalities responsible for invasion and metastasis of human malignancies, might prove a more appropriate endpoint for treatment monitoring compared with volumetric changes as visualized by CT and MRI.

The biodistribution study in NMRI mice demonstrates that $^{123}$I-mAb 14C5 is cleared from the blood compartment in $t_{1/2,\beta}$ = 130.42 ± 100.00 h). This slow blood clearance can be attributed to the fairly high molecular weight of the protein (150 kDa) and is comparable with existing radiolabeled antibodies that are generally known to exhibit a slow clearance from the blood compartment. As a result, blood-pool activity was at any time higher than tracer uptake in any of the other investigated organs (Table 3). In fact, an overall low tracer uptake was observed in most organs that, combined with a sufficient tumor uptake, should provide good imaging conditions for in vivo detection of CA14C5-expressing tumors and their subsequent metastases, not only in the thoracic or abdominal region but also in other regions, such as the head and neck region, skin, and oral mucosa. From the dosimetric point of view, the fairly high retention of activity in the blood compartment can also be considered as a benefit since the tracer distribution in the whole body—and, subsequently, the radiation burden to various organs—is thereby being decreased substantially.

**TABLE 3**
Biodistribution Results (%ID/g tissue) for $^{123}$I-mAb 14C5 in NMRI Mice ($n$ = 3)

| Tissue | Biodistribution time (h) | | | | | | | | |
|---|---|---|---|---|---|---|---|---|---|
| | 0.083 | 0.33 | 1 | 3 | 6 | 9 | 15 | 24 | 48 |
| Blood | 51.13 ± 2.38 | 48.19 ± 4.38 | 38.62 ± 1.02 | 31.28 ± 2.06 | 27.02 ± 2.09 | 21.51 ± 2.54 | 16.01 ± 3.91 | 14.33 ± 3.06 | 13.31 ± 1.39 |
| Brain | 1.26 ± 0.26 | 0.93 ± 0.02 | 0.90 ± 0.25 | 0.71 ± 0.08 | 0.66 ± 0.17 | 0.46 ± 0.18 | 0.32 ± 0.15 | 0.28 ± 0.05 | 0.27 ± 0.08 |
| Heart | 8.08 ± 1.94 | 8.74 ± 2.13 | 7.96 ± 0.74 | 4.24 ± 3.56 | 6.81 ± 1.78 | 5.23 ± 1.82 | 3.57 ± 1.21 | 2.98 ± 0.59 | 2.42 ± 0.05 |
| Lungs | 20.39 ± 3.74 | 20.29 ± 11.55 | 16.69 ± 3.58 | 10.96 ± 3.58 | 7.83 ± 1.01 | 6.24 ± 1.50 | 4.91 ± 1.41 | 4.00 ± 1.09 | 3.46 ± 1.06 |
| Stomach | 5.72 ± 3.37 | 6.38 ± 2.12 | 7.35 ± 2.98 | 12.78 ± 2.44 | 11.51 ± 7.49 | 5.99 ± 2.93 | 0.87 ± 0.06 | 1.10 ± 0.25 | 1.02 ± 0.68 |
| Spleen | 8.45 ± 0.41 | 9.21 ± 2.36 | 6.69 ± 0.50 | 5.79 ± 0.84 | 4.78 ± 0.79 | 3.73 ± 0.38 | 3.01 ± 1.14 | 2.27 ± 0.39 | 2.13 ± 0.80 |
| Liver | 15.12 ± 1.40 | 14.24 ± 0.65 | 10.58 ± 1.35 | 9.17 ± 0.96 | 7.95 ± 1.57 | 5.91 ± 0.59 | 3.68 ± 1.46 | 3.15 ± 0.31 | 2.69 ± 0.55 |
| Kidneys | 11.13 ± 1.07 | 9.57 ± 0.81 | 9.16 ± 0.93 | 7.88 ± 0.67 | 6.21 ± 0.63 | 4.66 ± 1.18 | 3.32 ± 1.21 | 2.99 ± 0.66 | 2.62 ± 0.17 |
| Small intestines | 2.01 ± 0.48 | 2.17 ± 0.39 | 3.11 ± 0.20 | 3.67 ± 0.06 | 3.30 ± 0.89 | 2.27 ± 0.24 | 1.23 ± 0.37 | 1.12 ± 0.25 | 0.92 ± 0.23 |
| Large intestines | 1.12 ± 0.32 | 1.04 ± 0.21 | 1.32 ± 0.16 | 2.17 ± 0.22 | 2.39 ± 0.53 | 1.96 ± 0.37 | 0.93 ± 0.25 | 0.84 ± 0.06 | 0.80 ± 0.19 |
| Bladder | 2.29 ± 0.82 | 2.67 ± 0.72 | 3.48 ± 2.50 | 5.76 ± 3.52 | 8.68 ± 5.16 | 7.68 ± 2.68 | 4.26 ± 1.14 | 3.74 ± 0.72 | 3.43 ± 2.61 |
| Body remainder | 3.44 ± 0.48 | 3.28 ± 0.57 | 3.66 ± 0.48 | 4.10 ± 0.40 | 4.11 ± 0.23 | 3.46 ± 0.25 | 2.79 ± 0.45 | 2.90 ± 0.21 | 2.81 ± 0.29 |
| Excretion* | 0.15 ± 0.24 | 0.24 ± 0.62 | 3.38 ± 1.75 | 7.22 ± 0.81 | 13.76 ± 3.00 | 28.03 ± 3.41 | 45.98 ± 9.64 | 43.55 ± 6.75 | 48.05 ± 5.24 |

*Excretion values (urine + feces) are expressed as %ID.

**TABLE 4**
Radiation Absorbed-Dose Estimates (mGy/MBq) for $^{123}$I-mAb 14C5 for Target Organs

| | $\%ID/g_{mice} = \%ID/g_{humans}$ | | $\%ID_{mice} = \%ID_{humans}$ | |
|---|---|---|---|---|
| Target organ | Average | SD | Average | SD |
| Adrenals | 0.01020 | 0.00152 | 0.01140 | 0.00305 |
| Brain | 0.00299 | 0.00032 | 0.00275 | 0.00033 |
| Breasts | 0.00641 | 0.00058 | 0.00570 | 0.00071 |
| Gallbladder wall | 0.01120 | 0.00226 | 0.01510 | 0.00565 |
| LLI wall | 0.01390 | 0.00079 | 0.02580 | 0.00364 |
| Small intestine | 0.01150 | 0.00208 | 0.02490 | 0.01270 |
| Stomach | 0.00899 | 0.00164 | 0.02920 | 0.01380 |
| ULI wall | 0.01050 | 0.00130 | 0.02440 | 0.00625 |
| Heart wall | 0.00903 | 0.00211 | 0.01340 | 0.00437 |
| Kidneys | 0.01210 | 0.00370 | 0.02400 | 0.00958 |
| Liver | 0.01370 | 0.00774 | 0.02740 | 0.01820 |
| Lungs | 0.01320 | 0.00489 | 0.01020 | 0.00379 |
| Muscle | 0.00878 | 0.00061 | 0.00846 | 0.00107 |
| Ovaries | 0.01370 | 0.00079 | 0.01630 | 0.00288 |
| Pancreas | 0.01060 | 0.00142 | 0.01360 | 0.00394 |
| Red marrow | 0.00816 | 0.00063 | 0.00804 | 0.00118 |
| Bone surfaces | 0.01480 | 0.00102 | 0.01370 | 0.00155 |
| Skin | 0.00583 | 0.00035 | 0.00525 | 0.00049 |
| Spleen | 0.01000 | 0.00124 | 0.01730 | 0.00317 |
| Testes | 0.01000 | 0.00034 | 0.00897 | 0.00036 |
| Thymus | 0.00851 | 0.00071 | 0.00751 | 0.00082 |
| Thyroid | 0.00839 | 0.00045 | 0.00704 | 0.00039 |
| Urine bladder wall | 0.12100 | 0.00084 | 0.12000 | 0.00147 |
| Uterus | 0.01960 | 0.00075 | 0.02070 | 0.00241 |
| Total body dose | 0.00926 | 0.00090 | 0.00955 | 0.00177 |
| Effective dose (mSv/MBq) | 0.01720 | 0.00178 | 0.02230 | 0.00483 |

LLI = lower large intestine; ULI = upper large intestine.

All of these findings seem to reflect the generally observed hepatic uptake and urinary excretion of radiolabeled proteins, their related metabolites, and trapping of some free iodine by the stomach. In spite of the predominant urinary excreted radioactivity, the cumulative excreted activity over time remains relatively low and can be attributed to the high molecular weight of the radioligand. Subsequently, the rather slow urinary excretion results in a radiation dose estimate for kidneys and urine bladder wall in humans of 0.0121–0.0240 and 0.1200–0.1210 mGy/MBq administered, respectively. In contrast, low-molecular-weight antibody fragments or peptides are generally being excreted through kidneys and urine much faster and to a substantially higher extent.

Initially, the predominant lung uptake very early after $^{123}$I-mAb 14C5 administration might seem to limit the usefulness of the molecule for imaging tumor invasion in the thoracic region—for example, invasive ductal breast carcinomas, lung spinocellular carcinomas, or adenocarcinomas of the thyroid gland. However, the favorable kinetics of tracer clearance from the lungs should result in good imaging conditions for this region at later time points (>2 h) after injection. If the fairly high retention of activity in the blood is taken into account, delayed imaging of tumor uptake in this region may be required anyway, to increase target-to-background ratios. On the other hand, imaging of tumors in the abdominal region—for example, adenocarcinomas of the colon, stomach, and ovaries—around 3–6 h after injection might be impeded somehow due to interfering bowel activity originating in the stomach and liver. In this regard, the presence of a strong tracer uptake in abdominal tumors might be a prerequisite for in vivo imaging of tumor invasion and metastasis during that time frame in this particular region. Alternatively, tumor uptake of the radioligand in the abdomen could easily be assessed at earlier or later time points considering the physical $t_{1/2}$ of $^{123}$I (13.2 h). The moderate accumulation of radioactivity in the abdominal region might be explained by the occurrence of some enterohepatic clearance. Alternatively, this activity uptake could indicate slowly ongoing deiodination of $^{123}$I-mAb 14C5 in vivo, with the production of some free iodine and its subsequent trapping in the stomach. However, the low absorbed radiation dose estimate for the thyroid, as determined by the dosimetry study, does not seem to reflect any significant formation of free iodine due to deiodination of the $^{123}$I-mAb 14C5 so far. In any case, these assumptions remain to be verified by human biodistribution studies with the tracer since species differences in the metabolism of radiolabeled proteins between laboratory animals and humans have been reported previously.

The MIRDOSE software provides a calculation of the effective dose for human adults as defined in the ICRP Publication 60 (*30*). Based on the estimated effective dose of 0.017–0.022 mSv/MBq obtained in our dosimetry study, both patients and volunteers could easily be investigated with 222 MBq $^{123}$I-mAb 14C5, allowing planar and SPECT imaging. Subsequently, the corresponding effective dose of 3.8–4.9 mSv is still 12%–32% lower compared with the reported average effective dose per patient from nuclear medicine procedures in Europe (*31*). As a result of the moderately low effective dose, $^{123}$I-mAb 14C5 could be administered in doses up to 230–295 MBq before reaching the 5-mSv upper-limit average effective dose of Category IIb of ICRP Publication 62 (*32*). To our knowledge, these dosimetry data provide the first evidence that $^{123}$I-mAb 14C5 could be applied safely in humans near the 300-MBq level and, therefore, should allow further evaluation of the radiolabeled antibody in future clinical trials without causing substantial radiotoxicity to the vital organs.

## CONCLUSION

In summary, $^{123}$I-mAb 14C5 can be produced in high radiochemical yields and purities while maintaining good in vitro stability over time. The tracer was shown to bind with high specificity and nanomolar affinity to SK-BR-3 and HeLa carcinoma cells, which were both characterized by a high CA14C5 receptor density. Therefore, efficient RID of

such tumor types in vivo by means of $^{123}$I-mAb 14C5 seems feasible. The favorable biodistribution characteristics of the tracer, in combination with a sufficient tumor uptake, should provide good imaging conditions in the thoracic or abdominal region when studying carcinomas of different origin. Furthermore, the estimated effective dose for human adults should easily allow safe administration of megabecquerel (millicurie) amounts of $^{123}$I-mAb 14C5 for the performance of human clinical trials. $^{123}$I-mAb 14C5 could offer new perspectives for RID of primary and metastatic breast cancer, but also spinocellular carcinomas of the head and neck region, of the lungs, skin, and stomach, and colon and ovarian carcinomas. Additionally, radioimmunoconjugates of mAb 14C5 or smaller fragments thereof with β-emitting radionuclides, such as $^{131}$I, $^{90}$Y, or $^{188}$Re, could provide new approaches in RIT of breast cancer metastasis and other types of carcinomas by specific targeting of cell substrate adhesion molecules involved in tumor growth and invasion.

## REFERENCES


1. Kreis T, Vale R. *Guidebook to the Extracellular Matrix, Anchor, and Adhesion Proteins.* Oxford, UK: Oxford University Press; 1999.
2. Alberts B, Bray D, Lewis J, Raff M, Roberts K, Watson JD. Cell junctions, cell adhesion, and the extracellular matrix. In: Alberts B, Bray D, Lewis J, Raff M, Roberts K, Watson JD, eds. *Molecular Biology of the Cell.* 3rd ed. New York, NY: Garland Publishing; 1994:chapter 19, part IV.
3. Jockusch BM, Bubeck P, Giehl K, et al. The molecular architecture of focal adhesions. *Annu Rev Cell Dev Biol.* 1995;11:379–416.
4. Jiang WG, Puntis MC, Hallett MB. Molecular and cellular basis of cancer invasion and metastasis: implications for treatment. *Br J Surg.* 1994;81:1576–1590.
5. Albelda SM. Role of integrins and other cell adhesion molecules in tumor progression and metastasis. *Lab Invest.* 1993;68:4–17.
6. Cavallaro U, Christofori G. Cell adhesion in tumor invasion and metastasis: loss of the glue is not enough. *Biochim Biophys Acta.* 2001;1552:39–45.
7. Yurchenco PD. Assembly of laminin and type IV collagen into basement membrane networks. In: Yurchenco PD, Birk DE, Mecham RP, eds. *Extracellular Matrix Assembly and Structure.* San Diego, CA: Academic Press; 1994.
8. Anderson JC. Biochemical basis of connective tissue disease. In: Gardner DL, ed. *Pathological Basis of the Connective Tissue Diseases.* London, UK: Arnold; 1992:173–226.
9. Behrens J. The role of cell adhesion molecules in cancer invasion and metastasis. *Breast Cancer Res Treat.* 1993;24:175–184.
10. Dedhar S, Saulnier R. Alterations in integrin receptor expression on chemically transformed human cells: specific enhancement of laminin and collagen receptor complexes. *J Cell Biol.* 1990;110:481–489.
11. Pignatelli M, Cardillo MR, Hanby A, Stamp GW. Integrins and their accessory adhesion molecules in mammary carcinomas: loss of polarization in poorly differentiated tumors. *Hum Pathol.* 1992;23:1159–1166.
12. Takeichi M. Cadherin cell adhesion receptors as a morphogenetic regulator. *Science.* 1990;251:1451–1455.
13. De Potter C, Schelfhout AM, De Smet FH, et al. A monoclonal antibody directed against a human cell membrane antigen prevents cell substrate adhesion and tumor invasion. *Am J Pathol.* 1994;144:95–103.
14. Coene E, Schelfhout AM, De Ridder L, De Potter C. Generation of a monoclonal antibody directed against a human cell substrate adhesion molecule and the expression of the antigen in human tissues. *Hybridoma.* 1997;16:77–83.
15. Giffels P, Köhler S, De Potter C, et al. MAb 14C5 against a human cell substrate adhesion molecule for inhibition of tumor growth in-vivo [abstract]. *Eur J Cancer.* 1997;33(suppl 5):96.
16. Wagner U, Köhler S, Prietl G, et al. Monoclonal anti-idiotype antibodies in immunotherapy of ovarian carcinoma (MAb ACA125) and breast carcinoma (MAb ACA14C5) [in German]. *Zentralbl Gynakol.* 1999;121:190–195.
17. Coene E, Willems K, Verbiest L, Wagner U, Schlebusch H, De Potter C. Expression patterns and functional activity of the human 14C5 cell substrate adhesion molecule [abstract]. *Eur J Cancer.* 1997;33(suppl 5):96.
18. Lahorte C, Burvenich I, Bacher K, et al. Synthesis, biodistribution and dosimetry of the $^{123}$I-14C5 MoAb in mice: a potential SPECT-ligand for radio-immunodetection of tumour growth and metastasis in vivo [abstract]. *Eur J Nucl Med.* 2002;29(suppl 1):S77.
19. Lahorte C, Dumont F, Slegers G, Van De Wiele C, Dierckx RA, Philippé J. Synthesis and in vitro stability of $^{123}$I-labelled annexin V: a potential agent for SPECT imaging of apoptotic cells. *J Labelled Compds Radiopharm.* 2000;43:739–751.
20. Bylund DB, Yamamura HI. Methods for receptor binding. In: Yamamura HI, ed. *Methods in Neurotransmitter Receptor Analysis.* New York, NY: Raven Press; 1990:1–35.
21. Loevinger R, Budinger T, Watson E. *MIRD Primer for Absorbed Dose Calculations.* New York, NY: The Society of Nuclear Medicine; 1991:1–17.
22. Cristy M, Eckerman K. *Specific Absorbed Fractions of Energy at Various Ages From Internal Photon Sources.* ORNL/TM-8381/VII. Oak Ridge, TN: Oak Ridge National Laboratory; 1987:7–29.
23. Stabin MG. MIRDOSE: personal computer software for internal dose assessment in nuclear medicine. *J Nucl Med.* 1996;37:538–546.
24. Cloutier RJ, Smith SA, Watson EE, Snyder WS, Warner GG. Dose to the fetus from radionuclides in the bladder. *Health Phys.* 1973;25:147–161.
25. Vanholme B. Detection and purification of a cell substrate antigen involved in the invasion and metastasis of breast cancer [dissertation]. Gent, Belgium: Gent University; 1999.
26. Burvenich I. Characterization of the 14C5 antigen involved in cell substrate adhesion, invasion and metastasis of breast carcinoma cells [dissertation]. Gent, Belgium: Gent University; 2001.
27. Coussens L, Yang-Feng TL, Liao YC, et al. Tyrosine kinase receptor with extensive homology to EGF receptor shares chromosomal location with neu oncogene. *Science.* 1985;230:1132–1139.
28. Press MF, Pike MC, Chazin VR, et al. Her-2/neu expression in node-negative breast cancer: direct tissue quantification by computarized image analysis and association of overexpression with increased risk of recurrent disease. *Cancer Res.* 1993;53:4960–4970.
29. Fischman AJ, Khaw BA, Strauss HW. Quo vadis radioimmune imaging. *J Nucl Med.* 1989;30:1911–1915.
30. International Commission on Radiological Protection. *1990 Recommendations of the International Commission on Radiological Protection.* ICRP Publication 60. *Ann ICRP.* Oxford, UK: Pergamon Press; 1991;21:6–10.
31. Beekhuis H. Population radiation absorbed dose from nuclear medicine procedures in the Netherlands. *Health Phys.* 1988;54:287–291.
32. International Commission on Radiological Protection. *Radiological Protection in Biomedical Research.* ICRP Publication 62. *Ann ICRP.* Oxford, UK: Pergamon Press; 1991;22:12–13.

## STIC-ILL

**From:** Davis, Minh-Tam
**Sent:** Wednesday, September 15, 2004 3:39 PM
**To:** STIC-ILL
**Subject:** Reprint request for 09/721864

NPL X Adonis X
MIC BioTech X MAIN
NO Vol NO NOS
Ck Cite Dupl Request
Call # 9/15 VD

1) 07821600 PMID: 3390350
Uptake of indium-111-labeled monoclonal antibody ZME-018 as a function of tumor size in a patient with melanoma.
Macey D J; Denardo S J; Denardo G L; Goodnight J K; Unger M W
Department of Radiology, University of California Davis Medical Center, Sacramento 95817.
American journal of physiologic imaging (UNITED STATES) 1988, 3 (1) p1-6, ISSN 0885-8276 Journal Code: 8610225

2) Rapid imaging of human melanoma xenografts using an scFv fragment of the human monoclonal antibody H11 labelled with 111In.
Reilly R M; Maiti P K; Kiarash R; Prashar A K; Fast D G; Entwistle J; Dan ; Narang S A; Foote S; Kaplan H A
Division of Nuclear Medicine, Toronto General Hospital, University Health Network, ON, Canada. raymond.reilly@utoronto.ca
Nuclear medicine communications (England) May 2001, 22 (5) p587-95, ISSN 0143-3636 Journal Code: 8201017

3) Treatment-related parameters predicting efficacy of Lym-1 radioimmunotherapy in patients with B-lymphocytic malignancies.
Lamborn K R; DeNardo G L; DeNardo S J; Goldstein D S; Shen S; Larkin E C; Kroger L A
Brain Tumor Research Center, Department of Neurological Surgery, University of California San Francisco Medical Center, San Francisco, California 94143, USA.
Clinical cancer research - an official journal of the American Association for Cancer Research (UNITED STATES) Aug 1997, 3 (8) p1253-60, ISSN 1078-0432 Journal Code: 9502500

4) 4368891 PMID: 10365793
Biodistribution of filamentous phage-Fab in nude mice.
Yip Y L; Hawkins N J; Smith G; Ward R L
School of Medicine (St. Vincent's Hospital), University of NSW, Sydney, Australia.
Journal of immunological methods (NETHERLANDS) May 27 1999, 225 (1-2) p171-8, ISSN 0022-1759 Journal Code: 1305440

5) Radiolabeling, biodistribution, and dosimetry of (123)I-mAb 14C5: a new mAb for radioimmunodetection of tumor growth and metastasis in vivo.
Lahorte Christophe M M; Bacher Klaus; Burvenich Ingrid; Coene Elisabeth D ; Cuvelier Claude; De Potter Christian; Thierens Hubert; Van de Wiele Christophe; Dierckx Rudi A; Slegers Guido
Department of Radiopharmacy, Faculty of Pharmaceutical Sciences, Gent University, Gent, Belgium. christophe.lahorte@ugent.be
Journal of nuclear medicine - official publication, Society of Nuclear Medicine (United States) Jun 2004, 45 (6) p1065-73, ISSN 0161-5505 Journal Code: 0217410

Thank you
MINH TAM DAVIS
ART UNIT 1642, ROOM 3A24, MB 3C18
272-0830

ELSEVIER

Journal of Immunological Methods 225 (1999) 171–178

JOURNAL OF IMMUNOLOGICAL METHODS

# Biodistribution of filamentous phage-Fab in nude mice

Yum L. Yip [a,b], Nicholas J. Hawkins [c], Glenn Smith [b], Robyn L. Ward [a,b,*]

[a] *School of Medicine (St. Vincent's Hospital), University of NSW, Sydney, NSW 2052, Australia*
[b] *CRC for Biopharmaceutical Research, Darlinghurst, NSW 2010, Australia*
[c] *School of Pathology, University of NSW, Sydney, NSW 2052, Australia*

Received 6 January 1999; accepted 1 March 1999

**Abstract**

In vivo panning of peptide libraries in mice has allowed the isolation of peptides which target the vasculature of specific organs. The application of this approach to phage displaying Fab fragments (phage-Fab) could lead to the isolation of antibodies which recognize novel tumor antigens. In this study, we have evaluated the biodistribution of phage-Fab in nude mice. Balb/c nude mice were injected intravenously with $10^9$ TU of phage displaying the anti-colon cancer Fab c30.6. Blood samples were collected at nine time points over a period of 72 h and three groups of four mice were sacrificed at 4 min, 24 h and 72 h. Normal tissues (liver, colon, spleen, kidneys, lungs, skeletal muscle) and faeces were collected at these time points and the number of viable phage in each sample was determined. The distribution of phage in tissues was also examined by immunohistochemical analysis of paraffin-embedded tissues. Regression analysis of plasma kinetic data showed that the half-life and the volume of distribution of phage was 3.6 h and 1 ml, respectively. Phage uptake occurred predominantly in lungs, kidneys, spleen and liver. Relatively few phage were distributed to colon and muscle, and phage were eliminated from the circulation by 72 h. Immunohistochemical analysis showed phage to be mainly within the vasculature at 4 min, whereas notable phage extravasation was observed at 24 h and 72 h. In conclusion, this study provides information on the in vivo behavior of phage-Fab which will be useful in the design of in vivo panning strategies. By choosing appropriate time points for tissue collection, it may be possible to isolate novel Fabs against both intra- and extravascular targets. 

*Keywords:* Biodistribution; Phage-Fab; Nude mice

## 1. Introduction

Antibody phage display has allowed the isolation of human antibodies recognizing a range of different antigens, including cell surface-expressed tumor antigens. Antibodies have been selected by panning phage libraries against purified antigens (Clark et al.,

*Abbreviations:* DAB, diaminobenzine tetrahydrochloride;; HRP, horseradish peroxidase; i.v., intravenous; PEG, polyethylene glycol; PMSF, phenylmethylsulphonylfluoride; TU, transducing unit

* Corresponding author. Department of Medical Oncology, St. Vincent's Hospital, Darlinghurst, NSW 2010, Australia. Tel.: +61-2-92958412; Fax: +61-2-92958451; E-mail: r.ward@garvan.unsw.edu.au

0022-1759/99/$ - see front matter 
PII: S0022-1759(99)00044-7

1997; Desai et al., 1998) or against whole tumor cells (Cai and Garen, 1995; Pereira et al., 1997; Figini et al., 1998). The clinical application of these tumor-specific antibodies will depend on their ability to target tumor in vivo. Unfortunately, numerous studies have failed to demonstrate a correlation between the in vitro binding characteristics of antibodies and their in vivo tumor targeting properties (Matzku et al., 1987; Andrew et al., 1990; Boerman et al., 1990; Shockley et al., 1992b). Parameters such as antigen expression level and accessibility, as well as tumor physiology, have a profound influence on in vivo antibody targeting (Jain, 1990; Shockley et al., 1992a; Sung et al., 1992), yet these parameters cannot easily be predicted by in vitro studies.

Recently, peptides that selectively localize to the vasculature of various tissues have been isolated by the in vivo panning of random peptide libraries in mice (Pasqualini and Ruoslahti, 1996; Rajotte et al., 1998). This approach has considerable potential in the isolation of antibodies with good in vivo targeting properties. In particular, panning phage displayed Fab libraries in live animals may allow the identification of antibodies that recognize biologically relevant tumor targets, and may also facilitate the discovery of novel surface tumor antigens.

The successful application of in vivo panning to the isolation of tumor specific antibodies must inevitably be predicated on an understanding of the pharmacokinetics of phage-Fab. This includes a knowledge of the biodistribution of phage in different tissues, their clearance from the circulation, and their capacity for extravasation into the interstitial compartment. An understanding of the last point is of particular importance in those studies seeking to isolate Fab with reactivity against extravascular antigens. To gain a better understanding of these parameters, we have investigated the pattern of distribution of phage-Fab in nude mice.

## 2. Materials and methods

### 2.1. Balb/c nude mice

Six to eight week old female Balb/c nude mice were purchased from Animal Resource Centre (Canning Vale, Western Australia), and were held in micro-isolators. All experiments were conducted with the approval of the Institutional Animal Experimentation Ethics Committee.

### 2.2. Amplification of phage from single colony

The Fab region of the chimeric anti-colon cancer antibody c30.6 (Mount et al., 1994) was PCR amplified and cloned into the MCO1 phage display vector (Ward et al., 1996). The nucleotide sequence of the antibody was verified by dideoxy-sequencing. A single *E. coli* XL1-Blue colony harbouring the c30.6 clone was grown overnight at 37°C in 2YT supplemented with 50 μg/ml carbenicillin, 10 μg/ml tetracycline and 2% glucose (2YT/carb/tet/glu). The overnight culture (1 ml) was inoculated into 100 ml fresh 2YT/carb/tet/glu and grown for 3 h at 37°C with shaking. VCSM13 helper phage ($5 \times 10^{11}$) were added and the culture was incubated for an additional 2 h at 37°C with shaking. Cells were pelleted at $1600 \times g$, resuspended in 100 ml fresh 2YT/carb/tet containing 70 μg/ml kanamycin and grown overnight with shaking at 30°C. The next day, cells were pelleted at $6000 \times g$ and the phage in the supernatant were precipitated at 4°C with 1/5 volume 20% PEG 6000/2.5 M NaCl. Phage were pelleted by centrifugation at $10{,}000 \times g$ and resuspended in PBS to a final concentration of $10^{14}$ TU/ml.

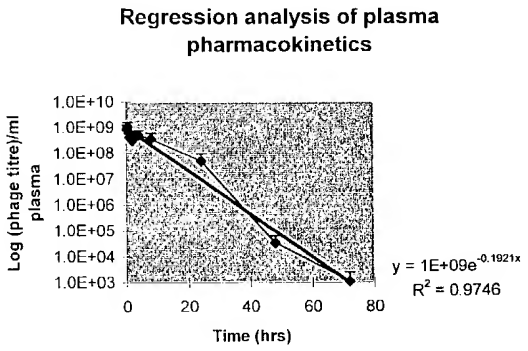


Fig. 1. Plasma pharmacokinetics of phage c30.6 in nude mice injected with $1 \times 10^9$ TU. The mean phage titre at each time point in three mice is shown together with S.E.

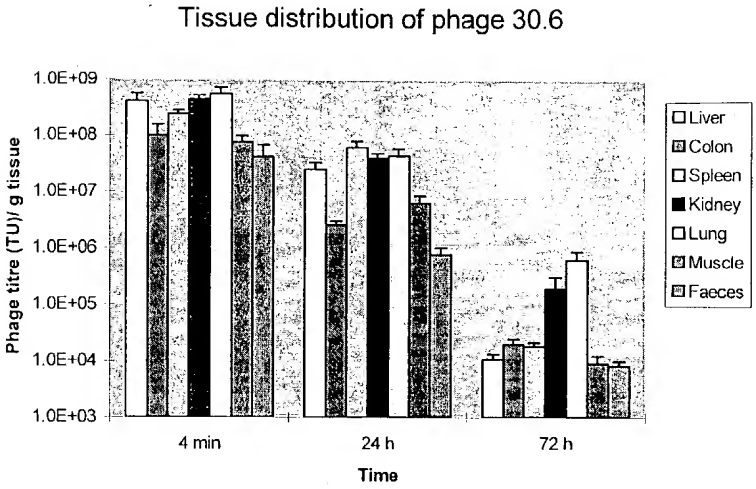


Fig. 2. Distribution of phage in tissues after 4 min, 24 h and 72 h following i.v. injection of $1 \times 10^9$ TU of phage c30.6. Values expressed as phage transducing unit (TU) per gram of tissue. Bars represent standard error (S.E.)

### 2.3. Calculation of plasma kinetic data

Three groups of three nude mice were injected i.v. with $1 \times 10^9$ c30.6 phage in a volume of 100 μl PBS. Blood samples were taken from the first group of mice at 4 min, 30 min, 1 h; from the second group of mice at 2 h, 4 h, 8 h; and from the third group of mice at 24 h, 48 h and 72 h. A 50 μl aliquot of plasma was incubated with 1 ml of log phase *E. coli* XL1-Blue for 30 min at 37°C without shaking. Following the addition of 10 ml of LB supplemented with 20 μg/ml carbenicillin, the cultures were incubated for another 1 h with shaking. Various dilutions of the culture were plated in duplicate on LB agar supplemented with 10 μg/ml carbenicillin and phage titres were determined by colony counting. Log percentage of initial injected phage was plotted against time, and assessed by regression analysis. The half-life ($t_{1/2}$) of the phage and the volume of distribution ($V_d$) were calculated using standard methods (Welling, 1986).

### 2.4. Quantitative distribution study of phage in mouse tissues

Three groups of four nude mice were injected i.v. with $1 \times 10^9$ c30.6 phage in a volume of 100 μl PBS. Mice were sacrificed at 4 min, 24 h and 72 h after injection. Faeces and normal tissues (liver, colon, spleen, kidneys, lungs, skeletal muscle) were weighed and assayed for the presence of infective phage. Tissues were ground into fine pieces in 1 ml of DMEM (Trace Biosciences, NSW, Australia) supplemented with 1 mM PMSF and protease inhibitor cocktail tablet (Boehringer Mannheim, NSW, Australia) (DMEM-PI). The mixture was clarified by centrifugation at $2000 \times g$ and the supernatant was kept for phage titering. The tissue pellets were washed three times in 3 ml of DMEM-PI supplemented with 0.1% BSA, and resuspended in 1 ml 0.1 M glycine pH 3.0 for 10 min at room temperature. This solution was neutralized with 1/10 volume of 1 M Tris pH 8.0 prior to centrifugation. Aliquots from

Table 1
Tissue to blood ratio of phage c30.6 at various time points

| | Liver | Colon | Spleen | Kidneys | Lungs | Muscle | Faeces | Plasma |
|---|---|---|---|---|---|---|---|---|
| 4 min | 0.23 | 0.06 | 0.13 | 0.25 | 0.31 | 0.04 | 0.00 | 1 |
| 24 h | 0.07 | 0.01 | 0.16 | 0.10 | 0.12 | 0.02 | 0.00 | 1 |
| 72 h | 5.0 | 9.1 | 8.2 | 86.4 | 286 | 4.1 | 3.8 | 1 |

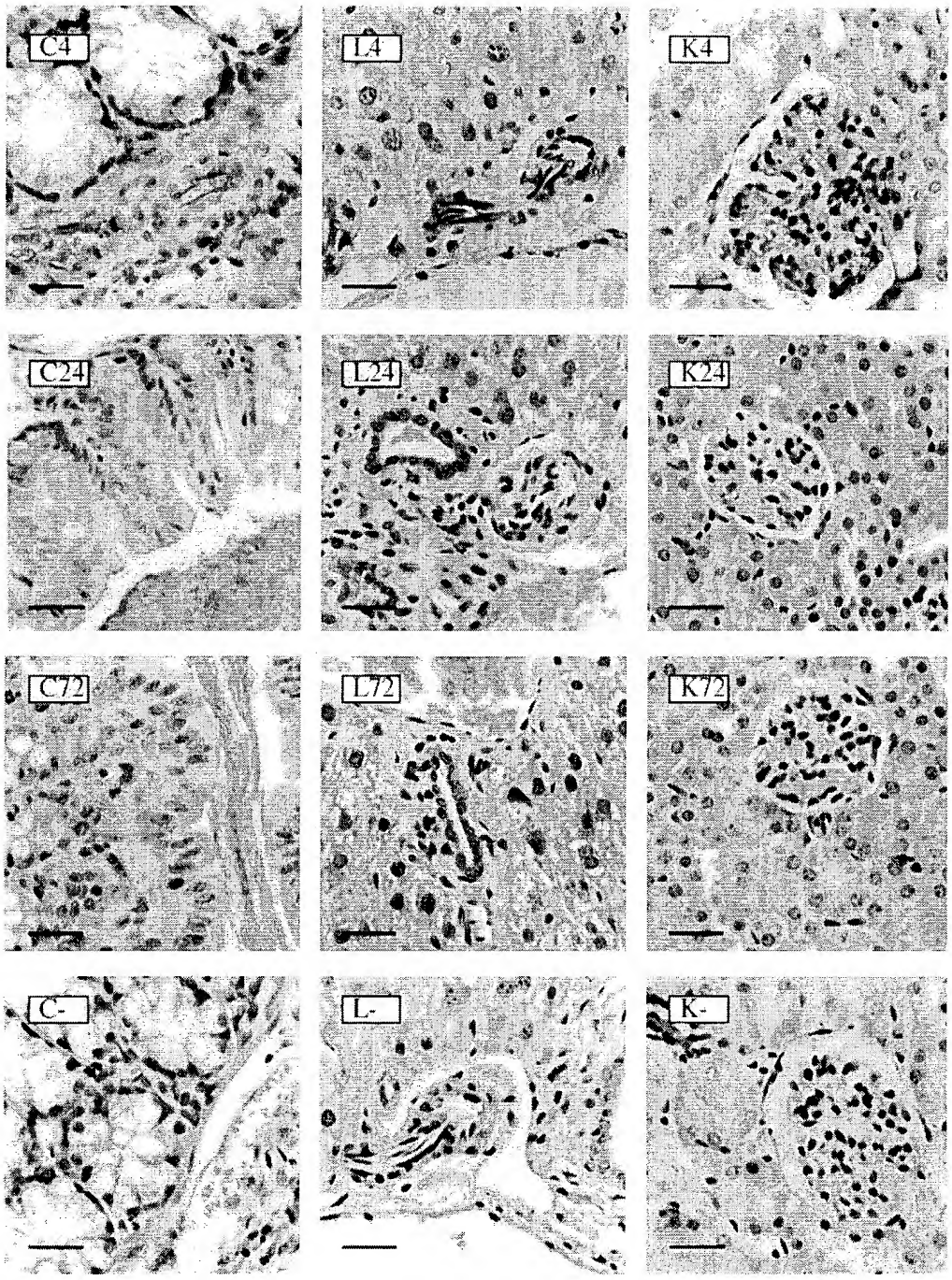


Fig. 3. Immunohistochemical staining of mouse tissue sections (C = colon, L = liver, K = kidney) after i.v. injection of phage c30.6 (4 = 4 min, 24 = 24 h, 72 = 72 h). Tissue sections were stained with a sheep anti-M13 antibody followed by a secondary HRP-conjugated donkey anti-sheep antibody. Negative controls (−) were stained with the HRP-conjugated donkey anti-sheep antibody only. Bar represents 50 μm.

the supernatant, washes and glycine elution were used to infect 1 ml of log phase XL1-Blue for 30 min at 37°C with no shaking, and phage titres determined as described above.

### 2.5. Immunohistochemical staining of mouse tissue sections

Paraffin-embedded tissue sections were prepared from mice injected with phage. The sections were dewaxed, rehydrated and endogenous peroxidase activity was blocked with 3% $H_2O_2/H_2O$ for 5 min at room temperature. The sections were then blocked with normal rabbit serum for 1 h at 37°C, and incubated with 10 μg/ml sheep anti-M13 (Pharmacia Biotech, NSW, Australia) in 2% BSA/TBS. Following one wash in TBS for 5 min, donkey anti-sheep-HRP (2 μg/ml; Jackson ImmunoResearch, NSW, Australia) in 2% BSA/TBS was applied to the sections for 1 h at room temperature. Bound secondary antibody was detected by incubation with DAB substrate (Sigma, NSW, Australia), and sections were counterstained in Harris hematoxylin, dehydrated and mounted. All sections were assessed by two of the authors (NJH, YLY).

## 3. Results

### 3.1. Distribution of phage-Fab in plasma and tissue

The phage titres in the plasma at different time points were determined and log percentage of initial injected phage was plotted against time (Fig. 1). By using regression analysis it was determined that the half-life of phage in plasma was 3.6 h and the volume of distribution was 1.0 ml.

Titres of phage were determined in supernatant, washes and glycine elution of each tissue. At all time points, nearly all phage (90%) were recovered from the supernatant of ground tissues. Only 10% of the phage were found in the washes and 0.1% were isolated from the glycine elution. On this basis, supernatants were used in all subsequent assessments of the phage biodistribution (Fig. 2).

At 4 min and 24 h, phage were found predominantly in the liver, spleen, kidneys and lungs. Phage concentrations in colon, muscle and faeces were approximately one order of magnitude lower at those time points. At 72 h, the remaining phage had accumulated in the lungs and kidneys, and few phage ($< 10^4$ TU) were recovered from other tissues. In all tissues, the tissue:blood ratio of phage c30.6 was less than 1.0 at both 4 min and 24 h, indicating that phage were primarily found in the plasma at these times (Table 1). At 72 h, the tissue:blood ratio was greater than 1.0 in all tissues examined. Few phage were left in plasma suggesting that phage had been cleared from the circulation. At this time point, phage had accumulated mostly in the lungs (ratio = 286) and kidneys (ratio = 86).

### 3.2. Immunohistochemical analysis of phage distribution

Tissues collected at 4 min, 24 h and 72 h were embedded in paraffin, and 5 μm sections were stained with a sheep anti-M13 antibody. At 4 min, there was distinct staining of the lumenal surface of the capillary endothelium in all organs examined (Fig. 3). In particular, intense staining was found within the glomerular capillary loops at 4 min. No evidence of tissue uptake was found at this time point. At 24 h, however, phage were found to have left the vascular compartment, and were present in the parenchyma of liver, the red pulp of spleen, the pulmonary interstitium, the proximal convoluted tubules of kidneys and in faeces. No staining was found in the bowel wall or in skeletal muscle. At 72 h, the pattern of staining remained essentially unchanged from 24 h for all tissue sections, although the intensity of staining was reduced.

## 4. Discussion

In vivo panning represents a significant new application of phage display technology, with the panning steps moving from an in vitro system to a dynamic system dependent on circulation within a viable organism. The strategy involves the injection of phage into a mouse, with recovery from tissues followed by reamplification in vitro, and finally, the injection of amplified phage into a second mouse (Pasqualini and Ruoslahti, 1996). To fully realize the potential of this approach, a number of technical questions must be answered, and in particular, the

most appropriate time for tissue collection must be determined. Our study focused on the temporal distribution of phage-Fab in nude mice. These animals were chosen since they are routinely used in preclinical studies of antibody tumor targeting. The experiments were also performed with a monoclonal phage population (phage c30.6) known to have no specific activity against mouse tissues. Because of this, phage titres found in different organs could be expected to represent the background titres in the first round of an actual panning experiment, where only a tiny proportion of specific binding phage-Fab are present in the library.

The distribution of phage-Fab in normal tissues over time shows two main patterns. In one group of tissues, which includes liver, spleen, kidneys and lungs, the uptake of phage at 4 min and at 24 h was significantly greater than that seen in colon and skeletal muscle (Fig. 2). At 4 min, this difference could in part be due to the higher perfusion and capillary permeability of the liver, lungs and kidneys when compared with colon and skeletal muscle (Covell et al., 1986). At 24 h, the number of phage recovered from each organ was decreased by 10-fold but the pattern of distribution remained essentially unchanged, with a slightly lower tissue:blood ratio than at 4 min (Fig. 2 and Table 1). This suggests that while phage were nearly all distributed by 4 min, the majority of phage-Fab was still in the tissue blood volume during the first 24 h. Following distribution of phage, it is expected that normal blood flow would wash away non-specific or low affinity phage, thus mimicking the washing steps of in vitro panning. At 72 h, phage were eliminated from the circulation, and thus those remaining in the tissues represented extravasated and trapped phage. The distribution of phage was also influenced by the normal structure and function of individual organs. Not unexpectedly, high phage uptake was found in the liver, lungs and spleen because of uptake into the reticulo-endothelium system, a finding also reported by Pasqualini et al. (1997).

A further factor which clearly influenced the tissue distribution of phage-Fab was their size. The filamentous phage M13 are shaped like flexible filaments with a diameter of 65 Å and a length of 9300 Å (Glucksman et al., 1992), whilst the dimension of the Fab they display is 80 Å × 50 Å × 40 Å (Poljak et al., 1973). As such, it is likely that the extravasation of phage would be restricted by the continuous endothelium of capillaries in tissues such as skeletal muscle, skin, connective tissues and brain (Clough, 1991). However, in organs such as liver, spleen, lungs and kidneys, immunohistochemical staining demonstrated that phage extravasation occurred by 24 h. The vasculature of the liver and spleen are discontinuous and contain open fenestrae (600 Å in diameter) backed by a discontinuous basement membrane (Clough, 1991). The extravasation of phage in these tissues is likely to occur through this route. Thus the ability of phage to extravasate is related not only to the circulation time, but also to the ultrastructure of the vasculature in different tissues. Given the heterogeneous and leaky nature of the tumor vasculature (Dvorak et al., 1988), it is possible that by 24 h, phage may extravasate into the tumor interstitium, although high tumor interstitial pressure may reduce the penetration of phage-Fab (Jain, 1990).

Our study suggests that in nude mice, phage are largely eliminated by both hepatic and renal excretion. The phage are probably filtered through the glomeruli (strongly stained at 4 min) and enter the proximal convoluted tubule by 24 h. While there was strong immunohistochemical staining of faeces by 24 h, the phage titres were low at this time point. This suggests that the majority of staining in faeces was due to the presence of phage protein fragments, probably following elimination in bile. Immunohistochemical detection of phage clearly does not necessarily indicate the presence of intact phage. However, with the exception of faeces, positive immunohistochemical staining in tissues was found to correlate closely with phage infectivity.

Since the c30.6 Fab displayed on the surface of the phage does not bind to normal mouse tissues (Mount et al., 1994), the biodistribution pattern we found in this study should be applicable to any phage-Fab population. This was verified by conducting similar experiments with phage displaying Fab reactive with tetanus toxoid and with Fabs against human carcinoembryonic antigen which are known to be non reactive with mouse tissue. In both cases, a similar distribution pattern was observed (results not shown).

In conclusion, our study provides basic pharmacokinetic data relevant to the design of in vivo

panning experiments. It is clear that the timing of phage retrieval will be influenced both by the organ being examined and the specific location of the target antigen in relation to the microvasculature. While 4 min appears to be the best time point for the isolation of Fab against intravascular antigens, the 24 h or the 72 h time points may prove superior for the isolation of antibodies against extravascular antigens. A disadvantage of the 72 h time point is the low phage titre which may be insufficient for subsequent panning rounds. The future studies will therefore involve the panning of an antibody library in tumor-bearing nude mice using 24 h as a time point for tissue collection.

## Acknowledgements

The authors wish to thank A/Prof. Ken Williams, St Vincent's Hospital, and Dr. Andrew McLachlan, University of Sydney, for valuable discussions regarding the pharmacokinetics of phage in mice. Yum L Yip is the recipient of the Australian Postgraduate Award.

## References

Andrew, S.M., Johnstone, R.W., Russell, S.M., McKenzie, I.F., Pietersz, G.A., 1990. Comparison of in vitro cell binding characteristics of four monoclonal antibodies and their individual tumor localization properties in mice. Cancer Res. 50, 4423.

Boerman, O., Massuger, L., Makkink, K., Thomas, C., Kenemans, P., Poels, L., 1990. Comparative in vitro binding characteristics and biodistribution in tumor-bearing athymic mice of anti-ovarian carcinoma monoclonal antibodies. Anticancer Res. 10, 1289.

Cai, X., Garen, A., 1995. Anti-melanoma antibodies from melanoma patients immunized with genetically modified autologous tumor cells: selection of specific antibodies from single-chain Fv fusion phage libraries. Proc. Natl. Acad. Sci. USA 92, 6537.

Clark, M.A., Hawkins, N.J., Papaioannou, A., Fiddes, R.J., Ward, R.L., 1997. Isolation of human anti-c-erbB-2 Fabs from a lymph node-derived phage display library. Clin. Exp. Immunol. 109, 166.

Clough, G., 1991. Relationship between microvascular permeability and ultrastructure. Prog. Biophys. Mol. Biol. 55, 47.

Covell, D.G., Barbet, J., Holton, O.D., Black, C.D., Parker, R.J., Weinstein, J.N., 1986. Pharmacokinetics of monoclonal immunoglobulin G1, F(ab')2, and Fab' in mice. Cancer Res. 46, 3969.

Desai, S.A., Wang, X., Noronha, E.J., Kageshita, T., Ferrone, S., 1998. Characterization of human anti-high molecular weight-melanoma-associated antigen single-chain Fv fragments isolated from a phage display antibody library. Cancer Res. 58, 2417.

Dvorak, H.F., Nagy, J.A., Dvorak, J.T., Dvorak, A.M., 1988. Identification and characterization of the blood vessels of solid tumors that are leaky to circulating macromolecules. Am. J. Pathol. 133, 95.

Figini, M., Obici, L., Mezzanzanica, D., Griffiths, A., Colnaghi, M.I., Winter, G., Canevari, S., 1998. Panning phage antibody libraries on cells: isolation of human Fab fragments against ovarian carcinoma using guided selection. Cancer Res. 58, 991.

Glucksman, M.J., Bhattacharjee, S., Makowski, L., 1992. Three-dimensional structure of a cloning vector. X-ray diffraction studies of filamentous bacteriophage M13 at 7 Å resolution. J. Mol. Biol. 226, 455.

Jain, R.K., 1990. Physiological barriers to delivery of monoclonal antibodies and other macromolecules in tumors. Cancer Res. 50, 814s.

Matzku, S., Bruggen, J., Brocker, E.B., Sorg, C., 1987. Criteria for selecting monoclonal antibodies with respect to accumulation in melanoma tissue. Cancer Immunol. Immunother. 24, 151.

Mount, P.F., Sutton, V.R., Li, W., Burgess, J., McKenzie, I.F.C., Pietersz, G.A., Trapani, J.A., 1994. Chimeric (mouse/human) anti-colon cancer antibody c30.6 inhibits the growth of human colorectal cancer xenografts in *scid/scid* mice. Cancer Res. 54, 6160.

Pasqualini, R., Ruoslahti, E., 1996. Organ targeting in vivo using phage display peptide libraries. Nature 380, 364.

Pasqualini, R., Koivunen, E., Ruoslahti, E., 1997. Alpha v integrins as receptors for tumor targeting by circulating ligands. Nature Biotechnol. 15, 542.

Pereira, S., Maruyama, H., Siegel, D., Van Belle, P., Elder, D., Curtis, P., Herlyn, D., 1997. A model system for detection and isolation of a tumor cell surface antigen using antibody phage display. J. Immunol. Methods 203, 11.

Poljak, R.J., Amzel, L.M., Avey, H.P., Chen, B.L., Phizackerley, R.P., Saul, F., 1973. Three-dimensional structure of the Fab' fragment of a human immunoglobulin at 2.8-Å resolution. Proc. Natl. Acad. Sci. USA 70, 3305.

Rajotte, D., Arap, W., Hagedorn, M., Koivunen, E., Pasqualini, R., Ruoslahti, E., 1998. Molecular heterogeneity of the vascular endothelium revealed by in vivo phage display. J. Clin. Invest. 102, 430.

Shockley, T.R., Lin, K., Nagy, J.A., Tompkins, R.J., Yarmush, M.L., Dvorak, H.F., 1992a. Spatial distribution of tumor-specific monoclonal antibodies in human melanoma xenografts. Cancer Res. 52, 367.

Shockley, T.R., Lin, K., Sung, C., Nagy, J.A., Tompkins, R.J., Dedrick, R.L., Dvorak, H.F., Yarmush, M.L., 1992b. A quantitative analysis of tumor specific monoclonal antibody uptake by human melanoma xenografts: effects of antibody immuno-

logical properties and tumor antigen expression levels. Cancer Res. 52, 357.

Sung, C., Shockley, T.R., Morrison, P.F., Dvorak, H.F., Yarmush, M.L., Dedrick, R.L., 1992. Predicted and observed effects of antibody affinity and antigen density on monoclonal antibody uptake in solid tumors. Cancer Res. 52, 377.

Ward, R.L., Clark, M.A., Lees, J., Hawkins, N.J., 1996. Retrieval of human antibodies from phage-display libraries using enzymatic cleavage. J. Immunol. Methods 189, 73.

Welling, R.G., 1986. Pharmacokinetics: process and mathematics. Am. Chem. Soc. Monogr. 185, 213.

STIC ILL

5/1185

**From:** Davis, Minh-Tam
**Sent:** Wednesday, September 15, 2004 3:39 PM
**To:** STIC-ILL
**Subject:** Reprint request for 09/721864

NPL ___ Adonis ___
MIC ___ BioTech ___ MAIN ___
NO ___ Vol NO ___ NOS ___
Ck Cite ___ Dupl Request ___
Call # ___
9/15 VD

1) 07821600 PMID: 3390350
Uptake of indium-111-labeled monoclonal antibody ZME-018 as a function of tumor size in a patient with melanoma.
Macey D J; Denardo S J; Denardo G L; Goodnight J K; Unger M W
Department of Radiology, University of California Davis Medical Center, Sacramento 95817.
American journal of physiologic imaging (UNITED STATES) 1988, 3 (1) p1-6, ISSN 0885-8276 Journal Code: 8610225

2) Rapid imaging of human melanoma xenografts using an scFv fragment of the human monoclonal antibody H11 labelled with 111In.
Reilly R M; Maiti P K; Kiarash R; Prashar A K; Fast D G; Entwistle J; Dan ; Narang S A; Foote S; Kaplan H A
Division of Nuclear Medicine, Toronto General Hospital, University Health Network, ON, Canada. raymond.reilly@utoronto.ca
Nuclear medicine communications (England) May 2001, 22 (5) p587-95, ISSN 0143-3636 Journal Code: 8201017

3) Treatment-related parameters predicting efficacy of Lym-1 radioimmunotherapy in patients with B-lymphocytic malignancies.
Lamborn K R; DeNardo G L; DeNardo S J; Goldstein D S; Shen S; Larkin E C; Kroger L A
Brain Tumor Research Center, Department of Neurological Surgery, University of California San Francisco Medical Center, San Francisco, California 94143, USA.
Clinical cancer research - an official journal of the American Association for Cancer Research (UNITED STATES) Aug 1997, 3 (8) p1253-60, ISSN 1078-0432 Journal Code: 9502500

4) 4368891 PMID: 10365793
Biodistribution of filamentous phage-Fab in nude mice.
Yip Y L; Hawkins N J; Smith G; Ward R L
School of Medicine (St. Vincent's Hospital), University of NSW, Sydney, Australia.
Journal of immunological methods (NETHERLANDS) May 27 1999, 225 (1-2) p171-8, ISSN 0022-1759 Journal Code: 1305440

5) Radiolabeling, biodistribution, and dosimetry of (123)I-mAb 14C5: a new mAb for radioimmunodetection of tumor growth and metastasis in vivo.
Lahorte Christophe M M; Bacher Klaus; Burvenich Ingrid; Coene Elisabeth D ; Cuvelier Claude; De Potter Christian; Thierens Hubert; Van de Wiele Christophe; Dierckx Rudi A; Slegers Guido
Department of Radiopharmacy, Faculty of Pharmaceutical Sciences, Gent University, Gent, Belgium. christophe.lahorte@ugent.be
Journal of nuclear medicine - official publication, Society of Nuclear Medicine (United States) Jun 2004, 45 (6) p1065-73, ISSN 0161-5505 Journal Code: 0217410

Thank you
MINH TAM DAVIS
ART UNIT 1642, ROOM 3A24, MB 3C18
272-0830

1 2 3 4 5

AMERICAN JOURNAL OF PHYSIOLOGIC IMAGING 3:1–6 (1988)

# Uptake of Indium-111-Labeled Monoclonal Antibody ZME-018 as a Function of Tumor Size in a Patient With Melanoma

DANIEL J. MACEY, PhD, SALLY J. DENARDO, MD, GERALD L. DENARDO, MD, JAMES K. GOODNIGHT, MD, and MICHAEL W. UNGER, PhD

*Departments of Radiology (D.J.M., S.J.D., G.L.D.), Internal Medicine (G.L.D.), and Surgery (J.K.G.), University of California Davis Medical Center, Sacramento, California 95817; Hybritech Inc. (M.W.U.), San Diego, California 92121*

ABSTRACT **The accumulation of an Indium-111-labeled monoclonal antibody (MoAb), ZME-018, in melanoma tumors in a patient was determined by sequential, quantitative gamma camera imaging. The amount and concentration of In-111 in each tumor changed in a characteristic pattern with time, reaching a peak at day 3 followed by a steady clearance. The concentration of In-111 in the tumor and the ratios of tumor to whole-body or blood decreased as the size of the tumor increased. These results were interpreted to indicate that the fraction of active, perfused tumor decreased as the melanoma lesions increased in size. The maximum number of MoAb molecules bound per melanoma cell was calculated to be abut 35,000. The implications of these observations for radioimmunoimaging and therapy are significant.**

**Key words: Necrotic tumor fraction, antibody quantitation, melanoma antigen in vivo, In-111 antibody dosimetry, pharmacokinetics of antibody**

## INTRODUCTION

Studies of osteosarcoma xenografts in nude mice have indicated that the amount of Indium-111-labeled monoclonal antibody (MoAb) 791T/36 increased linearly as a function of tumor size for tumors in the range 0.2–0.8 g, implying that the concentration of this MoAb was independent of size over this range [1]. In a study of human tumors implanted in nude mice the concentrations of several radiolabeled MoAbs decreased as the tumor size increased in the range 0.03–1.6 g [2]. This characteristic was independent of the MoAb and the target antigen. These apparently contradictory results may reflect observations that the MoAb uptake in a tumor depends on many factors including differences in blood flow and the amount of necrosis, levels of circulating antigen, and species specificity [3,4], so that their relevance to tumors in patients is not obvious.

In the present report, the amount and concentration of radiolabeled anti-melanoma MoAb ZME-018 in melanoma in a patient were found to depend on tumor size. The implications of this observation for radioimmunoimaging and radioimmunotherapy are significant.

## MATERIALS AND METHODS

### Radiopharmaceutical

The In-111 ZME-018 was supplied by Hybritech Inc.[1] This IgG2a MoAb was obtained by immunizing BALB/c mice with a melanoma cell line M21 [5]. The antibody was purified by fractionation and chromatography of ascites. The target antigen of ZME-018 is a high molecular weight glycoprotein of 240 kD.

One milligram of the MoAb ZME-018 was labeled with 4 mCi of In-111 using a modification of the Krejcarek technique [6]. Excess diethylene triamine pentaacetic acid (DTPA) was added to chelate any unbound In-111. Nineteen milligrams of unlabeled MoAb was then added, and the preparation was diluted with 60 ml of saline. A labeling efficiency of 86% was achieved, and the remaining In-111 was present as In-111 DTPA. The radiopharmaceutical eluted on high-performance liquid chromatography (HPLC) TSK 3000 as a major peak at 150 kD and a minor In-111-DTPA peak. The immunoreactivity of the radiopharmaceutical was 75%. The radiopharmaceutical was assayed with a Capintec

[1]Hybritech Inc., San Diego.

This work was supported by the Department of Energy Grant #DE FG03-84ER60233.

Received October 26, 1987; accepted November 13, 1987.

Address reprint requests to Gerald L. DeNardo, M.D., Section of Radiodiagnosis and Therapy, University of California Davis Medical Center, 4301 X Street, FOLB II-e, Sacramento, CA 95817.

dose calibrator and was verified by counting the dose with a gamma camera of known sensitivity for In-111. The radiopharmaceutical was administered intravenously to the patient over 30 minutes. The dose was corrected for the residue in the syringe and calculated to be 3.84 mCi.

### Imaging

A large-field-of-view gamma camera with a 300-kev collimator was used for imaging. Energy discrimination with 20% windows on each of the 173- and 246-kev photons of In-111 was used. The camera was interfaced to a computer system, and all images were acquired in a 128 × 128 word mode matrix for data analysis using a light pen to define manually regions of interest (ROI). The static images were terminated by the first of either 1 million counts or 600 s. Anterior and posterior images of the whole body (WBS) were acquired immediately after administration of the labeled MoAb. Analogous, conjugate images of the head, chest, abdomen, pelvis, and thigh regions were then acquired. Conjugate WBS and static images were also acquired at 1, 3, 6, 7, and 9 days. A dual laser system was used with marks drawn on the patient's skin to reposition the patient.

### Quantitation of tumor and organ uptake

The images on day 1 and subsequent days indicated 20 focal areas of tumor uptake in this patient with histologically proven malignant melanoma. Several areas of uptake were noted in the anterior pelvic and upper thigh areas. Four of these areas corresponded to superficial tumors of approximately spherical shape. These tumors were chosen for study because their diameters could be measured with calipers and their In-111 content could be quantitated accurately from the geometry of counting small volume sources. Irregular ROIs were drawn manually with a light pen on the anterior image of the pelvis to outline each of the lesions and a corresponding mirrored background ROI on the contralateral side of the patient (Fig. 1). The counts from each tumor after background subtraction were converted to microcuries using a sensitivity measured with a 10-ml volume of In-111 solution. This method of quantitation had been validated by comparing the gamma camera counts of a superficial melanoma from another patient before and after excision, and the agreement was found to be within 10%. The concentration of MoAb in each tumor was calculated assuming uniform distribution of the MoAb and was converted to percentage injected dose (%ID), microcuries per gram ($\mu$Ci/g) or %ID per gram (%ID/g).

Assuming the molecular weight of the ZME-018 MoAb molecule to be 150 kD, the maximum number of MoAb molecules and In-111 atoms per melanoma cell was calculated from the uptake data for the 2.8-g tumor (Appendix).

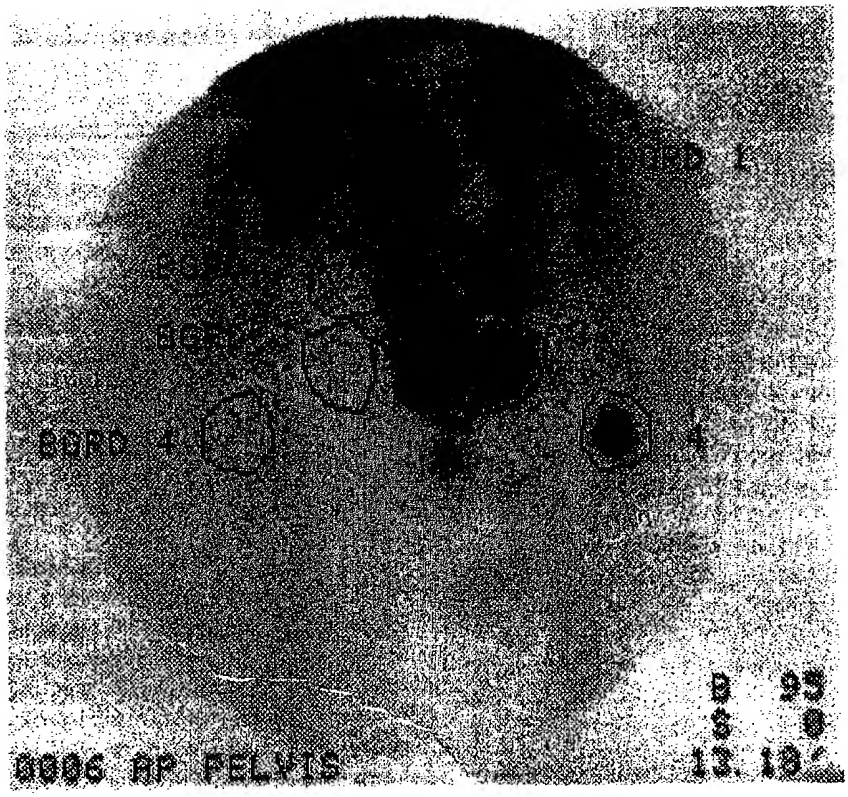


Fig. 1. Anterior image of the pelvic region of the patient was obtained 1 day after injection of In-111 ZME-018. Regions of interest were drawn to define the four melanoma sites and the appropriate mirror-image background region for each tumor. Note the difference in background with position on the body. The uptake between tumor 3 and background region 3 is in the scrotum.

### Liver and spleen uptake

The uptake of MoAb in the liver was measured by converting the number of counts within an irregular ROI drawn on the anterior image to microcurie content using a measured sensitivity derived from a liver volume filled with In-111 in an abdominal phantom.[2] No background subtraction was used because phantom studies indicated that background subtraction led to significant underestimates of the total radionuclide content [7].

The posterior image was used to quantitate MoAb uptake in the spleen. Background subtraction was used in this case to remove the contribution of surrounding radioactivity detected in a ROI. The effective depth of the spleen was measured as the distance of the centroid of this organ from the posterior wall of the abdomen on X-ray computed axial tomographic images. A linear attenuation coefficient (LAC) of 0.125/cm was derived from the counts detected from a small source of In-111 imaged at the effective splenic depth of 7 cm in water. A first-order attenuation correction factor was used to correct the spleen counts to obtain radionuclide content and %ID.

### Whole-body retention

The geometric mean (GM) of the number of counts in anterior and posterior conjugate views of the whole body was used to determine the whole-body retention. The geometric mean of counts in subsequent, conjugate views was expressed as a percentage of the geometric mean of counts in the immediate WBS images.

### Blood retention and cumulated urine

Whole-blood and urine samples were counted with a NaI well detector. A standard of measured activity prepared from the radiopharmaceutical dose was used to convert the blood and urine counts to %ID. The blood volume was assumed to be 7.5% of body weight [8].

### Target-to-nontarget ratios

The concentration of MoAb in each tumor was calculated from the decay-corrected uptake and tumor volume. The whole-body retention was used to calculate the nontarget MoAb concentration per unit mass on each day. For each day the ratio of the concentration of MoAb in the tumor to that of the whole body was derived from the relationship

$$\frac{\text{Tumor}}{\text{Whole Body}} = \frac{\text{Tumor Concentration as \%ID/g}}{\text{Whole-Body Concentration as \%ID/g}}$$

The ratio of MoAb concentration in each tumor to that of the blood on each imaging day was calculated from the relationship

$$\frac{\text{Tumor}}{\text{Blood}} = \frac{\text{Tumor Concentration as \%ID/g}}{\text{Whole-Blood Retention as \%ID/g}}$$

These ratios assume correctly that the total tumor uptake of MoAb is a small fraction of the administered dose.

[2]Alderson abdominal phantom with liver and spleen.

### "Necrotic" fraction

Large tumors are known to contain ischemic and necrotic tissue. An attempt to predict this fraction in tumors was made using two assumptions for the accumulation of MoAb. First, the smallest tumor (2.8 g) was assumed to contain only active melanoma tissue with a uniform distribution of the MoAb. Second, all the larger tumors were assumed to contain both "active" and "necrotic" tissue, and their active fraction was assumed to accumulate MoAb at the same concentration as the small tumor. The active volume (ATV) in ml for any tumor was defined as

$$\text{ATV} = \frac{\text{MoAb Uptake in Large Tumor}}{\text{MoAb Uptake in 2.8-g Tumor}}$$

Therefore, the fraction of necrosis in the larger tumors of measured volume (MV) is given by f where

$$f = (MV - ATV)/MV$$

$$\text{or} \quad ATV = MV(1 - f)$$

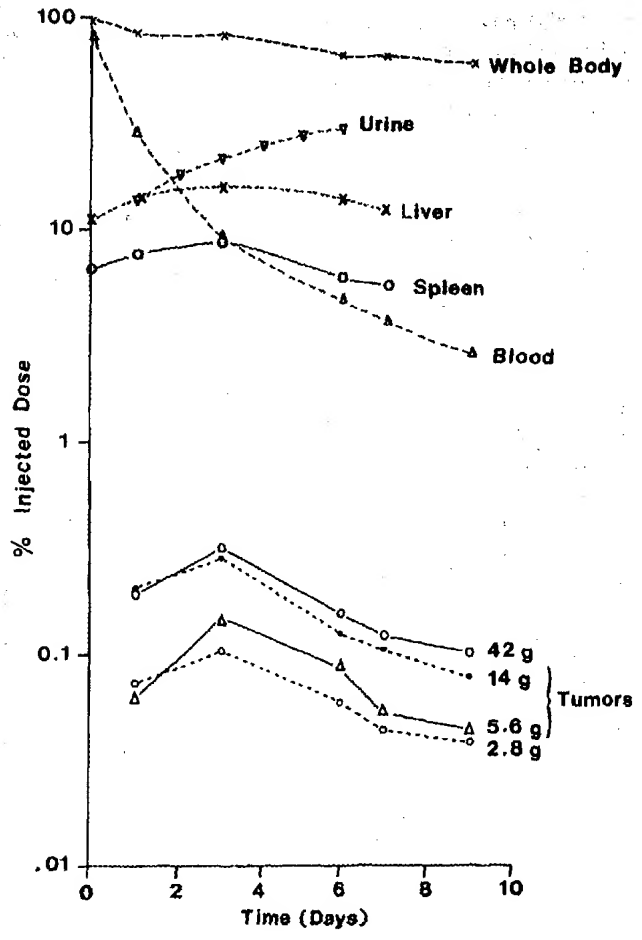


Fig. 2. Change in the amount of In-111 in the tumors, whole body, blood volume, liver, and spleen with time. Cumulative urinary excretion is also shown.

These equations were used to predict the active and necrotic fractions in the larger melanoma tumors.

## RESULTS

Clearance of In-111 from the body during the first 24 h corresponded to the In-111 in the radiopharmaceutical that was not bound to the MoAb (Fig. 2). The biologic half-time for clearance from the patient after the first 24 h was 18 days and corresponded to the reciprocal of urinary clearance. After a steady accumulation to day 3, In-111 in the liver and spleen was slowly cleared in parallel to that of the whole body.

The concentration of In-111 in each of the tumors increased to a peak at day 3 and was followed by a constant clearance (Fig. 3A). The concentration of In-111 decreased with increase in tumor size (Fig. 3B). The ratio of In-111 concentration in each tumor to the corresponding whole-body concentration on each day increased and decreased in a characteristic pattern (Fig. 4A). The peak tumor-to-whole-body concentration ratio ranged from 37 to 7.2 on day 3 for the 2.8 g and 41.6 g tumors, respectively. In contrast, the ratio of MoAb concentration in each tumor to the corresponding blood concentration increased to day 3 followed by little change to day 9 (Fig.4B).

The ratio of the peak MoAb concentration attained in each tumor to the whole-body retention measured on the same day decreased markedly with increase in tumor size (Fig. 5A) and tumor surface area (Fig. 5B). The calculated fractions of "active" and "necrotic" tissue for each tumor changed markedly with increase in tumor size (Fig. 6).

## DISCUSSION

These studies demonstrate in a patient the influence of tumor size on MoAb accumulation for the first time and confirm the relevance of reported studies of human tumors implanted in mice [2]. Quantitation of MoAb in each tumor in vivo was characterized by accumulation and clearance phases suggestive of specific uptake in the melanoma tissue. The MoAb uptake in each of the lesions was less than 1% ID, and the MoAb uptake in the 20 tumors was less than 5% ID. Therefore, the tumor burden influenced the total-body retention of the MoAb and the tumor-to-whole-body concentration ratios to a limited extent. Furthermore, the clearance from the whole body was similar to that from the tumors.

The concentration of MoAb in the tumors was inversely related to tumor size. The smallest tumor demonstrated a maximum tumor-to-whole-body concentration ratio of 37 when the morphometric volume of this tumor was considered to be the volume of accumulation as compared with a peak value of 7.2 attained by the 41.6-g tumor. The maximum concentration of In-111 in the 2.8-g tumor was 20 In-111 atoms per tumor cell equivalent to 30,000 molecules of ZME-018 per cell (Appendix). This corresponded to about 35,000 molecules of ZME-018 per cell when corrected for In-111 not bound to MoAb in the radiopharmaceutical. Another study of this MoAb in melanoma reported lower tumor-to-surrounding-tissue counts [9].

With the use of the MIRD [10] approach for radiation-absorbed dosimetry and the use of an extrapolated absorbed fraction for this 2.8-g tumor, the radiation dose was estimated to be 10 rads compared to a total-body dose of 1.9 rads for the 3.84-mCi dose administered.

Quantitative pharmacokinetics in patients are required for each radiolabeled MoAb in order to select the optimal time for radioimmunoimaging and to administer radioimmunotherapy safely [11,12]. The efficacy of therapy depends on the ratio of the radiation doses that can be delivered to the

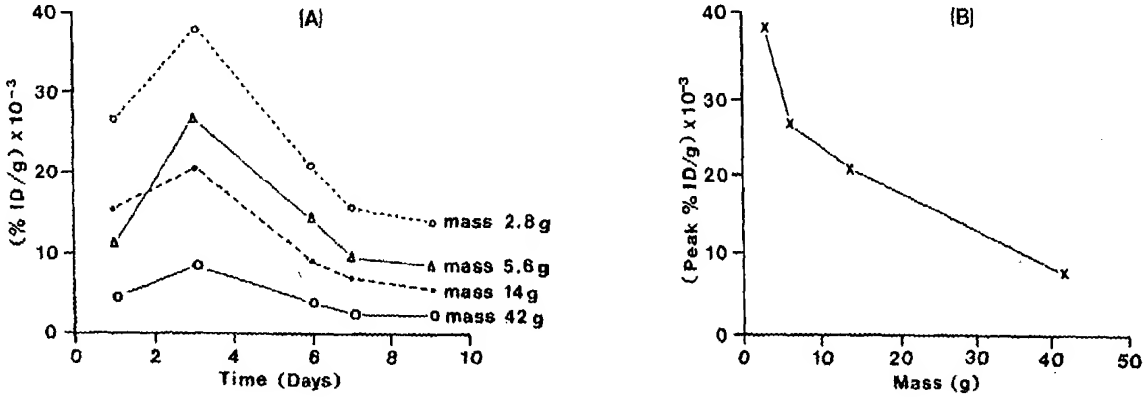


Fig. 3. A: Change in the concentration of In-111 in each tumor with time. B: Variation in the peak concentration of In-111 (day 3) with mass of each tumor.

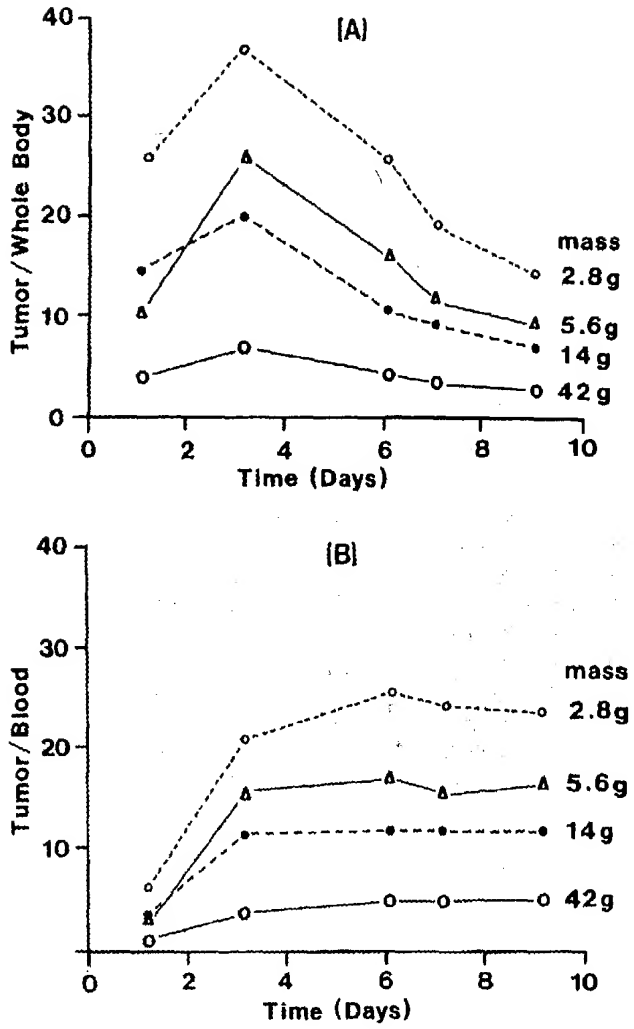


Fig. 4. Change in tumor-to-whole-body concentration ratio of In-111 (A) and tumor-to-blood concentration ratio of In-111 (B) with time. Note that there was equilibrium between each tumor and blood after day 3.

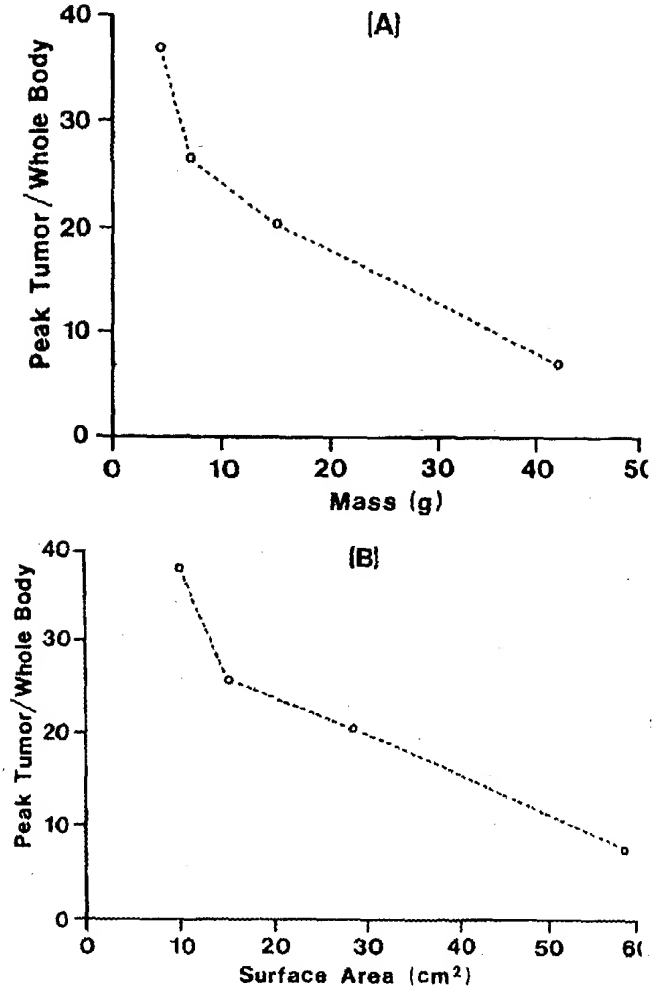


Fig. 5. Change in the peak concentration ratio of tumor to whole body of In-111 (day 3) with (A) mass and (B) surface area of each tumor.

tumor and normal tissues. The present results indicate that the concentration of this MoAb in tumor is dependent on tumor size, which in turn influences the spatial distribution of energy deposited in the tumor. Small melanoma tumors may be more effectively imaged and treated with radiolabeled MoAbs because of the increased concentration of radionuclide. Autoradiography and immunopathology studies have shown that necrosis, ischaemia, and poor diffusion limit the concentration of MoAb in tumors, particularly large tumors. Similar mechanisms lead to discrepancies between the morphologic volume and the physiologic volume of distribution of the radionuclide leading to underestimation of the true concentration of the radionuclide and the radiation-absorbed dose [13]. The range of the emissions and the exact location of the radionuclide in the tumor influence the radiotoxicity of a radionuclide [14].

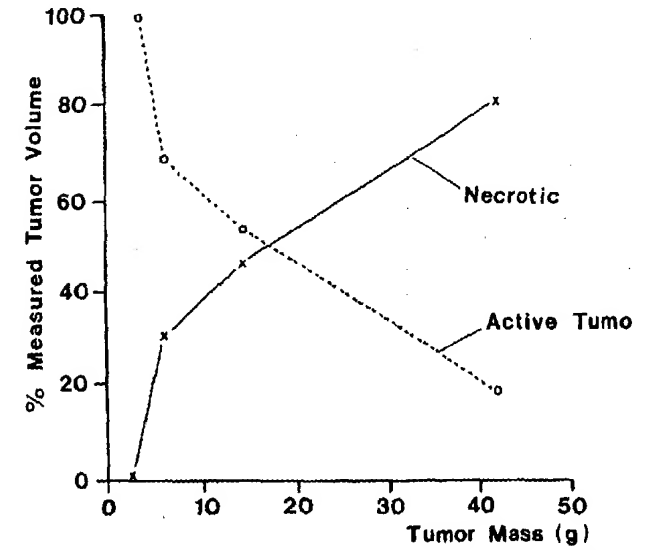


Fig. 6. Relationship of active and necrotic fractions to tumor size. The active and necrotic fractions were derived assuming the smallest tumor of 2.8 g contained only active tumor tissue.

We propose to perform similar studies of other tumors in patients in order to extend our observations. Volumes of tumors will be determined with calipers when superficially located or will be obtained by X-ray CT, ultrasound, or magnetic resonance imaging when located deep in the body.

## REFERENCES


1. Baldwin RW, Pimm MV: Antitumor monoclonal antibodies for radioimmunodetection of tumors and drug targeting. Cancer Metab Rev 2:89–106, 1983.
2. Hagan PJ, Halpern SE, Dillman RO, Shawler DL, Johnson DL, Chen A, Lakshmy K, Frincke J, Bartholomew RM, Davis GS, Carlo D: Tumor size effect on monoclonal antibody uptake in tumor models. J Nucl Med 27:422–427, 1986.
3. Pimm MV, Baldwin RW: Effect of tumor size on monoclonal antibody uptake in tumor models. Letter to the Editor. J Nucl Med 27:1788–1790, 1986.
4. Rankin EM, McVie JG: Radioimmunodetection of cancer: Problems and potential. Br Med J [Clin Res] 287:1402–1404, 1983.
5. Wilson BS, Imai K, Natali AG, Ferrone S: Distribution and molecular characterization of a cell-surface and a cytoplasmic antigen detectable in human melanoma cells with monoclonal antibodies. Int J Cancer 28:293–300, 1981.
6. Krejcarek CE, Tucker KL: Covalent attachment of chelating groups to macromolecules. Biochem Biophys Res Commun 77:581–585, 1977.
7. DeNardo GL, DeNardo SJ, Macey DJ, Mills SL: Quantitative pharmacokinetics of radiolabeled monoclonal antibodies for imaging and therapy in patients. Proceedings of NATO Advanced Study Institute Meeting on Radiolabeled Monoclonal Antibodies for Imaging and Therapy—Potential, Problems and Properties. Pisa, Italy, July–August 1986. Plenum Publ. Corp.
8. Snyder WS, Cook MS, Nassett ES, Karhausen CR, Perry Howells G, Tipton IS: ICRP Vol 23: Report of the task group on reference man. Oxford: Pergamon Press, p 325, 1974.
9. Murray JL, Rosenblum MG, Lamki J, Glenn HJ, Krizan Z, Hersh EM, Plager CE, Bartholomew RM, Unger MW, Carlo D: Clinical Parameters related to optimal tumor localization of In-111 labeled monoclonal antibody ZME-018. J Nucl Med 28:25–33, 1987.
10. Ellett WH, Humes RM: Absorbed fractions for small volumes containing photon emitting radionuclides. MIRD pamphlet #8, J Nuc Med 12:Supl 5, 25–32, 1971.
11. DeNardo GL, Raventos AR, Hines HH, Scheibe PO, Macey DJ, Hays MT, DeNardo SJ: Requirements for a treatment planning system for radioimmunotherapy. Int J Radiation Oncology Biol Phys 11:335–348, 1985.
12. Larson SM, Brown JP, Wright PW, Carrasquillo JA, Hellstrom I, Hellstrom KE: Imaging of melanoma with I-131 monoclonal antibodies. J Nucl Med 24:123–129, 1985.
13. Rossi HH: Microscopic energy distributions in irradiated matter. In Attix FH, Roesch WC, Tochilin E (eds): "Radiation Dosimetry: Vol I Fundamentals", Ch 2. New York: Academic Press, pp 43–92, 1968.
14. Rao DV, Govelitz GF, Sastry KSR: Radiotoxicity of T-201 in mouse testes: Inadequacy of conventional dosimetry. J Nucl Med 24:145–153, 1983.


## APPENDIX

### Number of MoAb molecules per tumor cell

This calculation was based on absolute quantitation of the amount of In-111 in the smallest tumor (2.8 g). Assumptions were that 1) the accumulation of MoAb was uniform in this tumor, and 2) no more than one In-111 atom was attached to each MoAb molecule. When the accumulation of MoAb reached a maximum 3 days after injection, the amount of In-111 in this tumor was 4.1 $\mu$Ci, which was equivalent to a concentration of 1.46 $\mu$Ci/g. This concentration as a fraction of the administererd dose (3.84 mCi) was

$$\text{Fractional ID/g} = 1.46/3{,}840 = 3.8\times10^{-4}$$

Since 20 mg MoAb was administered, then

$$\text{MoAb/g} = (3.8\times10^{-4})\times(20\times10^{3}) = 7.6\ \mu\text{g/g}$$

and

$$\#\text{MoAb/g} = \frac{(6.02\times10^{23})\times(7.6\times10^{-6})}{1.5\times10^{5}} = 3\times10^{3}$$

Assuming cells of 10 $\mu m^3$, the # of cells/g = $10^9$. Therefore, #MoAb/cell = $3\times10^{13}/10^9 = 3\times10^4$. However, only 86% of administered In-111 was attached to MoAb, so actual #MoAb/cell = $3\times10^4/0.86 = 3.5\times10^4$. The peak concentration of In-111 on day 3 was 1.46 $\mu$Ci/g and corresponded to $1.9\times10^{10}$ atoms of In-111 per gram of tumor. Assuming there were $10^9$ cells per gram of tumor, each melanoma cell had about 20 In-111 atoms on day 3.